Nanostructured Electrocatalysts for Selective Triglyceride Hydrogenation

by

Adam C. Lausche

A dissertation submitted in partial fulfillment
of the requirements for the degree of
Doctor of Philosophy
(Chemical Engineering)
in The University of Michigan
2011

Doctoral Committee:

Professor Levi T. Thompson, Chair
Professor John W. Halloran
Professor Johannes W. Schwank
Assistant Professor Xiaoxia Lin
Assistant Professor Charles W. Monroe

"It is the glory of God to conceal a matter;

to search out a matter is the glory of kings."

Proverbs 25:2 (NIV)

ACKNOWLEDGEMENTS

I would like to thank my advisor, Prof. Levi Thompson, for being my mentor and advisor throughout my graduate career. He has encouraged me to learn a variety of experimental techniques and has helped me to think about my data in new ways and from new angles. I very much appreciate how he has encouraged my professional development through his helpful advice and by encouraging me to attend professional conferences. The members of my thesis committee - Prof. John Halloran, Prof. Johannes Schwank, Prof. Nina Lin, and Prof. Charles Monroe - also deserve thanks for their constructive criticism of my work and for their encouragement. I especially want to thank Prof. Monroe for spending so much time and effort to teach me the fundamentals of electrochemistry.

I want to thank the exceptional high school and undergraduate students who assisted me in carrying out the experiments in this work: Krista Blumberg, Jeff Abromowitz, Mike Dowling, Kevin Shallcross, and Chris Hilger. I also want to thank the post-docs and research scientists in our group who took the time to teach and train me how to do catalysis and electrocatalysis: Chang Kim, Fan Shi, Valarie Thomas, and Alice Sleightholme. Valarie Thomas deserves special thanks for starting up the vegetable oil hydrogenation project, including the construction of the SPE reactor system. Alice Sleightholme also deserves special thanks for sharing her extensive expertise in electrochemistry and her constructive criticism.

I sincerely want to thank my parents, Dave and Patty, for teaching me the value of hard work and integrity. Certainly they told me in words that those things are

important, but I'm sure that I learned more about them from watching my parents live them out in daily life. I understand that being a parent can be a difficult and sometimes thankless job. But I am so very grateful to have such loving, supportive, and fun parents.

I want to thank my wife, Angie, and my daughter, Lydia, who make coming home so much fun. I find that no matter what happens in the lab, I find great peace and joy when I'm with my family.

Finally, I want to thank my Lord and Savior, Jesus Christ. I have found that apart from my faith in God, my life would be perpetual motion without meaning or purpose. But through my faith in Jesus, I have found great meaning, purpose, and hope.

TABLE OF CONTENTS

LIST OF FIGURES

Figure

LIST OF TABLES

Table

LIST OF ABBREVIATIONS

AOCS American Oil Chemists' Society

BET Brunauer, Emmett, and Teller

CV cyclic voltammetry

DHE dynamic hydrogen electrode

FAME fatty acid methyl ester

GC gas chromatography

GC-FID Gas Chromatograph - Flame Ionization Detector

GDL gas diffusion layer

HER hydrogen evolution reaction

ICP Inductively Coupled Plasma

ICP-OES Inductively Coupled Plasma - Optical Emission Spectroscopy

LSV linear sweep voltammetry

MEA membrane electrode assembly

ML methyl linoleate

OCV open circuit voltage

RDE rotating disk electrode

RF radio frequency

SHE standard hydrogen electrode

SMSE saturated mercury sulfate reference electrode

SPE solid polymer electrolyte

TGA thermogravimetric analysis

TPR temperature programmed reaction

XRD X-ray diffraction

CHAPTER I

Introduction

1.1 Summary

This chapter gives an introduction to electrochemical synthesis as an alternative to traditional thermochemical routes for chemical production. Previous researchers have reported the use of noble metal catalysts in solid polymer electrolyte (SPE) reactors for triglyceride hydrogenation, which resulted in products with superior selectivities as compared to those produced in the thermochemical reactor. Electrochemical reactors, however, are unlikely to be relevant on an industrial scale without less expensive hydrogenation catalysts. Early transition metal carbides and carbide-supported metal catalysts have been reported to have activities and selectivities comparable to those of noble metals. These catalysts may provide an interesting alternative to noble metals for triglyceride hydrogenation in the SPE reactor. This chapter concludes with the overall goals and scope of the thesis, as well as an overview of subsequent chapters.

1.2 Electrochemical Synthesis

Electrochemical processes are often heterogeneous. Water electrolysis, for example, is typically performed with two metal electrodes (anode and cathode) separated by an aqueous electrolyte (Figure 1.1a). When a voltage is applied by an external

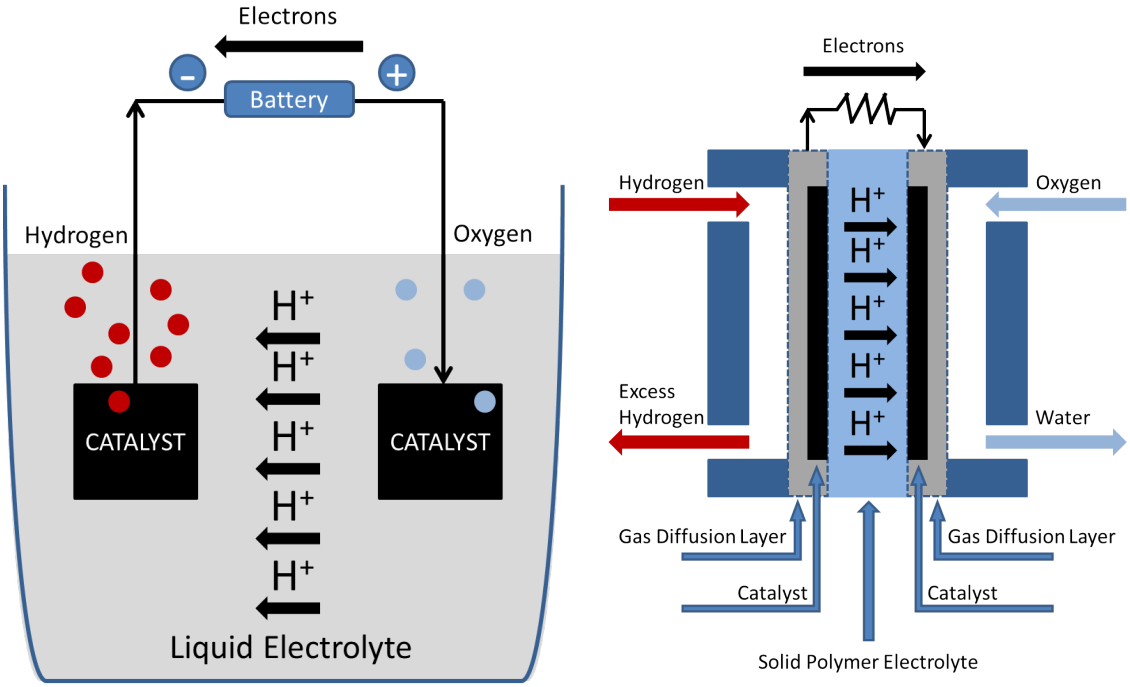

(a) Electrolyzer

(b) Fuel cell

Figure 1.1: Two schematics of electrochemical cells, which store (electrolyzers) and release (fuel cells) electrical energy in the form of chemical bonds.

power supply, two complementary chemical reactions (H_2 and O_2 production) occur at the interfaces between the electrodes and the liquid electrolyte. The fuel cell performs the same reactions, although in the opposite direction (i.e., H_2 and O_2 are consumed and H_2O and electrical energy are produced) (Figure 1.1b). In this case, however, the most common reactor design involves the use of a solid polymer electrolyte (SPE) with the metal electrodes finely dispersed on a gas diffusion layer, since the reactants in this case are gaseous. In both examples, these reactions happen at the electrochemical interfaces, where they either release or store electrical energy in the form of chemical bonds.

Aluminum production provides a good example of the advantages an electrochemical reactor can offer over traditional thermochemical synthesis. Although it is the earth's most abundant metal (8.3% by weight) [1], aluminum is never found in its elemental form in nature. Initially metallic aluminum was produced thermochemically,

using the Deville process invented in 1859 [2], and at such high cost that the metal was more valuable than gold or silver [3]. Subsequently a process was invented independently by Charles Martin Hall [4] and Paul Héroult to reduce alumina (Al_2O_3) to aluminum metal using electrolysis. This made the bulk production of aluminum economically feasible for the production of, for example, aircrafts [3].

With proper reactor design, we can also enhance separation between reactants and products, lower operating temperatures, and improve mass transfer [5]. The potential to drive such processes using inexpensive, renewable electricity presents the opportunity to decrease the environmental footprint of processes that have typically relied on fossil fuel-derived energy. Because of these potential advantages, we believe that there are significant opportunities for using electrochemical methods to drive other reactions that are typically performed thermochemically, such as triglyceride hydrogenation.

1.3 Triglyceride Hydrogenation

Industrial oil hydrogenation began with the bench top work performed by Sabatiér in 1897 [6], and was later patented by Normann in 1903 [7]. Proctor and Gamble purchased the US patent rights in 1909 and soon after began marketing Crisco, an inexpensive vegetable oil-based product that provided an alternative to the expensive animal shortenings on the market [8]. The batch and semi-batch thermochemical reactor designs used today have not changed significantly since that time [9]. A mixture of vegetable oil, hydrogen gas, and solid catalyst are pumped into the reactor and heated to reaction temperature (e.g., 140-160 °C) and pressure (3-5 atm H_2 gas). The mixture is vigorously agitated to keep the hydrogen gas bubbles as small as possible. Under these conditions, hydrogen adsorbs on the surface of the catalyst and reduces double bonds in the oil to single bonds, which raises the melting point of the oil and reduces the characteristic *fishy* odor [10]. Due to their low cost and

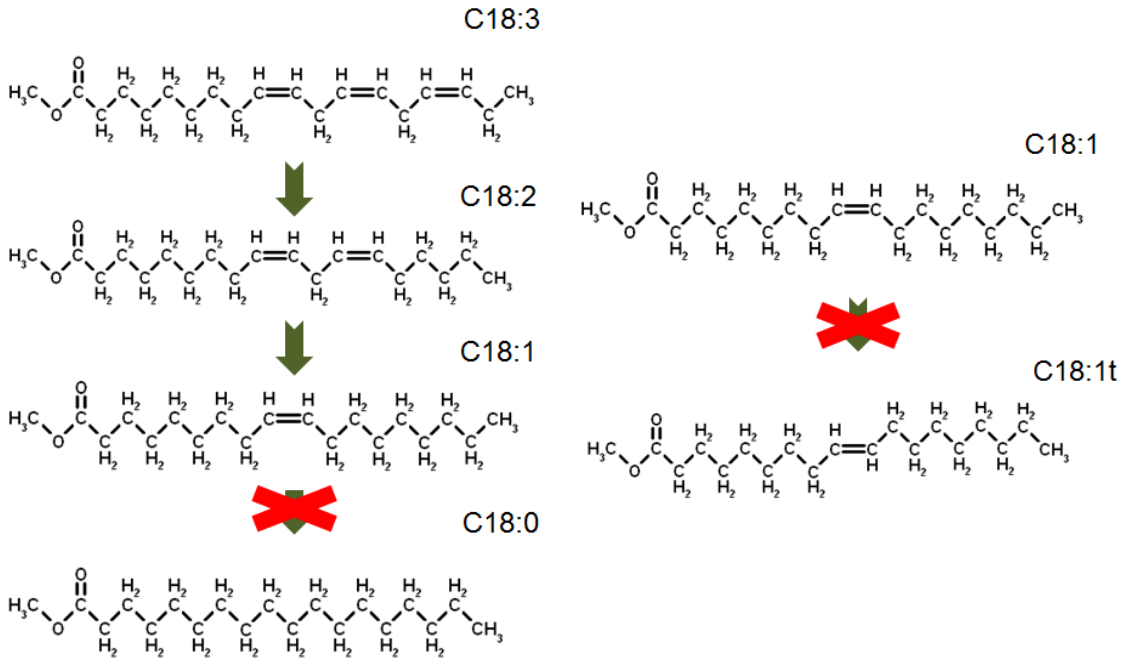

(a) Saturated fat selectivity (b) Trans fat selectivity

Figure 1.2: Schematics of two types of reaction selectivities for triglyceride hydrogenation.

high activity, nickel catalysts are typically used for hydrogenation, but Pd and other platinum group metals have also been demonstrated to be active [11].

The primary challenges associated with triglyceride hydrogenation deal with the activities and selectivities of the hydrogenation catalyst [12] (Figure 1.2). Vegetable oils typically contain a mixture of saturated, monounsaturated, and polyunsaturated carbon chains. One measure of catalyst selectivity is the preference for partial hydrogenation of the polyunsaturated carbon chains, since it is desirable to avoid the production of fully saturated chains. These fully saturated chains comprise the saturated fats, which are associated with increased risks of cardiovascular disease [13]. Another measure of catalyst selectivity involves limiting the geometric isomerization of the double bonds to the *trans* configuration. In the native oils, over 99% of the double bonds are in the *cis* configuration. Under hydrogenation conditions, the glyceride can be isomerized to the *trans* configuration. These *trans* fats are associated

with increased risks for coronary heart disease [14]. An ideal catalyst would produce monounsaturated fats (glycerides with exactly one carbon-carbon double bond) from feedstock, without producing *trans* or saturated fats.

In addition to catalyst type, the reactor operating parameters have been demonstrated to affect product selectivities significantly [12]. For example, an increase in the reactor temperature typically results in a decrease in the relative amounts of saturated fat production [12]. On the other hand, an increase in the reactor hydrogen pressure generally yields an increased saturated fat concentration. Previous researchers have related these trends to the fact that the hydrogenation reaction proceeds under mass-transfer limited conditions with respect to hydrogen in the stirred tank reactor [15]. The effect that these process parameters have on the product selectivities is therefore related to diffusion of hydrogen to the surface and the resulting changes in the surface coverage of hydrogen on the catalyst [12].

Triglyceride hydrogenation is believed to proceed via the Horiuti-Polanyi reaction scheme [16–18], which involves two individual hydrogenation steps (Figure 1.3). First, an adsorbed olefin reacts with an adsorbed hydrogen atom, producing a half-hydrogenated intermediate. This transformation is reversible. If a second hydrogen atom is available, the intermediate may react with it irreversibly to produce the fully reduced single bond. If a second atom is not available due to low hydrogen surface coverage, the intermediate may lose the original hydrogen atom and revert to the unsaturated state. Due to the differing stabilities of the *cis* and *trans* isomers, the *trans* configuration is thermodynamically favored at a 2 to 1 ratio [15].

The rates of hydrogenation and isomerization depend strongly on the surface coverage of hydrogen. Under conditions where the delivery of hydrogen is facile (e.g., high pressure, high agitation rates), the hydrogen coverage will be correspondingly high and the rates of isomerization will likely be low. Under conditions that result in the rapid consumption of surface hydrogen (e.g., high temperature, where high

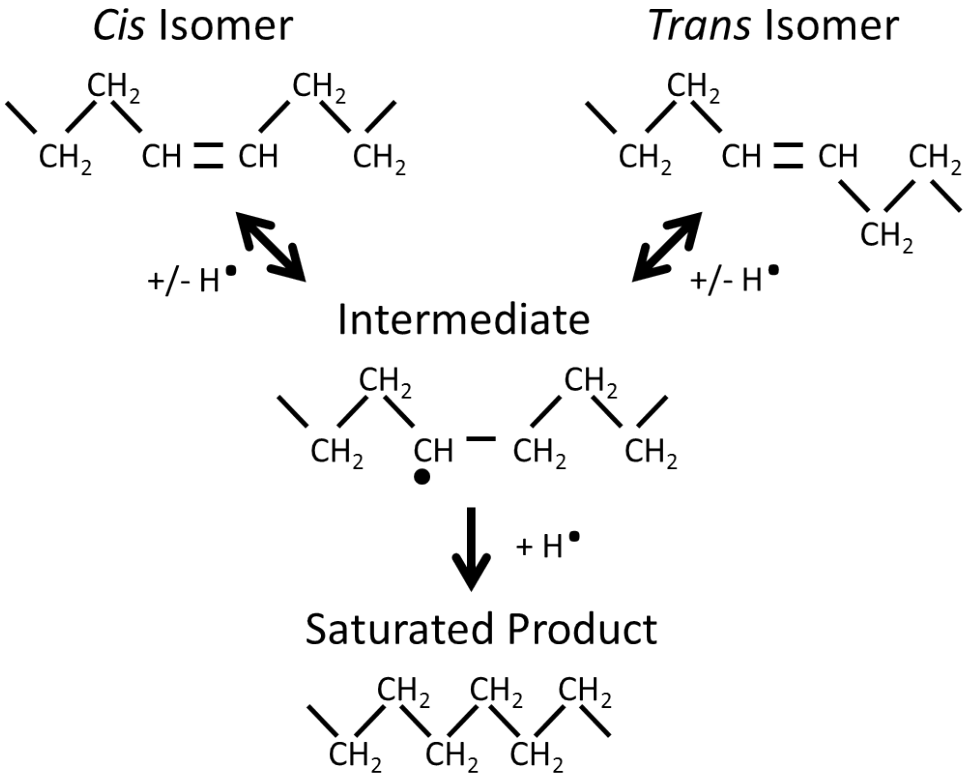

Figure 1.3: Horiuti-Polanyi reaction scheme for triglyceride hydrogenation.

reaction rates result in rapid consumption of surface hydrogen), the production of *trans* products will likely be higher [12]. The fact that reaction rates and reaction selectivities are linked in this way is a necessary consideration in the design of the thermochemical hydrogenation reactor. Since the hydrogen gas must dissolve and diffuse through the vegetable oil in order to react on the catalyst surface, the reaction rate will always be controlled by the solubility of hydrogen in the oil, which is usually low [15, 19].

1.4 Electrochemical Hydrogenation

The transfer of reactants and products to and from the catalyst surface is an important parameter in reactor design, because mass-transfer limitations can have negative effects on rates and product selectivities. Electrochemical reactors have potential advantages over thermochemical reactors, given a suitable electrolyte and reactor design. Furthermore, the applied voltage presents an additional operating parameter for controlling the reaction rates and selectivities. These advantages motivate our investigation of the utility of electrochemical reactors for the hydrogenation of triglycerides.

1.4.1 Electrochemical Reduction of Organics

Among the earliest reported work on electrochemical hydrogenation is that reported by Pomilio in 1915 [20]. He investigated the reduction of oleic acid to stearic acid, and suggested that the mass-transfer limitations in an aqueous electrolytic cell posed one of the main challenges for reducing unsaturated organics. In a 1942 review paper [21], Campbell *et al.* reported that a number of materials (Fe, Ni, Pt, and Pd) had been found to be active for alkene reduction [22, 23]. Work in this area developed in the 1960s with the systematic study of noble metal catalysts for hydrogenation [24, 25]. Since then a number of researchers have looked at how noble

and base metal catalysts can hydrogenate ketones [26–28], aldehydes [28–31], nitro compounds [28, 32, 33], nitriles [28], aromatics [32, 34], and alkenes [27, 28, 35]. One of the key design challenges of research reported in these papers was managing the mass-transfer of the unsaturated organic to the catalyst surfaces, since the research was carried out in reactors that were mass-transfer limited with respect to the organic reactant (Figure 1.4a).

The three-electrode cell consists of a reaction vessel with a catalytic working electrode, a counter electrode, and a reference electrode. The organic substrate is typically bubbled through (e.g., ethylene [35]) or dissolved in (e.g., acetone [26]) the electrolyte, which contains some source of protons (either H_3O^+ ions or H_2O). The solution may also be saturated with hydrogen gas, to provide another source of the reducing agent. As current is passed between the working and counter electrode, adsorbed hydrogen is formed on the catalyst surface, where it may react with the adsorbed organic substrate. The reaction vessel is usually stirred during this process, especially in cases where the reactants have poor solubilities in the electrolyte, since the reaction rate is typically mass-transport controlled [36].

It has also been suggested that the hydrogenation mechanism in an electrochemical reactor may depend on the character of the molecule being reduced. A key report in 1970 laid out a method for determining whether the rate determining step for hydrogenation was thermocatalytic, with the organic being hydrogenated by surface adsorbed hydrogen, or electrocatalytic, where the organic is protonated then reduced [37]. This method involves measuring the current through a reactor over a range of applied potentials both in the presence and the absence of the organic. The mechanism is determined by comparing the observed rates with those predicted by the thermocatalytic and electrocatalytic mechanisms. In the same year, Takehara *et al.* [27] tried this method with quinone and allyl alcohol, and found that the rate determining step for quinone hydrogenation was electrocatalytic, while allyl alcohol hydrogena-

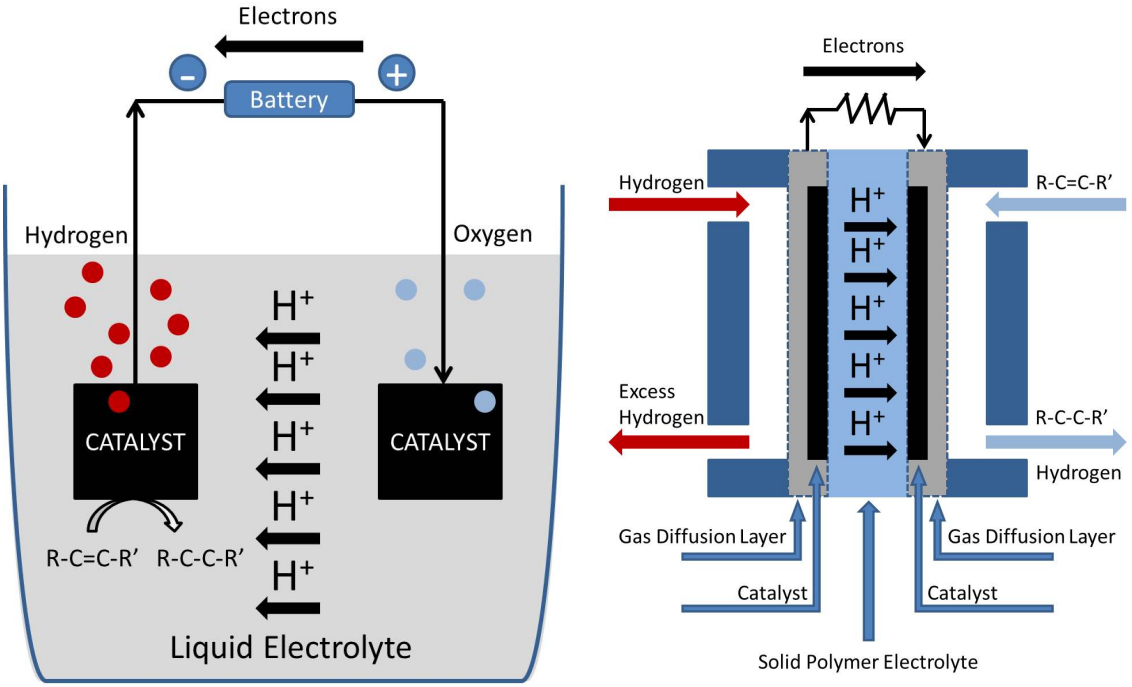

(a) Aqueous electrolyte hydrogenation cell

(b) SPE hydrogenation cell

Figure 1.4: Schematics of two electrochemical cell designs for the hydrogenation of organics.

tion followed a combination of pathways with thermocatalytic and electrocatalytic rate determining steps. The nature of the rate determining step is important, since electrochemical cells may have limited use if the applied potential cannot be used to affect the reaction rates and selectivities [36]. As such, it is necessary to explore the nature of the hydrogenation mechanism, in the context of the electrochemical reactor, in order to evaluate the utility of this approach for triglyceride hydrogenation.

1.4.2 Triglyceride Hydrogenation with a Solid Polymer Electrolyte Reactor

One type of electrochemical cell that potentially avoids the mass-transfer limitations of the aqueous electrochemical cell is the solid polymer electrolyte (SPE) reactor, which was first reported by Langer in 1963 [38, 39] (Figure 1.4b). Instead of transporting protons to the catalyst surface through a liquid electrolyte, this cell transports

them through a SPE to catalyst particles embedded in the polymer. Construction of this cell is similar to that of fuel cells, where hydrogen gas is flowed on one side of the SPE. Unlike a fuel cell, however, the unsaturated compound is flowed on the other side of the electrolyte, instead of oxygen gas. Under the applied potential, hydrogen dissociates to form protons and electrons. The protons are transported through the SPE, while the electrons flow through the external circuit. Hydrogen may then react with organics adsorbed on the cathode catalyst either as protons and electrons or as adsorbed hydrogen atoms. The significant improvement of this reactor design over the three-electrode cell is that the hydrogen is supplied separately from the organic to the catalyst surface, which potentially eliminates mass-transfer limitations.

Since the 1960s this reactor design has been implemented for the catalytic hydrogenation of a wide range of chemicals. Langer and coworkers extended their original work, which dealt with the hydrogenation of ethylene, to include the reduction of benzene [40], vinyl fluorides/chlorides [41], and nitric oxide [42–44], as well as the chlorination and bromination of olefins [45]. They reported that the rates and selectivities of the hydrogenation reaction are dependent on the applied potential and the hydrogenation catalyst, which suggests that the rate determining step may be electrocatalytic. Noble metal catalysts, such as Pt, Pd, and Ru, exhibited the highest activities. They also suggested that less expensive catalysts need to be developed for the technology to be industrially relevant. Lowrey and coworkers reported the use of the SPE reactor for fluorine production [46], although they reported corrosion of the Pt catalyst in those operating conditions. They suggested that catalysts need to be developed that are stable in the SPE reactor. More recently other researchers have reported the use of SPE reactors for hydrogen peroxide production [47], nitrobenzene reduction [48], and the hydrogenation of organic alcohols and acids [49]. They indicated that the rates for these reactions are also dependent on the applied potential, which again suggests that the rate determining step for these reactions may be

electrocatalytic.

Most recently Pintauro and coworkers demonstrated the electrocatalytic hydrogenation of triglycerides using a SPE reactor [5, 50–53]. Previously they had reported the electrocatalytic hydrogenation of soybean oil in an aqueous electrolyte hydrogenation reactor (e.g., Figure 1.4a), but this required the use of a non-food grade alcohol solvent (*tert*-butyl alcohol) to make the electrolyte and triglycerides miscible [54–56]. As an extension and improvement of this work, An *et al.* reported the use of a SPE reactor for triglyceride hydrogenation, which eliminated the need for this non-food grade solvent, since the hydrogenation reaction takes place at the interface of the SPE and the liquid triglyceride [50].

The utility of this reactor design was investigated with respect to two key objectives: 1) to decouple the delivery of reactants to the catalyst from the reaction rate, and 2) to control the reaction rates and selectivities using the applied potential. With respect to the first objective, they concluded that the delivery of hydrogen cannot be mass-transfer limited due to the reactor design [50, 51]. That is, since the hydrogen is delivered through the SPE, rather than co-fed with the oil (as in the thermochemical reactor and the aqueous electrolyte cell), hydrogen delivery should be facile under all conditions. The delivery of oil to the catalyst surface, however, was found to be somewhat dependent on the oil flow rate through the cathode and the thickness of the gas diffusion layer. An *et al.* reported that the hydrogenation rates were independent of these parameters, but the saturated fat and trans fat selectivities were dependent on the oil flow rate and gas diffusion layer (GDL) thickness. They determined that higher flow rates and thinner GDLs resulted in lower contact times with the catalyst surface, which in turn resulted in lower production of saturated and trans fats [52]. This suggests that the hydrogenation reaction may be mass-transfer limited with respect to the triglyceride in the SPE reactor under some operating conditions.

Pintauro and coworkers also found that hydrogenation rates increased with in-

creased current density (i.e., increased applied potential) [5, 52]. For example, using H_2O as the source of hydrogen, the hydrogenation rate for a Pd catalyst increased and then leveled off over the potential range 1.6 V to 2.3 V, while the rate for a Pt catalyst increased steadily over that range. The cause of this behavior, however, was not systematically studied. The authors attributed the changes to an imbalance in rates between the hydrogenation reaction and the HER, which also occurs at the cathode. No attempt was made to relate the reaction rates to any reaction mechanism, other than simply asserting a thermochemical mechanism, which involves the triglyceride being reduced by hydrogen adsorbed on catalyst surface sites (*) [51].

$$\text{R-C=C-R'} + 2\text{H}_{ads} \rightarrow \text{R-C-C-R'} + 2\ * \tag{1.1}$$

They also explored the rates and selectivities of a number of noble metal, base metal, and bimetallic Pd/base metal catalysts [52]. The rates for the noble metal catalysts (Pd, Pt, Rh, Ru, and Ir) tended to follow the same trends in activities and selectivities as the thermocatalytic hydrogenation reactor [11]. The base metal catalysts (Ni, Cd, Zr, Cr, Fe, Ag, Cu, and Co) were reported to have negligible activities. When used in combination with Pd, the bimetallic formulations did alter the observed rates and product selectivities. In general, the use of a bimetallic Pd-base metal catalyst tended to lower the observed rates, but also substantially improved the saturated and *trans* fat selectivities. In all cases, little effort was made to relate the rates and selectivities of these catalyst formulations to intrinsic properties of the materials, such as the electrochemical stabilities of the materials themselves.

1.4.3 Carbides and Carbide-supported Catalysts

One class of catalyst materials that has recently received increased interest for electrocatalytic applications are transition metal carbides and carbide-supported metals. These materials have been shown to exhibit activities and selectivities for certain reactions similar to those of platinum group metals [57], including CO hydrogenation [58] and benzene hydrogenation [59]. For these reactions, carbides have been reported to have activities similar to those of Pt and Ru. Since early transition metals are much less expensive these noble metals, these materials could potentially be interesting in a triglyceride electrochemical hydrogenation reactor.

Because they can be synthesized with high surface areas [60] and have high electrical conductivities [61–63], carbides have also been investigated for use as catalyst supports. Previous researchers have reported that their intrinsic activities present the opportunity to tune the performance of the supported metals [64, 65]. Tungsten carbide, in particular, has received increased interest especially in electrocatalytic applications [66–68]. W_2C was reported to improve the activity of a carbon supported Pt-Ru-W_2C catalyst for hydrogen oxidation, as well as being stable in an acidic environment [67, 68].

1.5 Research Goals and Organization of Text

The objective of research described in this thesis was to elucidate the fundamental electrochemical processes that occur during the electrocatalytic hydrogenation of triglycerides in a SPE reactor. We will investigate the triglyceride hydrogenation activities and selectivities of noble metal and base metal catalysts, since they have good electrical conductivities and are broadly used throughout the electrochemical literature [21, 24, 25, 52]. We will also investigate the utility of transition metal carbides and carbide-supported metals, since they have shown promise for other similar

reactions [58, 59, 67, 68]. We probe the fundamental characteristics that cause these materials to perform differently in the SPE reactor. We also demonstrate how to predict from these fundamental experiments whether a given catalyst will be effective as a hydrogenation electrocatalyst.

In order to accomplish these objectives, we employ a suite of thermochemical and electrochemical synthesis and characterization techniques. Chapter Two of this thesis gives a detailed description of the various experimental techniques that are employed, as well as some of the advantages of using techniques employed in this work. Also, a thorough description of catalyst synthesis and characterization is provided.

The effect of membrane acidity and applied potential on the electrochemical stability of the catalyst materials is examined in Chapter Three. We show that for certain materials the post-reaction catalyst loading is markedly decreased from the initial catalyst loading, via thermogravimetric analysis of the spent membrane electrode assemblies. These results are correlated to direct catalyst stability measurements by means of chronopotentiometry in a SPE electrochemical cell.

Chapter Four reports the activities and selectivities for the triglyceride hydrogenation reaction over the noble metal, base metal, carbide, and carbide-supported catalysts and compare them to available values from the literature. Previous studies have focused on the effect of process variables like oil flow rate, temperature, and turbulence on reaction rates under constant current operation. We discuss how varying the applied potential changes the rates and selectivities. Differences between the activities and selectivities of different catalysts are also described in this chapter.

In Chapter Five, a discussion of parameters governing catalyst activity and selectivity and the correlations between pure and mixed catalyst formulations is given, specifically with respect to the hydrogenation mechanisms. A detailed description of the mechanism for hydrogenation is discussed, with methyl linoleate, an 18 carbon methyl ester containing two double bonds. Over 50% of the glycerides in soybean oil

contain two double bonds. Methyl linoleate is used as a surrogate for the triglyceride reactant for determining the nature of hydrogenation mechanism in the SPE reactor.

In Chapter Six, the major conclusions of this work are presented and discussed, including an assessment of how these conclusions could impact the field of electrochemistry. A preliminary economic analysis is presented, which suggests that triglyceride hydrogenation in a SPE reactor could provide an economically viable alternative to the industrial thermochemical process. Finally, we give a detailed description of possible future directions for this work.

References

[1] D.R. Lide. *CRC handbook of chemistry and physics*. CRC Pr I Llc, 1996.

[2] A.G. Morachevskii. Henri Etienne Sainte-Claire Deville (To 150th Anniversary of the Development of the First Industrial Method for Production of Aluminum). *Russian Journal of Applied Chemistry*, 79(10):1731–1735, 2006.

[3] S. Venetski. Silver from clay. *Metallurgist*, 13(7):451–453, 1969.

[4] C.M. Hall. Process of Reducing Aluminum from JTS Fluoride Salts by Electrolysis, April 2 1889. US Patent 400,664.

[5] P.N. Pintauro, M.P. Gil, K. Warner, G. List, and W. Neff. Electrochemical hydrogenation of soybean oil with hydrogen gas. *Industrial & Engineering Chemistry Research*, 44(16):6188–6195, 2005.

[6] E.K. Rideal. Presidential address. Concepts in catalysis. The contributions of Paul Sabatier and of Max Bodenstein. *Journal of the Chemical Society (Resumed)*, pages 1640–1647, 1951.

[7] W. Normann. Process for converting unsaturated fatty acids or their glycerides into saturated compounds, 1903. British Patent 1 515.

[8] J. Burchenal. Food Product, 1915. US Patent 1,135,351.

[9] R.C. Hastert. Practical aspects of hydrogenation and soybean salad oil manufacture. *Journal of the American Oil Chemists' Society*, 58(3):169–174, 1981.

[10] T.L. Mounts, K. Warner, G.R. List, R. Kleiman, W.R. Fehr, E.G. Hammond, and J.R. Wilcox. Effect of altered fatty acid composition on soybean oil stability. *Journal of the American Oil Chemists' Society*, 65(4):624–628, 1988.

[11] P.N. Rylander. Hydrogenation of natural oils with platinum metal group catalysts. *Journal of the American Oil Chemists' Society*, 47(12):482–486, 1970.

[12] E.R. Cousins. Hydrogenation of fats and oils. Isomerization during hydrogenation. *Journal of the American Oil Chemists' Society*, 40(5):206–210, 1963.

[13] A. Mead, G. Atkinson, D. Albin, D. Alphey, S. Baic, O. Boyd, L. Cadigan, L. Clutton, L. Craig, C. Flanagan, et al. Dietetic guidelines on food and nutrition in the secondary prevention of cardiovascular disease–evidence from systematic reviews of randomized controlled trials (second update, January 2006). *Journal of Human Nutrition and Dietetics*, 19(6):401–419, 2006.

[14] D. Mozaffarian, M.B. Katan, A. Ascherio, M.J. Stampfer, and W.C. Willett. Trans fatty acids and cardiovascular disease. *New England Journal of Medicine*, 354(15):1601–1613, 2006.

[15] L.F. Albright. Mechanism of hydrogenation of triglycerides. *Journal of the American Oil Chemists' Society*, 40(5):16–29, 1963.

[16] Y.B. Vassiliev, V.S. Bagotzky, O.A. Khazova, V.V. Cherny, and A.M. Meretsky. Mechanism of adsorption, electroreduction and hydrogenation of compounds with ethylenic bonds on platinum and rhodium:: Part II. Comparison of the electroreduction and catalytic hydrogenation processes. *Journal of Electroanalytical Chemistry*, 98(2):273–282, 1979.

[17] P. Simon, A. Celkova, and S. Schmidt. A simplified Horiuti-Polanyi scheme for the hydrogenation of triacylglycerols. *Journal of the American Oil Chemists' Society*, 68(2):74–78, 1991.

[18] A. Bernas, P. Maki-Arvela, N. Kumar, B. Holmbom, T. Salmi, and D.Y. Murzin. Heterogeneously catalytic isomerization of linoleic acid over supported ruthenium catalysts for production of anticarcinogenic food constituents. *Industrial Engineerring Chemistry Research*, 42(4):718–727, 2003.

[19] E. Santacesaria, P. Parrella, M.S. Di Serio, and G. Borrelli. Role of mass transfer and kinetics in the hydrogenation of rapeseed oil on a supported palladium catalyst. *Applied Catalysis A: General*, 116(1-2):269–294, 1994.

[20] U. Pomilio. Elektrolytische Hydrierung von ungesattigten aliphatischen Sauren. *Zeitschrift für Elektrochemie und Angewandte Physikalische Chemie*, 21(17-18):444–448, 1915.

[21] K.N. Campbell and B.K. Campbell. The Addition of Hydrogen to Multiple Carbon-Carbon Bonds. *Chemical Reviews*, 31(1):77–175, 1942.

[22] C.L. Wilson. Analogies Between Electrolytic and Chemical Methods of Reduction. Experiments with Sorbic Acid. Remarks on Mechanism. *Transactions of The Electrochemical Society*, 75:353, 1939.

[23] K.N. Campbell and E.E. Young. The Addition of Hydrogen to Multiple Carbon-Carbon Bonds. IV. The Electrolytic Reduction of Alkyl and Aryl Acetylenes1. *Journal of the American Chemical Society*, 65(5):965–967, 1943.

[24] F. Beck and H. Gerischer. Elektrochemische Gesichtspunkte zur katalytischen Hydrierung an Platinkontakten in gepufferten Losungen. *Zeitschrift für Elektrochemie, Berichte der Bunsengesellschaft für Physikalische Chemie*, 65(6):504–517, 1961.

[25] V.F. Beck. Der Verlauf der Katalysatorbezugsspannung bei Hydrierungsreaktionen in Losung. *100 Jahre BASF: aus der Forschung*, page 107, 1965.

[26] X. De Hemptinne and K. Schunck. Electrochemical reduction of acetone. Electrocatalytic activity of platinized platinum. *Transactions of the Faraday Society*, 65:591–597, 1969.

[27] Z. Takehara. Hydrogenation of some organic compounds in acidic aqueous solutions on noble metal catalysts. *Electrochimica Acta*, 15(6):999–1012, 1970.

[28] M. Antonietta Casadei and D. Pletcher. The influence of conditions on the electrocatalytic hydrogenation of organic molecules. *Electrochimica Acta*, 33(1):117–120, 1988.

[29] K. Park, P.N. Pintauro, M.M. Baizer, and K. Nobe. Flow Reactor Studies of the Paired Electro-Oxidation and Electroreduction of Glucose. *Journal of the Electrochemical Society*, 132:1850, 1985.

[30] K. Park, P.N. Pintauro, M.M. Baizer, and K. Nobe. Current efficiencies and regeneration of poisoned Raney nickel in the electrohydrogenation of glucose to sorbitol. *Journal of Applied Electrochemistry*, 16(6):941–946, 1986.

[31] V. Anantharaman and P.N. Pintauro. The Electrocatalytic Hydrogenation of Glucose. *Journal of the Electrochemical Society*, 141:2729, 1994.

[32] P.N. Pintauro and J.R. Bontha. The role of supporting electrolyte during the electrocatalytic hydrogenation of aromatic compounds. *Journal of Applied Electrochemistry*, 21(9):799–804, 1991.

[33] Y. Song and P.N. Pintauro. The electrochemical synthesis of aminonitriles I. H-cell studies with adiponitrile and azelanitrile. *Journal of Applied Electrochemistry*, 21(1):21–27, 1991.

[34] D. Robin, M. Comtois, A. Martel, R. Lemieux, A.K. Cheong, G. Belot, and J. Lessard. The electrocatalytic hydrogenation of fused poly cyclic aromatic compounds at Raney nickel electrodes: the influence of catalyst activation and electrolysis conditions. *Canadian Journal of Chemistry*, 68(7):1218–1227, 1990.

[35] M. Byrne and A.T. Kuhn. Electro-catalytic reduction of ethylene on platinum and ruthenium. *Journal of the Chemical Society, Faraday Transactions 1: Physical Chemistry in Condensed Phases*, 68:355–368, 1972.

[36] G.C. Bond, G. Webb, M.D. Birkett, and A.T. Kuhn. *The catalytic hydrogenation of organic compounds–a comparison between the gas–phase, liquid–phase, and electrochemical routes*, pages 61–89. RSC Publishing, 1983.

[37] C. Wagner. Considerations on the mechanism of the hydrogenation of organic compounds in aqueous solutions on noble metal catalysts. *Electrochimica Acta*, 15(6):987–997, 1970.

[38] S.H. Langer and H.P. Landi. Electrogenerative Hydrogenation. *Journal of the American Chemical Society*, 85(19):3043–3044, 1963.

[39] S.H. Langer and H.P. Landi. The Nature of Electrogenerative Hydrogenation. *Journal of the American Chemical Society*, 86(21):4694–4698, 1964.

[40] S.H. Langer, S.J. Pietsch, and G.P. Sakellaropoulos. Electrogenerative chemical reactors. *Energy*, 4(2):225–233, 1979.

[41] G.P. Sakellaropoulos and S.H. Langer. Electrocatalytic hydrogenation of ethylene over palladium at positive potentials. *Journal of Catalysis*, 67(1):77–89, 1981.

[42] S.H. Langer and K.T. Pate. Electrogenerative reduction of nitric oxide. *Nature*, 1980.

[43] S.H. Langer and K.T. Pate. Electrogenerative reduction of nitrogen oxides, March 23 1982. US Patent 4,321,313.

[44] M.J. Foral and S.H. Langer. The effect of preadsorbed sulfur on nitric oxide reduction on porous platinum black electrodes. *Electrochimica Acta*, 33(2):257–263, 1988.

[45] S.H. Langer, A.D. Miller, and S. Pietsch. Electrogenerative chloro-and bromofluorination of olefins from aqueous media; the electrogenerative cell as a chemical reactor. *Journal of Applied Chemistry and Biotechnology*, 27(1):176–180, 1977.

[46] R. Lowrey, M. Doyle, and T. Andersona. A Novel Fluorine Production Process in a Proton Exchange Membrane Reactor. *Electrochemical and Solid-state Letters*, 2(10):519–521, 1999.

[47] K. Otsuka, K. Hosokawa, I. Yamanaka, Y. Wada, and A. Morikawa. One-step oxidation of benzene to phenol applying a fuel cell system. *Electrochimica Acta*, 34(10):1485–1488, 1989.

[48] X.Z. Yuan, Z.F. Ma, Q.Z. Jiang, and W.S. Wu. Cogeneration of cyclohexylamine and electrical power using PEM fuel cell reactor. *Electrochemistry communications*, 3(11):599–602, 2001.

[49] X.Z. Yuan, Z.F. Ma, Q.G. He, J. Hagen, J. Drillet, and V.M. Schmidt. Electrogenerative hydrogenation of allyl alcohol applying PEM fuel cell reactor. *Electrochemistry Communications*, 5(2):189–193, 2003.

[50] W. An, J.K. Hong, and P.N. Pintauro. Current efficiency for soybean oil hydrogenation in a solid polymer electrolyte reactor. *Journal of Applied Electrochemistry*, 28(9):947–954, 1998.

[51] W. An, J.K. Hong, P.N. Pintauro, K. Warner, and W. Neff. The electrochemical hydrogenation of edible oils in a solid polymer electrolyte reactor. I. Reactor design and operation. *Journal of the American Oil Chemists' Society*, 75(8):917–925, 1998.

[52] W. An, J.K. Hong, P.N. Pintauro, K. Warner, and W. Neff. The electrochemical hydrogenation of edible oils in a solid polymer electrolyte reactor. II. Hydrogenation selectivity studies. *Journal of the American Oil Chemists' Society*, 76(2):215–222, 1999.

[53] K. Warner, W.E. Neff, G.R. List, and P. Pintauro. Electrochemical hydrogenation of edible oils in a solid polymer electrolyte reactor. Sensory and compositional characteristics of low trans soybean oils. *Journal of the American Oil Chemists' Society*, 77(10):1113–1118, 2000.

[54] G.J. Yusem and P.N. Pintauro. The electrocatalytic hydrogenation of soybean oil. *Journal of the American Oil Chemists' Society*, 69(5):399–404, 1992.

[55] P.N. Pintauro. Electrocatalytic process for the hydrogenation of edible and non-edible oils and fatty acids, July 6 1993. US Patent 5,225,581.

[56] G. Yusem, P.N. Pintauro, P.C. Cheng, and W. An. Electrocatalytic hydrogenation of soybean oil in a radial flow-through Raney nickel powder reactor. *Journal of Applied Electrochemistry*, 26(10):989–997, 1996.

[57] R.B. Levy and M. Boudart. Platinum-like behavior of tungsten carbide in surface catalysis. *Science*, 181(4099):547, 1973.

[58] G.S. Ranhotra, A.T. Bell, and J.A. Reimer. Catalysis over molybdenum carbides and nitrides:: II. Studies of CO hydrogenation and C2H6 hydrogenolysis. *Journal of Catalysis*, 108(1):40–49, 1987.

[59] J.S. Lee, M.H. Yeom, K.Y. Park, I.S. Nam, J.S. Chung, Y.G. Kim, and S.H. Moon. Preparation and benzene hydrogenation activity of supported molybdenum carbide catalysts. *Journal of Catalysis*, 128(1):126–136, 1991.

[60] L. Volpe and M. Boudart. Compounds of molybdenum and tungsten with high specific surface area:: II. Carbides. *Journal of Solid State Chemistry*, 59(3):348–356, 1985.

[61] H.O. Pierson. *Handbook of chemical vapor depostion [ie deposition](CVD): principles, technology, and applications*. William Andrew, 1999.

[62] W.P. Leroy, C. Detavernier, R.L. Van Meirhaeghe, A.J. Kellock, and C. Lavoie. Solid-state formation of titanium carbide and molybdenum carbide as contacts for carbon-containing semiconductors. *Journal of Applied Physics*, 99:063704, 2006.

[63] L.W. Shacklette and W.S. Williams. Influence of order-disorder transformations on the electrical resistivity of vanadium carbide. *Physical Review B*, 7(12):5041, 1973.

[64] W. Setthapun. *Carbide and nitride supported methanol steam reforming catalysts*. PhD thesis, University of Michigan, 2007.

[65] N.M. Schweitzer, J.A. Schaidle, O.K. Ezekoye, X. Pan, S. Linic, and L.T. Thompson. High Activity Carbide Supported Catalysts for Water Gas Shift. *Journal of the American Chemical Society*, 2011.

[66] R. Venkataraman, H.R. Kunz, and J.M. Fenton. Development of new CO tolerant ternary anode catalysts for proton exchange membrane fuel cells. *Journal of the Electrochemical Society*, 150:A278, 2003.

[67] M.B. Zellner and J.G. Chen. Surface science and electrochemical studies of WC and W2C PVD films as potential electrocatalysts. *Catalysis Today*, 99(3-4):299–307, 2005.

[68] E.C. Weigert, D.V. Esposito, and J.G. Chen. Cyclic voltammetry and X-ray photoelectron spectroscopy studies of electrochemical stability of clean and Pt-modified tungsten and molybdenum carbide (WC and Mo2C) electrocatalysts. *Journal of Power Sources*, 193(2):501–506, 2009.

CHAPTER II

Experimental Methods

2.1 Introduction

The objective of research described in this dissertation was to understand the structure and function of electrocatalysts used in a solid polymer electrolyte (SPE)-type triglyceride hydrogenation reactor. To accomplish this objective, we have employed several thermochemical and electrochemical techniques to synthesize and characterize the materials.

Noble metal and base metal catalysts were used as received from vendors. Transition metal carbides were synthesized using a temperature programmed reaction (TPR) method from the transition metal oxide precursors. The carbide-supported metal catalysts were prepared using a wet impregnation technique and the unpassivated carbide surface. Techniques, such as X-ray diffraction (XRD), BET surface area analysis, Inductively Coupled Plasma (ICP) elemental analysis, and thermogravimetric analysis (TGA) were employed to characterize the structures and compositions of the catalysts.

Electrocatalyst performance characterization was accomplished using a SPE-type reactor, which circulated a mixture of triglycerides (i.e., soybean oil) on the cathode side and H_2 gas on the anode side. The reactor was operated isothermally for up to 72 hr, and product samples were taken periodically for analysis using gas chromatog-

raphy (GC).

Various electrochemical techniques, including cyclic voltammetry (CV), linear sweep voltammetry (LSV), and chronoamperometry, were used to characterize the stabilities of the materials. In some cases these were also used to interrogate the mechanisms of catalytic electrochemical reactions.

2.2 Catalyst Synthesis

2.2.1 Transition Metal Carbide Catalysts

Transition metal carbide catalysts were prepared via TPR of the respective oxide precursors. This method produces relatively high surface area materials, as opposed to reduction of the native metals [1, 2]. Prior to the development of the oxide TPR procedure, typical surface areas for carbides prepared by carburization of metal precursors were in the range of < 2 m^2 g^{-1} [3].

Oxide precursors were reduced in a quartz tube downflow reactor, supported on a plug of quartz wool. The reactor was heated in a temperature programmed manner, according to synthesis procedures described in the literature (see Table 2.1) [4, 5]. Reactants gases (15% CH_4/H_2) were continuously flowed through the reactor bed to provide a carburizing atmosphere. This reactant gas mixture provides a balance between providing sufficient carbon to replace the interstitial oxygen atoms and forming excess free carbon on the surface [2].

Upon completion of the temperature program, the reactor tube was quenched to room temperature. Before exposing the carbide materials to ambient air, a 1% O_2/He mixture was flowed through the catalyst bed at a low flow rate (1.2 L h^{-1}) to form a passivation layer on the surface. The unpassivated carbides spontaneously undergo bulk oxidation when exposed to the ambient air [1]. Previous researchers reported that passivation prevents this bulk oxidation, by forming an oxygen-rich carbide-like

surface [6–8].

2.2.2 Carbide-supported Metal Catalysts

Carbide-supported metal catalysts were prepared via wet impregnation of the carbide materials with metal precursors [7–9]. After completion of the carbide synthesis temperature program, the reactor tube was quenched to room temperature. Without exposure to ambient air or passivation gases, the catalyst was transferred to a flask containing 70 mL of a deaerated solution of the metal salt. The concentration of the salt solution was adjusted to give the desired catalyst weight loading. The solution was continuously bubbled with Ar gas to prevent dissolved O_2 from the atmosphere from oxidizing the carbide material. After 4 hr of bubbling at room temperature, the liquid was decanted and the wet catalyst was transferred to a new quartz tube reactor under a blanket of Ar gas. The adsorbed metal salt complex was reduced in H_2 gas as the reactor was heated in a temperature programmed manner (see Table 2.1). Again the reactor was quenched to room temperature and the catalyst was passivated in 1% O_2/He for 5 hr at room temperature.

2.3 Physical Characterization

2.3.1 X-ray Diffraction Analysis

XRD is a bulk characterization technique that uses X-ray radiation to interrogate the long-range crystal structure of a material [10]. Diffraction occurs whenever a wave passes through a regularly spaced object, and the wavelength is on the same order of magnitude as the object spacing. X-ray diffraction patterns consist of a plot of the relative intensity of diffracted X-rays versus the angle of diffraction. A typical diffraction pattern for crystalline solids will contain a set of peaks over a range of diffraction angles. These peaks correspond to different crystal planes in the material,

Table 2.1: Precursors and reactor conditions for transition metal carbide catalyst synthesis.

Catalyst	Precursor	Precursor Weight (g)	Flow Rate (mL min^{-1})[a]	R_1[b]	T_1 (°C)	S_1[c]	R_2[b]	T_2 (°C)	S_2[c]
VC	V_2O_5	0.4	400	0.28	157	0.0	7.7	987	1.0
NbC	Nb_2O_5	0.4	260	2.38	1100	1.0	-	-	-
Mo_2C	$(NH_4)_6Mo_7O_{24}{\cdot}4H_2O$	1.3	400	0.55[d]	350[d]	12.0[d]	1.5	590	2.0
W_2C	WO_3	1.1	200	0.28	250	0.0	7.5	650	5.0
Pd/W_2C	unpassivated W_2C	0.9	400	0.75	110	2.0	1.0	450	4.0

[a]Reducing gas is 15% CH_4/H_2 (Cryogenic Gases, certified mixture), unless otherwise noted
[b]Temperature ramp time (hr)
[c]Temperature soak time (hr)
[d]Reducing gas is 100% H_2 (Cryogenic Gases, pre-purified)

and can be used to differentiate between materials with different crystal structures. Bragg's Law (Equation 2.1) relates the diffraction angle to the spacing between each set of crystal planes, where n is an integer (1, 2, 3, ...), λ is the X-ray wavelength, d is the characteristic spacing of each crystal plane, and θ_{B} is the angle between the incident X-rays and the crystal planes.

$$n\lambda = 2d \sin \theta_{\mathrm{B}} \tag{2.1}$$

X-ray diffraction analysis can also provide information about the average crystallite size of a crystalline material. For a perfect, infinitely large crystal, Bragg's law dictates that one angle (θ_{B}) will satisfy the equation for each d-spacing. For a material that is polycrystalline with a small average crystallite size (less than approximately 1 micron), other angles $\theta = \theta_{\mathrm{B}} \pm d\theta$ will also diffract the rays incident on the crystal. Therefore, for very large crystals, the diffraction peak will be very narrow, while smaller crystals will have broader peaks. This relationship is expressed by the Scherrer equation (Equation 2.2) [11], which relates the average crystallite size (t) to the X-ray wavelength (λ), the peak width (usually approximated as the full width at half the maximum peak intensity, B), and the Bragg angle (θ_{B})

$$\mathrm{t} = \frac{0.9\lambda}{B \cos \theta_{\mathrm{B}}} \tag{2.2}$$

For this work a Rigaku Miniflex X-ray diffractometer was used, with Cu Kα radiation and a Ni filter ($\lambda = 1.540$ Å). The analysis was performed over the diffraction angle range $10° < 2\theta < 90°$, with a 0.02 degree step size and a 5 degree min^{-1} scan rate. Analysis of the XRD patterns was performed using the Jade Software v. 9.0 (Materials Data, Inc.) software package. Crystal phases were identified by comparison with standard references from the ICDD (International Center for Diffraction Data) PDF4 database (rev. 2009).

2.3.2 BET Surface Area Analysis

BET surface area analysis was first described by Brunauer, Emmett, and Teller (BET) in 1938 [12]. This theory generalizes the monolayer adsorption assumed by the Langmuir isotherm to multilayer adsorption. A given sample is degassed under vacuum at elevated temperatures (e.g., 100-400 °C) to remove any physisorbed contaminants. Then the sample is cooled to 77 K with liquid N_2 and covered with multiple monolayers of physisorbed N_2 molecules. BET derived an equation (Equation 2.3), which relates the volume of adsorbed gas on a sample, v, to the pressure, p, where v_m is the volume of gas adsorbed in one monolayer, p_0 is the saturation pressure of the gas, and c is a constant. This equation predicts the variation in gas volume adsorbed with partial pressure. At low pressures ($p << p_0$), the isotherm is concave, which corresponds to sub-monolayer adsorption of gases on the material surface. At high pressures ($p \rightarrow p_0$), the isotherm is convex, which corresponds to the formation of multiple layers of adsorbed gas.

$$\frac{p}{v(p_0 - p)} = \frac{1}{v_m c} + \frac{c-1}{v_m c}\frac{p}{p_0} \tag{2.3}$$

A plot of $\frac{p}{v(p_0-p)}$ versus p/p_0 is approximately linear for relative pressures between 0.05 and 0.20. By fitting a line through this region, the number of N_2 atoms in one monolayer of adsorbed gas (v_m) can be calculated from the slope and y-intercept. The surface area of the material can then be calculated by multiplying this number by the area occupied by one N_2 atom [13].

BET surface area measurements were performed using a Micromeritics ASAP 2000 BET analyzer. Approximately 0.1 g of material was degassed at 300 °C for 2 hr prior to surface area measurements.

2.3.3 ICP Elemental Analysis

The catalyst compositions were determined by Inductively Coupled Plasma - Optical Emission Spectroscopy (ICP-OES) using a Varian 710-ES analyzer (Figure 2.1). Catalyst samples were dissolved in 5% aqua regia (3 parts HCl-1 part HNO_3 (Fisher Scientific, certified ACS Plus)) in 30% H_2O_2 (Fisher Scientific, certified ACS) and diluted with deionized H_2O [14].

The samples and standards of known concentrations are sequentially introduced to the ICP instrument using a peristaltic pump through a nebulizer, which entrains atomized droplets in an Ar stream [15]. During analysis this mist flows to the ICP torch, which consists of three concentric quartz tubes, situated inside an radio frequency (RF) generator coil. The argon gas is ionized by the intense RF electromagnetic field generated by the RF coil. Metals dissolved in the samples and standards in the mist are likewise ionized. Electrons in the metals are rapidly lost and regained by the metal atoms, which results in the emission of radiation at wavelengths that are characteristic of the different elements.

The wavelengths and intensities of these emissions are detected by a CCD camera and recorded by the computer software. The intensities of these emissions are proportional to the concentrations of the dissolved metals. In order to quantify the various catalyst compositions, the emission spectra of dissolved samples were compared to those for a series of standard solutions of known concentrations (Inorganic Ventures).

2.3.4 Thermogravimetric Analysis

Catalyst performances were measured in a SPE electrochemical reactor, and the catalyst materials were supported on GDLs incorporated in a membrane electrode assembly (MEA). Thermogravimetric analysis was used to characterize the actual MEA catalyst loadings before and after reaction in the SPE reactor. Characterization of the post-reaction MEAs was performed using a TA Instruments SDT Q600

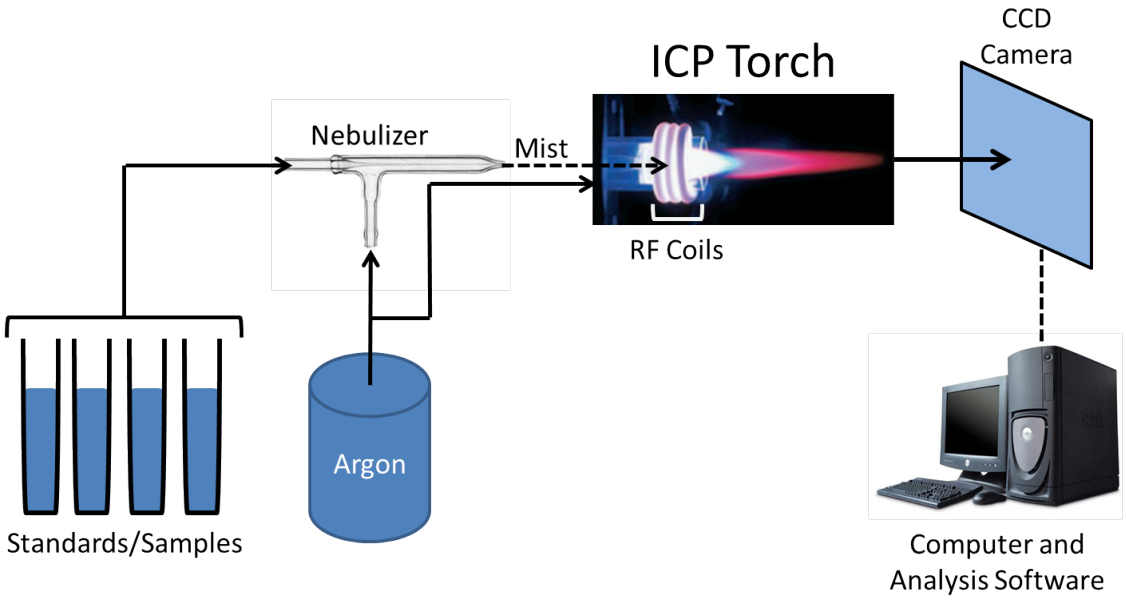

Figure 2.1: Schematic of ICP elemental analysis instrumentation.

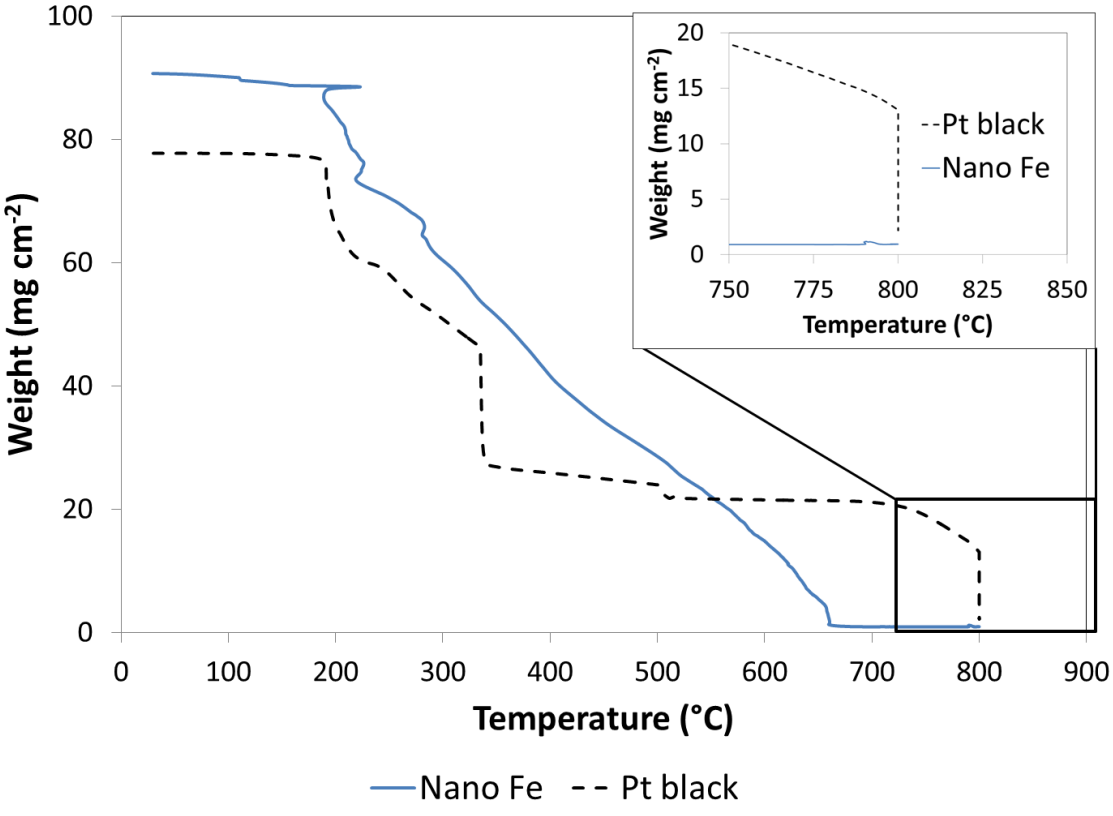

Figure 2.2: Thermogravimetric analysis of post-reaction MEA catalyst content in 0.05 L min^{-1} of 100% O_2 ramped at 40 °C min^{-1} to 800 °C.

thermogravimetric analyzer. A 1 cm^2 cross-section was excised from the spent MEA. Since the anode and cathode GDLs each contained $\sim$ 1 mg cm^{-2} of catalysts, the expected loading for this 1 cm^2 cross-section was $\sim$2 mg. The temperature of the TGA reaction chamber was ramped at 40 °C min^{-1} to 800 °C, and held for 5 min [16, 17]. A 100% O_2 gas (Cryogenic Gases, extra-dry grade) was flowed at 0.05 L min^{-1} to provide an oxidizing atmosphere. The weight changes in the MEA were measured as a function of time and temperature (Figure 2.2). The TGA data was analyzed using the TA Instruments Universal Analysis 2000 v. 4.3A software to determine the actual catalyst loadings.

2.4 Performance Characterization

2.4.1 SPE Reactor Operation

The triglyceride hydrogenation system consisted of a SPE fuel cell-type reactor (Figure 2.3). On the anode side, a mass flow controller and a humidification system provided humidified H_2 gas to the anode side of the stack. A backpressure regulator controlled the H_2 pressure at 10 psig. A heater/stirrer and liquid pump controlled the delivery of oil on the cathode side, which operated in a batch recycle manner. Hydrogenation reactions were performed isothermally between 60-80 °C with 100 mL oil circulated at 100 mL min^{-1} on the cathode, and 100 mL min^{-1} of H_2 gas on the anode. A Hewlett-Packard E3631A power supply controlled the current/potential of the reactor, which was operated either in constant current (0.5 A) or constant potential (0.25 - 1.0 V) modes. A Fuel Cell Test Station (Fuel Cell Technologies, Inc.) recorded the cell potential throughout reactor operation.

Membrane electrode assemblies (MEA) were prepared by hand painting thin coats of liquid catalyst suspension onto the GDL surfaces. Carbon GDLs used in this study were cut to size (1 in^2 or 6.45 cm^2), and used as received from the vendors (E-tek

cloth LT2500W ELAT© and Toray paper TGP-H-090). Liquid catalyst suspensions for cathode GDLs were prepared by mixing 21.1 mg of catalyst material with 120.7 μL of 5 wt% Nafion® perfluorinated resin solution (Sigma-Aldrich, density = 0.874 g/mL at 25 °C), 200 μL of isopropanol, and 200 μL of deionized H_2O. Liquid suspensions for anode GDLs consisted of 132.3 mg of 20 wt% Pt/C catalyst with 1.009 mL of 5 wt% Nafion® perfluorinated resin solution (Sigma-Aldrich), 600 μL of isopropanol, and 600 μL of deionized H_2O.The relative amounts of catalyst and Nafion® solution were calculated to give a dry composition of 80% catalyst and 20% Nafion® resin. Target catalyst loadings for the anode and cathode GDLs were 1 mg cm^{-2}. The anode catalyst was 20% Pt/C (Alfa Aesar), while the cathode catalyst varied for each experiment. The anode and cathode GDLs were assembled with a Nafion® 117 membrane via a hot pressing technique [18] at 135 °C and 700 psi for 5 min.

2.4.2 Product Composition Analysis

Liquid samples were taken periodically and characterized using standard methods reported by the American Oil Chemists' Society (AOCS) Methods Ce 1-62. Triglyceride samples were transesterified by mixing 150 μL of each sample with 1.5 mL hexane (Sigma-Alrich, ACS Reagent) and 80 μL 2N KOH (Sigma-Aldrich, 99.99%) in CH_3OH (Alfa Aesar, 99.8+% HPLC Grade) for one minute in a plastic centrifuge tube (AOCS Method Ce 2-66). The sample tubes were centrifuged at 5000 rpm for 30 seconds. Then 40 μL of the supernatant was further diluted with 1.5 mL hexane in a GC sample vial. The transesterification reaction separated the carbon chains from the glycerol backbone, thus creating fatty acid methyl esters (FAMEs). The resulting FAMEs were analyzed using GC using a Varian 450-GC instrument Gas Chromatograph - Flame Ionization Detector (GC-FID) equipped with a Varian CP 7487 column operating at 192 °C (AOCS Method Ce 1-62). The resulting GC-FID traces were analyzed using PeakSimple Chromatography Software v. 3.93 (SRI Instruments) to

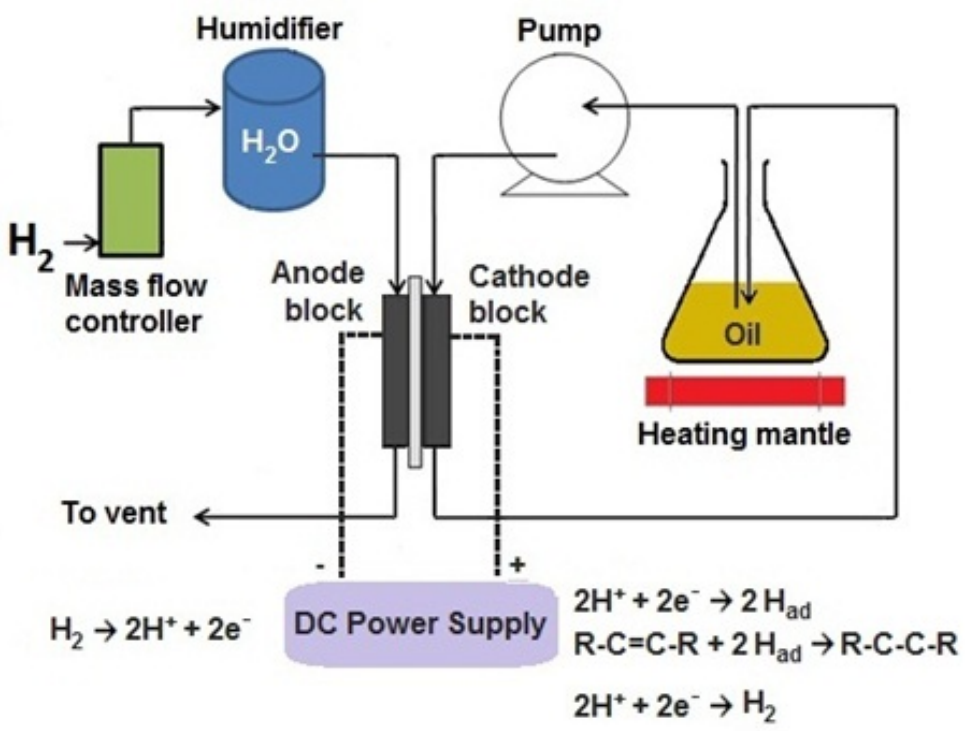

Figure 2.3: Schematic of a SPE triglyceride hydrogenation reactor.

determine the triglyceride composition. Product compositions for selected samples were independently verfied by third-party analysis (Thionville Laboratories Inc).

The FAMEs from the fresh soybean oil were composed of approximately 10% 16-carbon chains and 90% 18-carbon chains. The 16-carbon components (16 carbons with zero double bonds, denoted as C16:0) are fully saturated, and do not participate either as reactants or products in the hydrogenation reaction. They do, however, provide a convenient internal standard for GC-FID calibration, since their concentration does not change during the reaction. The 18-carbon FAMEs are comprised of a mixture of 4% methyl stearate (C18:0), 23% C18:1, 55% C18:2, and 8% C18:3, and hydrogenation results in reduction of selected double bonds. The electrochemical current efficiency (CE%) characterizes the efficiency with which protons that travel through the Nafion® SPE are involved in reducing double bonds, rather than recombining and evolving as H_2 gas or participating in other side reactions. Equation 2.4 characterizes this ratio of the change in the number of double bonds (as measured by

the change in composition of the triglyceride mixture) versus the integrated flux of protons through the membrane (that is, the product of the applied current, I, and the total time of the experiment, t)

$$\text{CE } \% = \frac{FM\left[\frac{2\Delta_{\text{C18:1}}}{MW_{\text{C18:1}}} + \frac{4\Delta_{\text{C18:2}}}{MW_{\text{C18:2}}} + \frac{6\Delta_{\text{C18:3}}}{MW_{\text{C18:3}}}\right]}{It} \tag{2.4}$$

where $\Delta_{\text{C18:1}}$, $\Delta_{\text{C18:2}}$, and $\Delta_{\text{C18:3}}$ are the changes in the weight fractions of the FAME components C18:1, C18:2, and C18:3, respectively; M is the mass (in grams) of soybean oil, F is Faraday's constant, and MW is the molecular weight of each FAME component.

2.5 Electrochemical Characterization

Electrochemical techniques can be used to characterize the kinetics and energetics of surface-electrolyte reactions [19]. Since these reactions involve the transfer of electrons under an applied potential, we can measure their rates by measuring the electron-transfer rates (i.e. current) as a function of potential.

CV is one method of characterizing these reactions via the linear variation of the applied potential over a given range. When the applied potential reaches one end of the potential region, the potential sweep is inverted. This cyclic potential sweep is typically carried out several times during a given experiment, and the current is measured as function of the applied potential. This can give information about the types of surface reactions that are redox active over this potential range [19].

For example, two such surface reactions occur on a Pt electrode in 0.5 M H_2SO_4 over the potential range from 0.0 V to 1.4 V vs standard hydrogen electrode (SHE), as illustrated in Figure 2.4. As the applied potential is linearly varied between 0.0 V and 0.4 V vs SHE, surface adsorbed hydrogen atoms are oxidized or reduced (Equation 2.5a). PtO is formed over the potential range 0.4 V to 1.4 V vs SHE by the

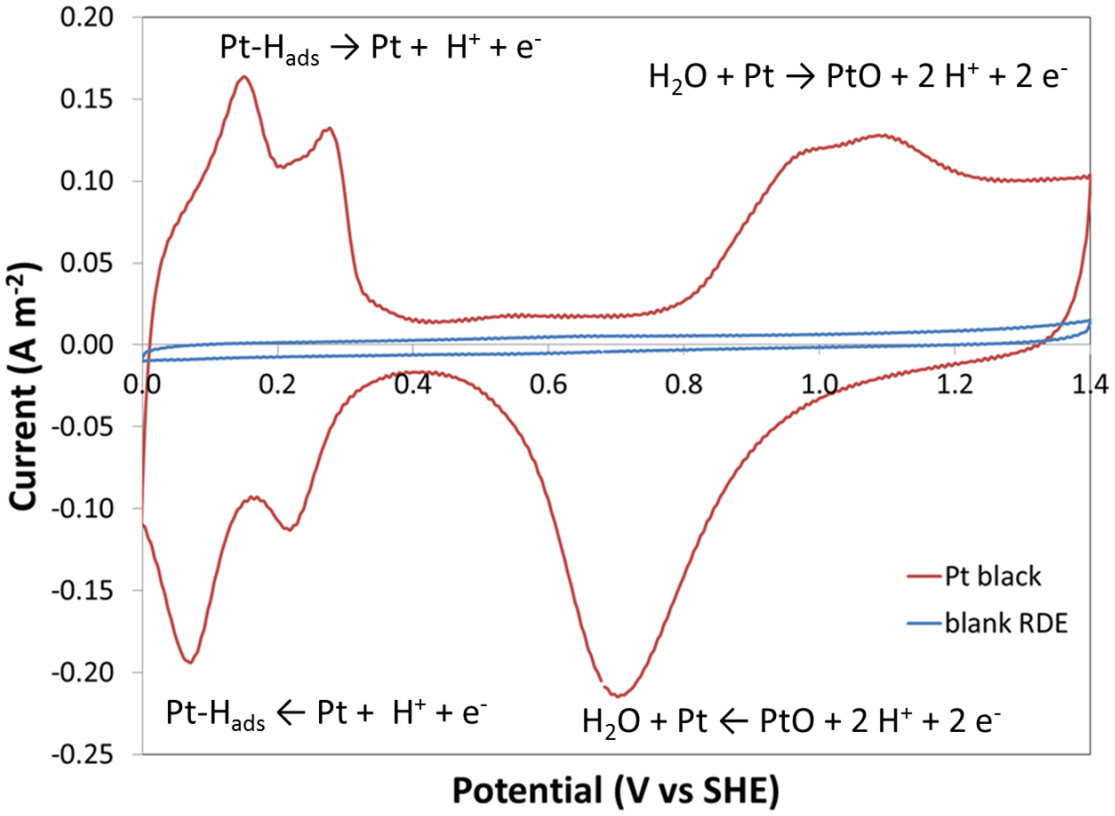

Figure 2.4: Cyclic voltammogram of Pt black supported on glassy carbon RDE at 0 rpm in 0.5 M H_2SO_4, initally bubbled with N_2 for 30 min and then covered with a N_2 blanket, with a scan rate of 200 mV s^{-1}.

reaction of Pt sites (*) with oxygen from H_2O [20] (Equation 2.5b). The oxidation of surface Pt sites produces two electrons, which results in the anodic (positive) current that is measured. On the reverse sweep, the PtO is reduced to Pt, which consumes electrons and results in the cathodic (negative) current.

$$H_{ads} \leftrightharpoons H^+ + e^- + * \qquad \text{Hydrogen Adsorption} \qquad (2.5a)$$

$$H_2O + * \leftrightharpoons O_{ads} + 2H^+ + 2e^- \qquad \text{Oxygen Adsorption} \qquad (2.5b)$$

The peaks that are observed for the two surface reactions are a result of the combination of the current-overpotential relationship and the limitations of mass-transfer of reactants to the electrode surface. The relationship between the applied potential and the observed current for a one-electron transfer reaction ($O + e^- \leftrightharpoons R$) is given by the Butler-Volmer equation (2.6), where i is the current density; i_0 is the exchange current density; C_O^s and C_O^b are the concentrations of species O at the surface and in the bulk electrolyte, respectively; C_R^s and C_R^b are the concentrations of species R at the surface and in the bulk electrolyte, respectively; α is the symmetry factor (usually assumed to be 0.5); and f is the ratio of Faraday's constant to the ideal gas constant and the temperature. The difference between the applied potential (E) and the equilibrium potential (E^0) is called the overpotential (η), which is effectively the driving force for the electrochemical reaction.

$$i = i_0\left[\frac{C_O^s}{C_O^b}\exp[-\alpha f\eta] - \frac{C_R^s}{C_R^b}\exp[(1-\alpha)f\eta]\right] \qquad (2.6)$$

The large peak associated with the reduction of O_{ads} at approximately 0.7 V vs SHE is the result of the interplay between the increasing driving force for O_{ads} reduction and the decreasing availability of that species. As the applied potential is swept in the negative direction from 1.4 V past the equilibrium potential of 0.8

V, the driving force for O_{ads} reduction increases exponentially and the driving force for O_{ads} formation becomes insignificant. At large overpotentials, $\exp(-\alpha f\eta) << \exp((1-\alpha)f\eta)$ and the Butler-Volmer equation simplifies to:

$$i = -i_0 \frac{C_{\mathrm{R}}^s}{C_{\mathrm{R}}^b} \exp[(1-\alpha)f\eta] \tag{2.7}$$

If the supply of O_{ads} and H^+ were infinite, the current density i would go to the limit of negative infinity as the overpotential increased. But the number of PtO sites is finite, so the O_{ads} reduction current density reaches a maximum at approximately 0.7 V vs SHE and subsequently decreases. This behavior is described in the Butler-Volmer equation by the term C_{R}^s, which decreases over time as the finite supply of O_{ads} is consumed.

2.5.1 Electrochemical Stability Characterization

Chronoamperometry provides one way to measure electrocatalyst stabilities in the SPE reactor. This method involves applying a constant potential across a cell and measuring the resulting current density. In the SPE reactor, this current is due to the HER, which is favored over the potential range used in this research (-1.0 V to -0.25 V vs SHE) (Figure 2.6a). The stabilities of the electrocatalysts were characterized using this chronoamperometry method in a solid-state SPE cell (Figure 2.5) [21]. The catalysts were supported on a gold wire microelectrode (d = 0.1 mm) and placed in physical contact with a SPE membrane. A platinum flag was used as the counter electrode, and a dynamic hydrogen electrode (DHE) was used as the reference electrode. Measurements were performed using an Autolab PGSTAT302N potentiostat (Metrohm AG).

A typical experiment consisted of physically abrading a small amount of catalyst material into the gold metal, positioning the electrode in contact with the SPE membrane (Nafion®), and applying a potential for up to 15 h. The potential applied in

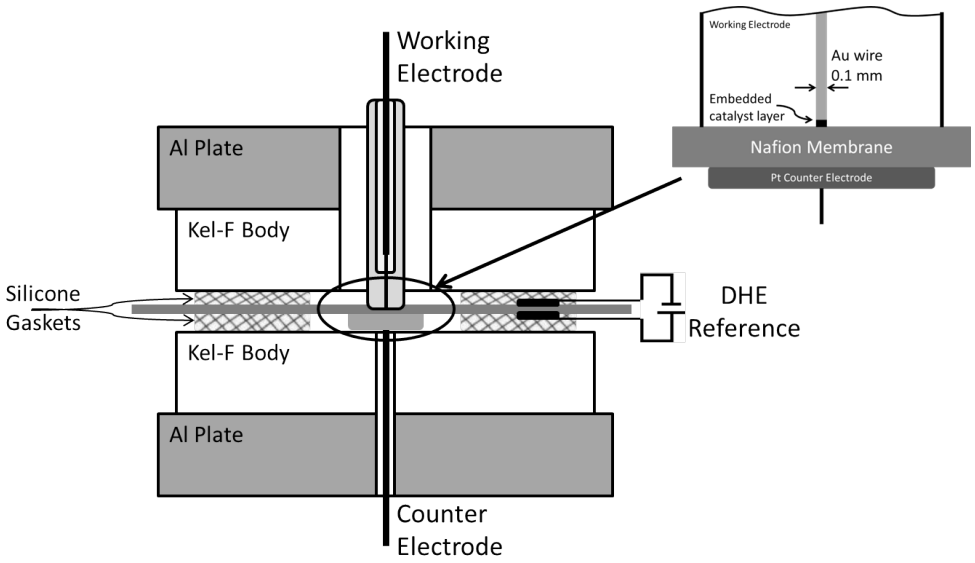

Figure 2.5: Schematic of a SPE cell for electrocatalyst stability characterization.

these experiments was -0.25 V vs SHE, which is the most oxidative of the potentials applied in the electrochemical hydrogenation experiments. The current density as a function of time was measured, and the stability of the catalyst was assessed by means of this current/time behavior (chronoamperometry) (Figure 2.6).

Some materials (e.g., Pt black) reached a steady-state current after an initial adjustment period, which was significantly different than the current from the blank Au microelectrode (Figure 2.6a). Other materials (e.g., Nano Fe) initially exhibited an anodic current, and then decayed to a current that is comparable to that of the blank microelectrode (Figure 2.6b). Using this method we directly characterized the electrochemical stabilities of the different catalyst materials. Catalysts that qualitatively retained their HER rates were concluded to be stable under the applied voltage. Catalysts that exhibited oxidative currents under the applied voltage or did not retain their HER rates were concluded to be unstable.

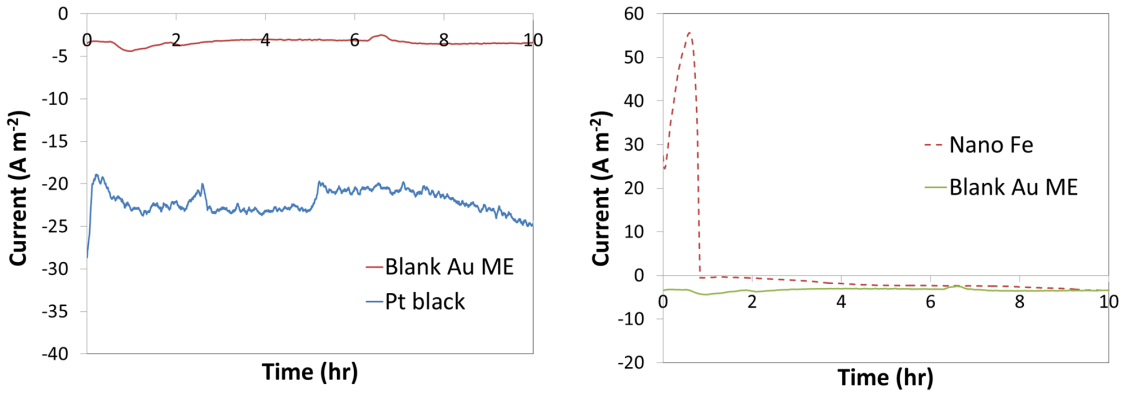

(a) Pt black stability

(b) Nano Fe stability

Figure 2.6: Chronoamperometry plots obtained for catalyst materials in SPE solid-state electrochemical cell at -0.25 V vs SHE and ∼20 °C.

2.5.2 Electrochemical Mechanism Characterization

The electrochemical mechanisms for the HER and the hydrogenation reaction were characterized over the various catalysts using a technique called linear sweep voltammetry (LSV). LSV is similar to CV, in that it involves the linear variation of the applied potential over a given potential range; but LSV differs from CV in that the potential is varied only in one direction and typically at a lower rate. Previous researchers have demonstrated that LSV can be used to determine the reaction mechanism for the HER in an electrochemical cell [22]. In this thesis, we describe the use of this method to determine the HER mechanism for noble metal, W_2C, and W_2C-supported Pd catalysts. We also extended this method to investigate the hydrogenation mechanisms for these catalysts.

LSV experiments were performed using a three-electrode cell with a liquid electrolyte (i.e. 0.5 M H_2SO_4 in H_2O for the HER or 0.5 M H_2SO_4 in 96% CH_3OH and H_2O for the hydrogenation reaction), along with a platinum wire counter electrode and a saturated mercury sulfate reference electrode (SMSE). All glassware used for electrochemical measurements was cleaned before use. The glassware was immersed in a solution of potassium permanganate (2 tsp L^{-1}) and concentrated sulfuric acid

(10 mL L^{-1}) overnight, and then rinsed with a solution of concentrated sulfuric acid (20 mL L^{-1}) and 30% hydrogen peroxide (20 mL L^{-1}) [23]. Finally, the glassware was rinsed with ultrapure H_2O (18 MΩ cm) and dried in an oven at 80 °C. Liquid electrolytes were likewise prepared using ultrapure H_2O and deaerated with pre-purified gases (i.e., N_2 or H_2) passed through a deoxygenating filter.

HER experiments were performed using a glassy carbon RDE. A small amount of catalyst suspended in isopropanol and ultrapure H_2O was pipetted onto the surface of the inverted RDE, which was rotated at 100 rpm. The liquid was allowed to dry for approximately 15 min. The catalyst was affixed to the RDE surface via a small aliquot (approximately 5 μL) of 5 wt% Nafion® perfluorinated resin solution (Sigma-Aldrich), which was pipetted onto the surface of the RDE and allowed to dry for another 15 min. Before LSV experiments were performed, the catalyst was electrochemically conditioned by performing CV between 0.0 V and 1.4 V vs SHE for 100 scans at 0.2 V s^{-1} [24, 25]. Catalysts were concluded to be conditioned when subsequent scans did not change.

Currents measured during LSV were normalized by the catalyst's electrochemical surface area, which was estimated by measuring the capacitance of the catalyst's electrochemical double layer. CVs were performed at several scan rates for each catalyst over a potential range that was free of adsorption events (e.g., 0.4 V to 0.5 V vs SHE in Figure 2.4). The difference in current between the forward and reverse passes over this potential range for each scan rate (in V s^{-1}) was calculated, and a plot of this difference vs scan rate was constructed. The slope of this plot has units of Farads, and corresponds to the capacitance of the catalyst's electrochemical double layer. The electrochemical surface area (cm^2) of the catalyst was estimated by dividing this capacitance by an estimated specific capacitance of 10 μF cm^{-2} [26].

2.5.2.1 HER Mechanism

A typical HER experiment consisted of suspending the electrode in an aqueous electrolyte (0.5 M H_2SO_4 in H_2O), and applying a linearly varying potential across the cell while measuring the resulting current. Using methods described in the literature, we analyzed this response to determine the rate determining step(s) for triglyceride hydrogenation over the different materials [22].

The HER is generally reported to occur via two elementary steps. The first step involves the reduction of a proton from the electrolyte to form an adsorbed hydrogen atom (the Volmer reaction). The second step may follow one of two reaction pathways. One of these (the Tafel reaction) involves the combination of two H_{ads} to form H_2. The second (the Heyrovský reaction) involves the combination of one H_{ads}, one H^+, and one H^- to form H_2.

$$H_{ads} + H^+ + e^- \rightleftharpoons H_2 \qquad \text{Heyrovský} \tag{2.8a}$$

$$2H_{ads} \rightleftharpoons H_2 \qquad \text{Tafel} \tag{2.8b}$$

$$H^+ + e^- \rightleftharpoons H_{ads} \qquad \text{Volmer} \tag{2.8c}$$

$$2H^+ + 2e^- \rightleftharpoons H_2 \qquad \text{Overall HER} \tag{2.8d}$$

The rates of these reaction steps are related to each other, because the mass balance for each participant in these elementary reactions (H_2, H^+, H_{ads}, e^-) must match the corresponding mass balance for the overall reaction. The reaction stoichiometry for the elementary and overall reactions can be expressed in matrix form. The rate of the overall reaction is the sum of the rates of the elementary steps multiplied by the stoichiometry of each step. This relationship is expressed in Equation 2.9, where r_i is the rate of reaction i.

$$
\begin{array}{cc} & \begin{array}{cccc} \mathrm{H^+} & \mathrm{e^-} & \mathrm{H}_{ads} & \mathrm{H_2} \end{array} \\ \begin{array}{c} \underline{\mathrm{H}} \\ \underline{\mathrm{T}} \\ \underline{\mathrm{V}} \\ \underline{\mathrm{HER}} \end{array} & \begin{bmatrix} \text{-1} & \text{-1} & \text{-1} & 1 \\ 0 & 0 & \text{-2} & 1 \\ \text{-1} & \text{-1} & 1 & 0 \\ \text{-1} & 0 & 2 & 0 \end{bmatrix} \end{array}
$$

$$
\underline{\mathrm{H}} r_{\mathrm{H}} + \underline{\mathrm{T}} r_{\mathrm{T}} + \underline{\mathrm{V}} r_{\mathrm{V}} = \underline{\mathrm{HER}} r_{\mathrm{HER}} \tag{2.9}
$$

We can express Equation 2.9 in terms of matrices, as well.

$$
\begin{array}{c} \\ \mathrm{H^+} \\ \mathrm{e^-} \\ \mathrm{H}_{ads} \\ \mathrm{H_2} \end{array}
\begin{bmatrix} -1 & 0 & -1 \\ -1 & 0 & -1 \\ -1 & -2 & 1 \\ 1 & 1 & 0 \end{bmatrix}
\begin{bmatrix} r_{\mathrm{H}} \\ r_{\mathrm{T}} \\ r_{\mathrm{V}} \end{bmatrix}
= \begin{bmatrix} -r_{\mathrm{H}} - r_{\mathrm{V}} \\ -r_{\mathrm{H}} - r_{\mathrm{V}} \\ -r_{\mathrm{H}} - 2r_{\mathrm{T}} + r_{\mathrm{V}} \\ r_{\mathrm{H}} + r_{\mathrm{T}} \end{bmatrix}
= \begin{bmatrix} -2 \\ -2 \\ 0 \\ 1 \end{bmatrix}
\begin{bmatrix} r_{\mathrm{HER}} \end{bmatrix}
$$

Using matrix multiplication, the following relationships can be calculated for each of the reaction participants.

$$
\begin{aligned}
\mathrm{H^+}: \quad & -r_{\mathrm{H}} - r_{\mathrm{V}} && = -2r_{\mathrm{HER}} \\
\mathrm{e^-}: \quad & -r_{\mathrm{H}} - r_{\mathrm{V}} && = -2r_{\mathrm{HER}} \\
\mathrm{H}_{ads}: \quad & -r_{\mathrm{H}} - 2r_{\mathrm{T}} + r_{\mathrm{V}} && = 0 \\
\mathrm{H_2}: \quad & r_{\mathrm{H}} + r_{\mathrm{T}} && = r_{\mathrm{HER}}
\end{aligned} \tag{2.10}
$$

It is convenient to rewrite these rates, which are mathematically equivalent, as current densities (since $i = nFr_k$, where n is the number of electrons, F is Faraday's constant, and r_K is the rate of reaction k).

$$\begin{aligned} i_{\mathrm{VH}}: &\quad 0.5(i_{\mathrm{V}} + i_{\mathrm{H}}) = i_{\mathrm{HER}} \\ i_{\mathrm{TH}}: &\quad i_{\mathrm{T}} + i_{\mathrm{H}} = i_{\mathrm{HER}} \\ i_{\mathrm{VT}}: &\quad i_{\mathrm{V}} - i_{\mathrm{T}} = i_{\mathrm{HER}} \end{aligned} \tag{2.11}$$

The reaction rate for each elementary step is the difference between the forward (i_+) and reverse (i_-) reaction rates for each elementary step.

$$i_{+H} = i_{\mathrm{H},0}\left(\frac{c^s_{\mathrm{H}_2}}{c^b_{\mathrm{H}_2}}\right)\left(\frac{1-\theta_{\mathrm{H}}}{1-\theta^e_{\mathrm{H}}}\right)\exp[\alpha f\eta] \tag{2.12a}$$

$$i_{-H} = i_{\mathrm{H},0}\left(\frac{c^s_{\mathrm{H}^+}}{c^b_{\mathrm{H}^+}}\right)\left(\frac{\theta_{\mathrm{H}}}{\theta_{\mathrm{H},0}}\right)\exp[-\alpha f\eta] \tag{2.12b}$$

$$i_{+T} = i_{\mathrm{T},0}\left(\frac{c^s_{\mathrm{H}_2}}{c^e_{\mathrm{H}_2}}\right)\left(\frac{1-\theta_{\mathrm{H}}}{1-\theta^e_{\mathrm{H}}}\right)^2 \tag{2.13a}$$

$$i_{-T} = i_{\mathrm{T},0}\left(\frac{\theta_{\mathrm{H}}}{\theta^e_{\mathrm{H}}}\right)^2 \tag{2.13b}$$

$$i_{+V} = i_{\mathrm{V},0}\left(\frac{\theta_{\mathrm{H}}}{\theta^{e}_{\mathrm{H}}}\right)\exp[\alpha f\eta] \tag{2.14a}$$

$$i_{-V} = i_{\mathrm{V},0}\left(\frac{c^{s}_{\mathrm{H}^+}}{c^{b}_{\mathrm{H}^+}}\right)\left(\frac{1-\theta_{\mathrm{H}}}{1-\theta^{e}_{\mathrm{H}}}\right)\exp[-\alpha f\eta] \tag{2.14b}$$

where $i_{\mathrm{V},0}$, $i_{\mathrm{T},0}$, $i_{\mathrm{H},0}$ are the exchange current densities for the Volmer, Tafel, and Heyrovský steps, respectively; θ_{H} and θ^{e}_{H} are the H surface coverage and the H surface coverage at equilibrium, respectively; $\mathrm{c}^{s}_{\mathrm{H}_2}$ and $\mathrm{c}^{b}_{\mathrm{H}_2}$ are the concentrations of H_2 dissolved in the electrolyte at the catalyst surface and in the bulk electrolyte, respectively; and $\mathrm{c}^{s}_{\mathrm{H}^+}$ and $\mathrm{c}^{b}_{\mathrm{H}^+}$ are the concentrations of H^+ in the electrolyte at the catalyst surface and in the bulk electrolyte, respectively.

Under reaction conditions, the concentration of a reactant at the catalyst surface may become depleted with respect to the concentration in the bulk, especially if the reactant is poorly soluble in the electrolyte. For the purposes of this analysis, the surface and bulk proton concentrations ($\mathrm{c}^{s}_{\mathrm{H}^+}$ and $\mathrm{c}^{b}_{\mathrm{H}^+}$) are assumed to be equal, since the electrolyte is highly acidic. The concentration of H_2 at the surface, however, is likely to be depleted, since H_2 is poorly soluble in the electrolyte.

The mass transfer of H_2 from the bulk to the surface can be described by the Nernst-Planck equation (2.15a), which indicates that the rate of H_2 diffusion to the electrode surface (ν_{H_2}) is proportional to the H_2 concentration gradient at the electrode. Assuming a linear concentration gradient from the bulk to the surface across a stagnation layer of thickness δ, the Nernst-Planck equation can be simplified to the following form(2.15b).

$$\nu_{H_2} = -D_{H_2}\frac{dC_{H_2}}{dx} \tag{2.15a}$$

$$\nu_{H_2} = -D_{H_2}\frac{C^b_{H_2} - C^s_{H_2}}{\delta} \tag{2.15b}$$

$$\frac{i}{nF} = -D_{H_2}\frac{C^b_{H_2} - C^s_{H_2}}{\delta} \tag{2.15c}$$

At steady-state, the transfer of H_2 to the electrode surface can be related to the observed current densities via the expression $\nu_{H_2} = \frac{i}{nF}$, where n is the number of electrons and F is Faraday's constant (Equation 2.15c). A limiting current densitiy (i_L) is reached when the concentration of H_2 at the surface ($C^s_{H_2}$) goes to zero.

$$i_L = -nFC^b_{H_2}\frac{D_{H_2}}{\delta} \tag{2.16}$$

This equation can be combined with Equation 2.15c to yield an expression relating the concentration of protons at the surface to that in the bulk electrolyte.

$$\frac{C^s_{H_2}}{C^b_{H_2}} = 1 - \frac{i}{i_L} \tag{2.17}$$

For a RDE, the limiting current is described by the Koutecky-Levich equation (2.18), where D_{H_2} is the diffusion rate of H_2, ω is the rotation rate, ν is the kinematic viscosity, and i_K is the kinetic current density [19]. The kinetic current density is that which would flow if there were no mass-transfer limitations in the system ($C^s_{H_2} = C^b_{H_2}$).

$$\frac{1}{i} = \frac{1}{i_K} + \frac{1}{i_L} = \frac{1}{i_K} + \frac{1}{0.62nFAD^{2/3}_{H_2}\omega^{1/2}\nu^{-1/6}C^b_{H_2}} \tag{2.18}$$

Three new mathematically equivalent descriptions of the HER current can be formed by combining Equations 2.11, 2.12, 2.13, 2.14, and 2.17.

$$i_{\mathrm{VH}} = \frac{i_{\mathrm{V},0}\left[\left(\frac{\theta_{\mathrm{H}}}{\theta^e_{\mathrm{H}}}\right)e^{\alpha f\eta} - \left(\frac{1-\theta_{\mathrm{H}}}{1-\theta^e_{\mathrm{H}}}\right)e^{-\alpha f\eta}\right] + i_{\mathrm{H},0}\left[\left(\frac{1-\theta_{\mathrm{H}}}{1-\theta^e_{\mathrm{H}}}\right)e^{\alpha f\eta} - \left(\frac{\theta_{\mathrm{H}}}{\theta^e_{\mathrm{H}}}\right)e^{-\alpha f\eta}\right]}{\frac{1}{F} + \frac{i_{\mathrm{H},0}}{j_L}\left(\frac{1-\theta_{\mathrm{H}}}{1-\theta^e_{\mathrm{H}}}\right)e^{\alpha f\eta}} \tag{2.19a}$$

$$i_{\mathrm{TH}} = \frac{i_{\mathrm{T},0}\left[\left(\frac{1-\theta_{\mathrm{H}}}{1-\theta^e_{\mathrm{H}}}\right)^2 - \left(\frac{\theta_{\mathrm{H}}}{\theta^e_{\mathrm{H}}}\right)^2\right] + i_{\mathrm{H},0}\left[\left(\frac{1-\theta_{\mathrm{H}}}{1-\theta^e_{\mathrm{H}}}\right)e^{\alpha f\eta} - \left(\frac{\theta_{\mathrm{H}}}{\theta^e_{\mathrm{H}}}\right)e^{-\alpha f\eta}\right]}{\frac{1}{2F} + \frac{i_{\mathrm{T},0}}{j_L}\left(\frac{1-\theta_{\mathrm{H}}}{1-\theta^e_{\mathrm{H}}}\right)^2 + \frac{i_{\mathrm{H},0}}{j_L}\left(\frac{1-\theta_{\mathrm{H}}}{1-\theta^e_{\mathrm{H}}}\right)e^{\alpha f\eta}} \tag{2.19b}$$

$$i_{\mathrm{VT}} = \frac{i_{\mathrm{V},0}\left[\left(\frac{\theta_{\mathrm{H}}}{\theta^e_{\mathrm{H}}}\right)e^{\alpha f\eta} - \left(\frac{1-\theta_{\mathrm{H}}}{1-\theta^e_{\mathrm{H}}}\right)e^{-\alpha f\eta}\right] - i_{\mathrm{T},0}\left[\left(\frac{1-\theta_{\mathrm{H}}}{1-\theta^e_{\mathrm{H}}}\right)^2 - \left(\frac{\theta_{\mathrm{H}}}{\theta^e_{\mathrm{H}}}\right)^2\right]}{\frac{1}{2F} - \frac{i_{\mathrm{T},0}}{j_L}\left(\frac{1-\theta_{\mathrm{H}}}{1-\theta^e_{\mathrm{H}}}\right)^2} \tag{2.19c}$$

Finally, in order to calculate current as a function of potential (Equation 2.21), it is necessary to determine the hydrogen coverage as a function of potential. We evaluated this coverage-potential dependence (Equation 2.22) by taking the difference of any two of these three equations (2.19a, 2.19b, and 2.19c) and set it equal to zero. For example, taking the equations for the VH and VT expressions:

$$\frac{i_{\mathrm{V},0}\left[\left(\frac{\theta_{\mathrm{H}}}{\theta^e_{\mathrm{H}}}\right)e^{\alpha f\eta} - \left(\frac{1-\theta_{\mathrm{H}}}{1-\theta^e_{\mathrm{H}}}\right)e^{-\alpha f\eta}\right] + i_{\mathrm{H},0}\left[\left(\frac{1-\theta_{\mathrm{H}}}{1-\theta^e_{\mathrm{H}}}\right)e^{\alpha f\eta} - \left(\frac{\theta_{\mathrm{H}}}{\theta^e_{\mathrm{H}}}\right)e^{-\alpha f\eta}\right]}{\frac{1}{F} + \frac{i_{\mathrm{H},0}}{j_L}\left(\frac{1-\theta_{\mathrm{H}}}{1-\theta^e_{\mathrm{H}}}\right)e^{\alpha f\eta}} - \frac{i_{\mathrm{V},0}\left[\left(\frac{\theta_{\mathrm{H}}}{\theta^e_{\mathrm{H}}}\right)e^{\alpha f\eta} - \left(\frac{1-\theta_{\mathrm{H}}}{1-\theta^e_{\mathrm{H}}}\right)e^{-\alpha f\eta}\right] - i_{\mathrm{T},0}\left[\left(\frac{1-\theta_{\mathrm{H}}}{1-\theta^e_{\mathrm{H}}}\right)^2 - \left(\frac{\theta_{\mathrm{H}}}{\theta^e_{\mathrm{H}}}\right)^2\right]}{\frac{1}{2F} - \frac{i_{\mathrm{T},0}}{j_L}\left(\frac{1-\theta_{\mathrm{H}}}{1-\theta^e_{\mathrm{H}}}\right)^2} = 0 \tag{2.20}$$

The process of fitting this model to a data set is iterative (Figure 2.7), since evaluating the dependence of the current on the potential (Equation 2.21) requires knowing the dependence of the coverage on the potential (Equation 2.22).

$$j = j(\eta, \theta^e, i_{\mathrm{H},0}, i_{\mathrm{T},0}, i_{\mathrm{V},0}) \tag{2.21}$$

$$\theta = \theta(\eta, \theta^e, i_{\mathrm{H},0}, i_{\mathrm{T},0}, i_{\mathrm{V},0}) \tag{2.22}$$

The fitting algorithm involves the input of an initial guess for the adjustable pa-

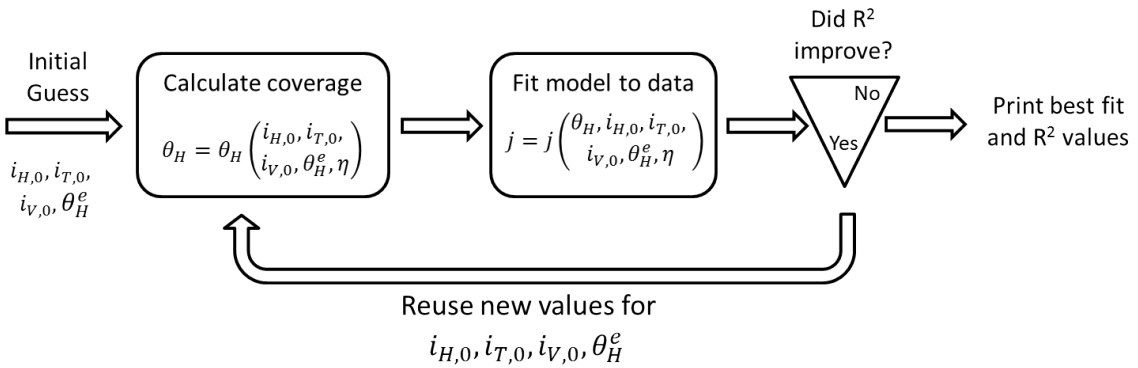

Figure 2.7: Protocol for fitting the Volmer-Heyrovský-Tafel model to LSV data for hydrogen evolution reaction. This scheme fits the VHT model by iteratively calculating j=j(η) and $\theta = \theta(\eta)$ (Equations 2.21 and 2.22) until the data and model converge.

rameters, and solving Equation 2.20 to get an expression for $\theta = \theta(\eta)$. Using this expression along with the initial guess, the model is fit to the data set using nonlinear regression and allowing the adjustable parameters to vary. These new values provide the input for determining the expression for $\theta = \theta(\eta)$. This process is repeated until the fit from the nonlinear regression ceases to improve during each successive iteration.

2.5.2.2 Hydrogenation Reaction Mechanism

During operation of the SPE hydrogenation reactor, both the HER and triglyceride hydrogenation reactions occur on the surface of the cathode catalyst. By extending the strategy employed in the previous section, previous researchers have demonstrated that it is possible to determine which mechanisms are prevalent for each of these reactions [27]. A typical hydrogenation reaction experiment consisted of suspending the electrode in the aqueous electrolyte (0.5 M H_2SO_4 in 96% CH_3OH and H_2O), and applying a linearly varying potential across the cell while measuring the resulting current. Methyl linoleate, which is the methyl ester of the 18 carbon glyceride containing two double bonds, was used as a surrogate for the triglyceride. In soybean oil, over 50% of the glycerides have two double bonds, so ML is a reasonable

approximation for esters from the triglyceride. The concentration of ML was varied over subsequent LSVs between 0 M and 3.86 x 10^{-3} M and the effect of ML on the current-voltage curve was measured. CH_3OH was added to the electrolyte to make it miscible with ML.

In addition to the equations from the previous section, two additional equations describe the adsorption and reaction of organics (e.g., methyl linoleate (ML)) on the surface of the catalyst. The surface coverage of ML is related to its bulk concentration in solution via a Langmuir adsorption isotherm:

$$\frac{\theta_{\mathrm{ML}}}{1-\theta_{\mathrm{ML}}} = \Gamma_{\mathrm{ML}} C_{\mathrm{ML}} \qquad \text{Langmuir Isotherm} \tag{2.23}$$

Previous researchers have proposed that, in an electrochemical cell, the rate determining step for hydrogenation can be either thermochemical (Equation 2.24a) or electrochemical (Equation 2.24b) [28, 29], where k_{Hyd} is the reaction rate constant, θ_{ML} is the surface coverage of ML, θ_{H} is the surface coverage of hydrogen, a and b are the reaction rate orders for the organic and hydrogen, respectively, α is the symmetry factor, f is the ratio of Faraday's constant to the ideal gas constant and temperature, and η is the overpotential.

$$r_{\mathrm{Hyd}} = k_{\mathrm{Hyd}} \theta_{\mathrm{ML}}^{a} \theta_{\mathrm{H}}^{b} \tag{2.24a}$$

$$r_{\mathrm{Hyd}} = k_{\mathrm{Hyd}} \theta_{\mathrm{ML}}^{a} \theta_{\mathrm{H}}^{b} \exp(\alpha f \eta) \tag{2.24b}$$

These expressions are used to modify the equations from the previous section to account for the effect of ML on curve from LSV.

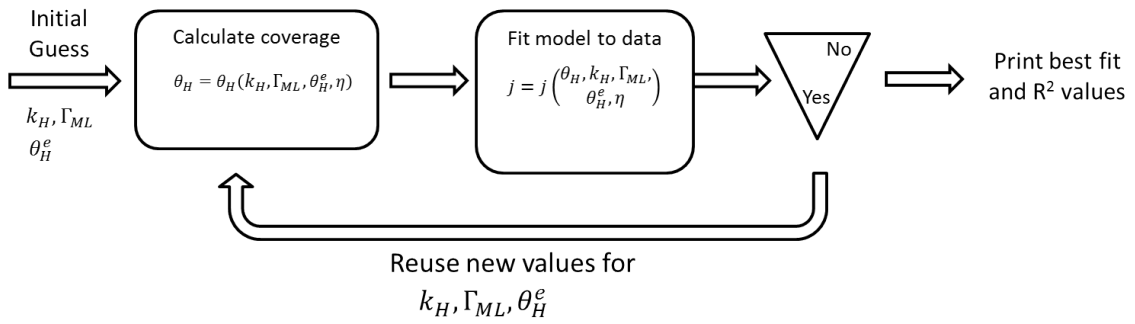

Figure 2.8: Protocol for fitting the Volmer-Heyrovský-Tafel hydrogenation model to LSV data for the hydrogen evolution and hydrogenation reactions. This scheme fits the VHT model by iteratively calculating j=j(η) and $\theta = \theta(\eta)$ (Equations 2.21 and 2.22) until the data and model converge.

$$i_{\mathrm{VH}} = \frac{i_{\mathrm{V},0}\left[\left(\frac{\theta_{\mathrm{H}}}{\theta_{\mathrm{H}}^e}\right)e^{\alpha f\eta} - \left(\frac{1-\theta_{\mathrm{H}}^e-\theta_{ML}}{1-\theta^e}\right)e^{-\alpha f\eta}\right] + i_{\mathrm{H},0}\left[\left(\frac{1-\theta_{\mathrm{H}}^e-\theta_{ML}}{1-\theta^e}\right)e^{\alpha f\eta} - \left(\frac{\theta_{\mathrm{H}}}{\theta_{\mathrm{H}}^e}\right)e^{-\alpha f\eta}\right]}{\frac{1}{F} + \frac{i_{\mathrm{H},0}}{j_L}\left(\frac{1-\theta_{\mathrm{H}}^e-\theta_{ML}}{1-\theta^e}\right)e^{\alpha f\eta}} - Fr_{Hyd} \tag{2.25a}$$

$$i_{\mathrm{TH}} = \frac{i_{\mathrm{T},0}\left[\left(\frac{1-\theta_{\mathrm{H}}^e-\theta_{ML}}{1-\theta^e}\right)^2 - \left(\frac{\theta_{\mathrm{H}}}{\theta_{\mathrm{H}}^e}\right)^2\right] + i_{\mathrm{H},0}\left[\left(\frac{1-\theta_{\mathrm{H}}^e-\theta_{ML}}{1-\theta^e}\right)e^{\alpha f\eta} - \left(\frac{\theta_{\mathrm{H}}}{\theta_{\mathrm{H}}^e}\right)e^{-\alpha f\eta}\right]}{\frac{1}{2F} + \frac{i_{\mathrm{T},0}}{j_L}\left(\frac{1-\theta_{\mathrm{H}}^e-\theta_{ML}}{1-\theta^e}\right)^2 + \frac{i_{\mathrm{H},0}}{j_L}\left(\frac{1-\theta_{\mathrm{H}}^e-\theta_{ML}}{1-\theta^e}\right)e^{\alpha f\eta}} - Fr_{Hyd} \tag{2.25b}$$

$$i_{\mathrm{VT}} = \frac{i_{\mathrm{V},0}\left[\left(\frac{\theta_{\mathrm{H}}}{\theta_{\mathrm{H}}^e}\right)e^{\alpha f\eta} - \left(\frac{1-\theta_{\mathrm{H}}^e-\theta_{ML}}{1-\theta^e}\right)e^{-\alpha f\eta}\right] - i_{\mathrm{T},0}\left[\left(\frac{1-\theta_{\mathrm{H}}^e-\theta_{ML}}{1-\theta^e}\right)^2 - \left(\frac{\theta_{\mathrm{H}}}{\theta_{\mathrm{H}}^e}\right)^2\right]}{\frac{1}{2F} - \frac{i_{\mathrm{T},0}}{j_L}\left(\frac{1-\theta_{\mathrm{H}}^e-\theta_{ML}}{1-\theta^e}\right)^2} - Fr_{Hyd} \tag{2.25c}$$

$$\begin{aligned}&\frac{i_{\mathrm{V},0}\left[\left(\frac{\theta_{\mathrm{H}}}{\theta_{\mathrm{H}}^e}\right)e^{\alpha f\eta} - \left(\frac{1-\theta_{\mathrm{H}}^e-\theta_{ML}}{1-\theta^e}\right)e^{-\alpha f\eta}\right] + i_{\mathrm{H},0}\left[\left(\frac{1-\theta_{\mathrm{H}}^e-\theta_{ML}}{1-\theta^e}\right)e^{\alpha f\eta} - \left(\frac{\theta_{\mathrm{H}}}{\theta_{\mathrm{H}}^e}\right)e^{-\alpha f\eta}\right]}{\frac{1}{F} + \frac{i_{\mathrm{H},0}}{j_L}\left(\frac{1-\theta_{\mathrm{H}}^e-\theta_{ML}}{1-\theta^e}\right)e^{\alpha f\eta}} \\ &- \frac{i_{\mathrm{V},0}\left[\left(\frac{\theta_{\mathrm{H}}}{\theta_{\mathrm{H}}^e}\right)e^{\alpha f\eta} - \left(\frac{1-\theta_{\mathrm{H}}^e-\theta_{ML}}{1-\theta^e}\right)e^{-\alpha f\eta}\right] - i_{\mathrm{T},0}\left[\left(\frac{1-\theta_{\mathrm{H}}^e-\theta_{ML}}{1-\theta^e}\right)^2 - \left(\frac{\theta_{\mathrm{H}}}{\theta_{\mathrm{H}}^e}\right)^2\right]}{\frac{1}{2F} - \frac{i_{\mathrm{T},0}}{j_L}\left(\frac{1-\theta_{\mathrm{H}}^e-\theta_{ML}}{1-\theta^e}\right)^2} = 0\end{aligned} \tag{2.26}$$

The process of fitting this new model to the data is iterative as well, but follows a slightly different procedure (Figure 2.8). First, the model is fit to the data for

the solution without ML (same procedure as Figure 2.7); this current-voltage data only involves the HER, so the two new parameters (Γ_{ML} and k_{Hyd}) do not apply. For subsequent data sets that involve increasing concentrations of ML, the exchange current densities for the three elementary steps ($v_{H,0}$, $v_{T,0}$, and $v_{V,0}$) are held constant. Only the equilibrium surface coverage (θ^e), and the hydrogenation parameters (Γ_{ML} and k_{Hyd}) are varied during nonlinear regression. The form of the rate expression assumed to be correct is the one that provides the best fit for the data over the whole range of potentials and ML concentrations.

References

[1] L. Volpe and M. Boudart. Compounds of molybdenum and tungsten with high specific surface area:: II. Carbides. *Journal of Solid State Chemistry*, 59(3):348–356, 1985.

[2] J.S. Lee, S.T. Oyama, and M. Boudart. Molybdenum carbide catalysts:: I. Synthesis of unsupported powders. *Journal of Catalysis*, 106(1):125–133, 1987.

[3] G.C. Bond, G. Webb, S.T. Oyama, and G.L. Haller. *The catalytic hydrogenation of organic compounds–a comparison between the gas–phase, liquid–phase, and electrochemical routes*, pages 333–365. RSC Publishing, 1982.

[4] J. Patt, D.J. Moon, C. Phillips, and L. Thompson. Molybdenum carbide catalysts for water–gas shift. *Catalysis Letters*, 65(4):193–195, 2000.

[5] S.T. Oyama and D.F. Cox. New catalysts for coal processing: Metal carbides and nitrides. Technical report, Federal Energy Technology Center, Morgantown, WV (US); Federal Energy Technology Center, Pittsburgh, PA (US), 1999.

[6] J.J. Patt. *Carbide and nitride catalysts for the water gas shift reaction*. PhD thesis, University of Michigan, 2003.

[7] W. Setthapun. *Carbide and nitride supported methanol steam reforming catalysts*. PhD thesis, University of Michigan, 2007.

[8] W. Setthapun, S.K. Bej, and L.T. Thompson. Carbide and Nitride Supported Methanol Steam Reforming Catalysts: Parallel Synthesis and High Throughput Screening. *Topics in Catalysis*, 49(1):73–80, 2008.

[9] N.M. Schweitzer, J.A. Schaidle, O.K. Ezekoye, X. Pan, S. Linic, and L.T. Thompson. High Activity Carbide Supported Catalysts for Water Gas Shift. *Journal of the American Chemical Society*, 2011.

[10] B.D. Cullity and S.R. Stock. *Elements of X-ray Diffraction*, volume 2. Addison-Wesley Reading, MA, 1978.

[11] P. Scherrer. Bestimmung der Grosse und der inneren Struktur von Kolloidteilchen mittels Rontgenstrahlen. *Gottinger Nachrichten,(2)*, pages 98–100, 1918.

[12] S. Brunauer, P.H. Emmett, and E. Teller. Adsorption of Gases in Multimolecular Layers. *Journal of the American Chemical Society*, 60(2):309–319, 1938.

[13] P.H. Emmett and S. Brunauer. The use of low temperature van der Waals adsorption isotherms in determining the surface area of iron synthetic ammonia catalysts. *Journal of the American Chemical Society*, 59(8):1553–1564, 1937.

[14] M. Archer, R.I. McCrindle, and E.R. Rohwer. Analysis of cobalt, tantalum, titanium, vanadium and chromium in tungsten carbide by inductively coupled plasma-optical emission spectrometry. *Journal of Analytical Atomic Spectrometry*, 18(12):1493–1496, 2003.

[15] J.M. Mermet. Is it still possible, necessary and beneficial to perform research in ICP-atomic emission spectrometry? *Journal of Analytical Atomic Spectrometry*, 20(1):11–16, 2005.

[16] B. Liu and S. Creager. Carbon xerogels as pt catalyst supports for polymer electrolyte membrane fuel-cell applications. *Journal of Power Sources*, 195(7):1812–1820, 2010.

[17] M.S. Mamat, S.A. Grigoriev, K.A. Dzhus, D.M. Grant, and G.S. Walker. The performance and degradation of pt electrocatalysts on novel carbon carriers for pemfc applications. *International Journal of Hydrogen Energy*, 35(14):7580–7587, 2010.

[18] E.A. Ticianelli, C.R. Derouin, A. Redondo, and S. Srinivasan. Methods to advance technology of proton exchange membrane fuel cells. *Journal of the Electrochemical Society*, 135:2209, 1988.

[19] A.J. Bard and L.R. Faulkner. *Electrochemical methods: fundamentals and applications*. A1bazaar, 2006.

[20] H. Angerstein-Kozlowska, B.E. Conway, and W.B.A. Sharp. The real condition of electrochemically oxidized platinum surfaces: Part I. Resolution of component processes. *Journal of Electroanalytical Chemistry*, 43(1):9–36, 1973.

[21] J. Jiang and A. Kucernak. Investigations of fuel cell reactions at the composite microelectrode— solid polymer electrolyte interface. I. Hydrogen oxidation at the nanostructured Pt Nafion membrane interface. *Journal of Electroanalytical Chemistry*, 567(1):123–137, 2004.

[22] P.M. Quaino, M.R. Gennero de Chialvo, and A.C. Chialvo. Hydrogen Electrode Reaction: A Complete Kinetic Description. *Electrochimica Acta*, 52(25):7396–7403, 2007.

[23] A.E.S. Sleightholme. *Electrochemical Studies of Fuel Cell Catalysts*. PhD thesis, Imperial College London, 2006.

[24] A. Bonakdarpour, R. Löbel, S. Sheng, T.L. Monchesky, and J.R. Dahn. Acid stability and oxygen reduction activity of magnetron-sputtered ptta ($0 \leq x \leq 1$) films. *Journal of the Electrochemical Society*, 153:A2304, 2006.

[25] G.C.K. Liu, D.A. Stevens, J.C. Burns, R.J. Sanderson, G. Vernstrom, R.T. Atanasoski, M.K. Debe, and J.R. Dahn. Oxygen reduction activity of dealloyed pt(1-x)ni(x) catalysts. *Journal of the Electrochemical Society*, 158:B919–B926, 2011.

[26] B.E. Conway. Electrochemical capacitors: Their nature, function, and applications. *Electrochemistry Encyclopedia*, 2003.

[27] V. Anantharaman and P.N. Pintauro. The Electrocatalytic Hydrogenation of Glucose. *Journal of the Electrochemical Society*, 141:2729, 1994.

[28] C. Wagner. Considerations on the mechanism of the hydrogenation of organic compounds in aqueous solutions on noble metal catalysts. *Electrochimica Acta*, 15(6):987–997, 1970.

[29] Z. Takehara. Hydrogenation of some organic compounds in acidic aqueous solutions on noble metal catalysts. *Electrochimica Acta*, 15(6):999–1012, 1970.

CHAPTER III

Electrocatalyst Stabilities in a SPE Reactor

3.1 Introduction

The catalytically active portion of the SPE reactor is the MEA, which consists of catalyst layers, GDLs, and a Nafion® 117 SPE. Liquid catalyst suspensions, consisting of catalyst, isopropanol, H_2O, and a Nafion® resin, were applied to the GDLs using a hand painting technique that involves repeated applications, drying, and weighing to attain a specified weight loading. After a final drying of the painted GDL to remove the suspension solvents, the prepared GDLs are hot-pressed into the SPE.

While the catalyst loading is known before the reaction, the different electrochemical stabilities of the catalyst materials in the context of the acidic Nafion® membrane may reduce catalyst loading during reactor operation. In this chapter, the stabilities of noble metal, base metal, carbide, and carbide-supported metal catalysts were characterized using two methods. First, we fabricated MEAs with noble metal, base metal, carbide, and carbide-supported Pd catalysts and used them in a SPE reactor. We determined the post-reaction catalyst weights of the MEAs using TGA to ascertain any differences between the pre- and post-reaction loadings. Second, we used in-situ chronopotentiometry measurements in a Nafion®-based solid-state cell under conditions similar to those in the SPE cell, to measure the electrochemical

stabilities of the catalysts.

3.2 Experimental

3.2.1 Thermogravimetric Analysis

A TA Instruments SDT Q600 TGA was used to characterize the post-reaction catalyst loadings of the SPE reactor MEAs. The TGA temperature was increased at 40 °C min^{-1} to 800 °C, and held there for 5 min [1, 2], while 0.05 L min^{-1} of 100% O_2 gas was flowed through the TGA to provide an oxidizing atmosphere. Changes in the MEA weight were measured as a function of time and temperature. The final weight of the remaining catalyst material was recorded using the TA Instruments Universal Analysis 2000 v. 4.3A software. Each catalyst was tested twice, and the MEA catalyst content was reported as the average of those two replicates.

3.2.2 Chronoamperometry in Solid Polymer Electrolyte Cell

Direct electrocatalyst stability measurements were performed with a SPE three-electrode cell, which was similar in construction to that used for triglyceride hydrogenation reactions (Figure 2.5) [3]. The cell consisted of a Nafion® membrane sandwiched between two Kel-F plates. A gold microelectrode was used as the working electrode with the electrocatalysts being physically abraded into the embedded gold metal wire. A 1 cm^2 platinum flag was used as the counter electrode, and a DHE, consisting of two 1 cm^2 platinum flags, was used as the reference electrode. A potential of -0.25 V vs SHE was applied and the corresponding current was measured for up to 10 hr, in order to simulate the potential of the SPE-hydrogenation reactor during operation.

3.3 Results and Discussion

3.3.1 Thermogravimetric Analysis of Spent MEAs

After measuring the triglyceride hydrogenation activities and selectivities of the different catalyst materials in the SPE reactor, the MEAs were tested to determine their post-reaction catalyst contents. Figure 3.1 shows the TGA of Pt black and Nano Fe MEAs, which illustrates oxidation of the Nafion® membrane and carbon GDL supporting material as a function of time. The difference in initial weights was due to differing amounts of residual soybean oil in the MEA from reactor operation, which was combusted along with the SPE and GDL materials. The Pt black MEA had a final weight loading of 2.0 ± 0.1 mg cm^{-2}, while the Nano Fe MEA had a final loading of 1.0 ± 0.1 mg cm^{-2}. Presumably the remaining material from the Nano Fe MEA is the 1 mg cm^{-2} Pt from the anode, while the Pt black MEA retained both the 1 mg cm^{-2} from the anode as well as the 1 mg cm^{-2} from the cathode. The GDL and SPE materials were tested separately using TGA; they completely combusted and did not have any residual weight.

The final weight loadings of the noble metal, base metal, carbide and carbide-supported metal catalysts are listed in Table 3.1. The noble metal catalysts and some of the base metal catalysts (i.e. Nano Ag and Nano Cu) have weight loadings close to the initial value of 2.0 mg cm^{-2}, which suggests that they were stable. The rest of the base metal catalysts had loadings close to 1.0 mg cm^{-2}, which indicates that they were not stable (i.e., formed products that were removed from the MEA). The carbide and carbide-supported metal catalysts have loadings between 1 and 2 mg cm^{-2}, so it is unclear from the TGA results whether they were stable [4].

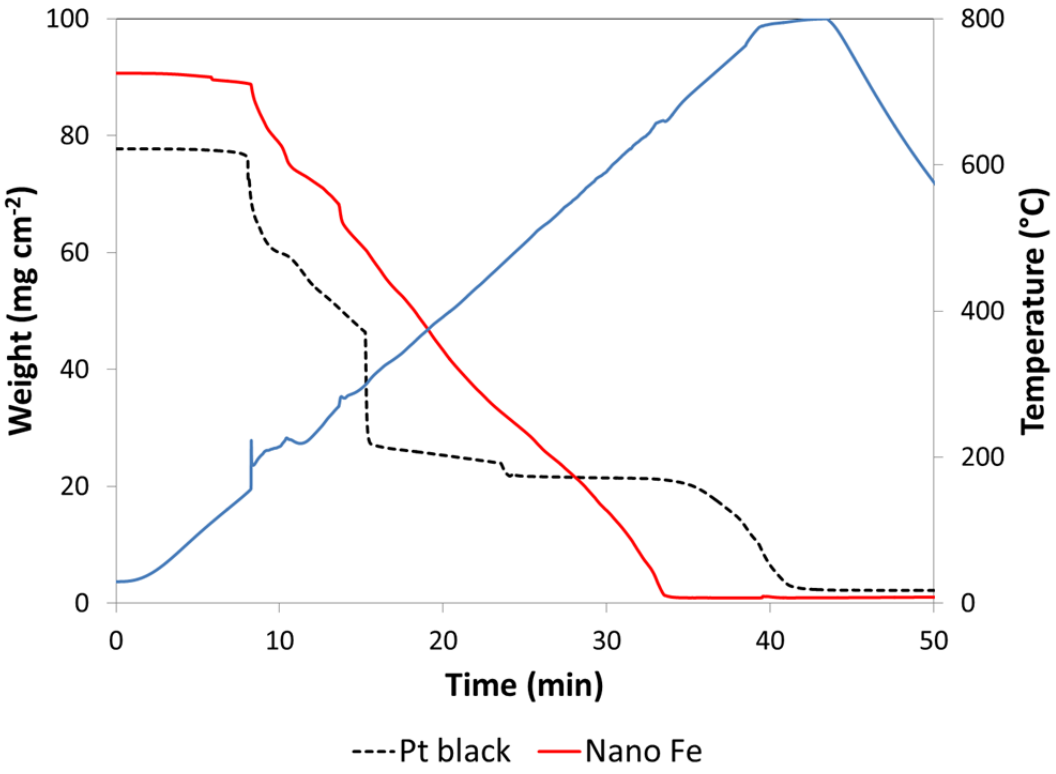

Figure 3.1: Thermogravimetric oxidation of post-reaction Pt black and Nano Fe MEAs in 0.05 L min^{-1} of 100% O_2 ramped at 40 °C min^{-1} to 800 °C.

Table 3.1: Noble metal, base metal, carbide and W_2C-supported Pd catalyst post-reaction MEA loadings and predicted stabilities from Pourbaix diagrams.

Catalyst	Post-TGA Weight (mg cm^{-2})	Predicted Stabilities[a]
Pt black	2.0 ± 0.1	Stable
Rh black	1.6 ± 0.2	Stable
Ru black	1.8 ± 0.1	Stable
Ir black	1.7 ± 0.1	Stable
Nano Pd	2.3 ± 0.2	Stable
Nano Fe	1.0 ± 0.1	Unstable
Nano Cu	1.4 ± 0.1	Stable
Nano Co	1.19 ± 0.1	Unstable
Nano Ni	0.92 ± 0.09	Unstable
Nano Ag	1.4 ± 0.1	Stable
VC	1.7 ± 0.1	Unstable
Mo_2C	1.8 ± 0.1	Unstable
NbC	1.3 ± 0.1	Unstable
W_2C	1.73 ± 0.04	Unstable
3% Pd/W_2C	1.82 ± 0.04	Stable
6% Pd/W_2C	1.7 ± 0.4	Stable

[a]Stabilities as predicted from the Pourbaix diagram at pH = 0 and E = -0.25 V. [5]

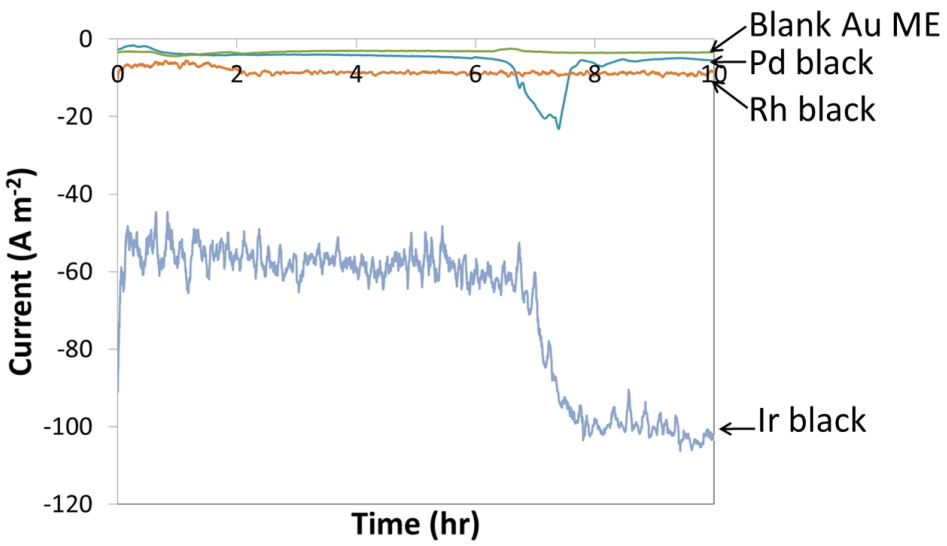

Figure 3.2: Chronoamperometry stability measurements of Pd, Rh, and Ir catalysts in a SPE-cell at -0.25 V vs SHE.

3.3.2 Electrochemical Stability Measurements

The noble metal, base metal, carbide, and carbide-supported metal catalyst stabilities were directly characterized in a SPE-type three-electrode cell. In Figure 3.2, the measured currents for HER for the noble metal catalysts are shown over a 10 h period at -0.25 V vs SHE. These materials exhibited HER currents that were relatively stable. The variations in current that many of the catalysts initially exhibited was likely due to oxidation of surface impurities, since the catalysts were not electrochemically cleaned. Typically catalysts were cycled at high scan rate (e.g., 0.2 to 0.5 V s^{-1}) for up to 100 scans, in order to remove any adsorbed species [6, 7]. Thus the catalyst activities had temporary excursions from their long-term stable current due to this surface oxidation. The currents for certain base metal (Cu and Ag) catalysts (W_2C and 6% Pd/W_2C) are shown in Figure 3.4, which were also stable over the 10 hr measurements.

Other base metals (e.g., Fe, Co, and Ni) and carbide catalysts (e.g., VC, NbC, and Mo_2C) exhibited some evidence of corrosion or electrochemical transformation. The base metals initially had anodic (positive) currents over a period of a few hours, and

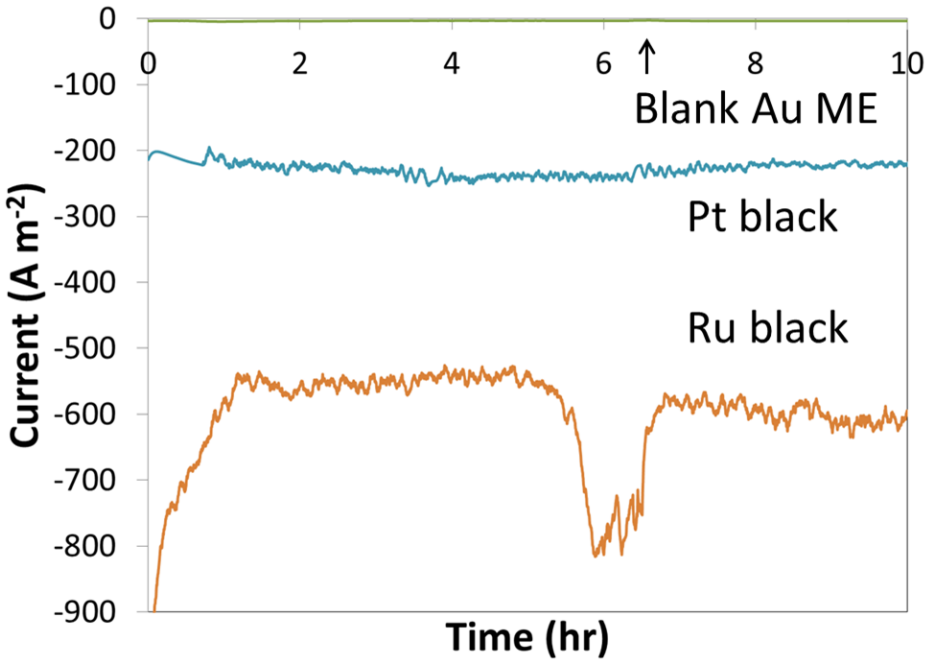

Figure 3.3: Chronoamperometry stability measurements of Pt and Ru catalysts in a SPE-cell at -0.25 V vs SHE.

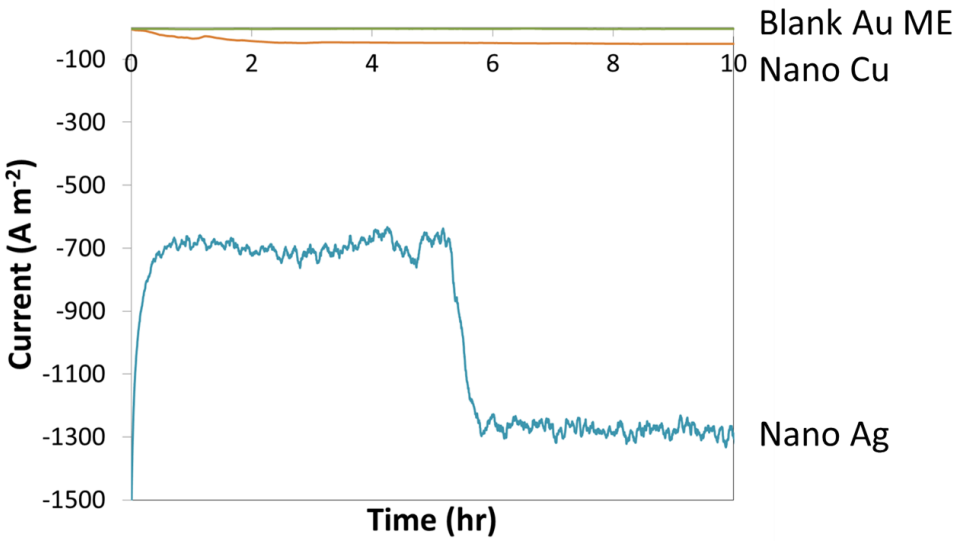

Figure 3.4: Chronoamperometry stability measurements of Cu and Ag base metal catalysts in a SPE-cell at -0.25 V vs SHE.

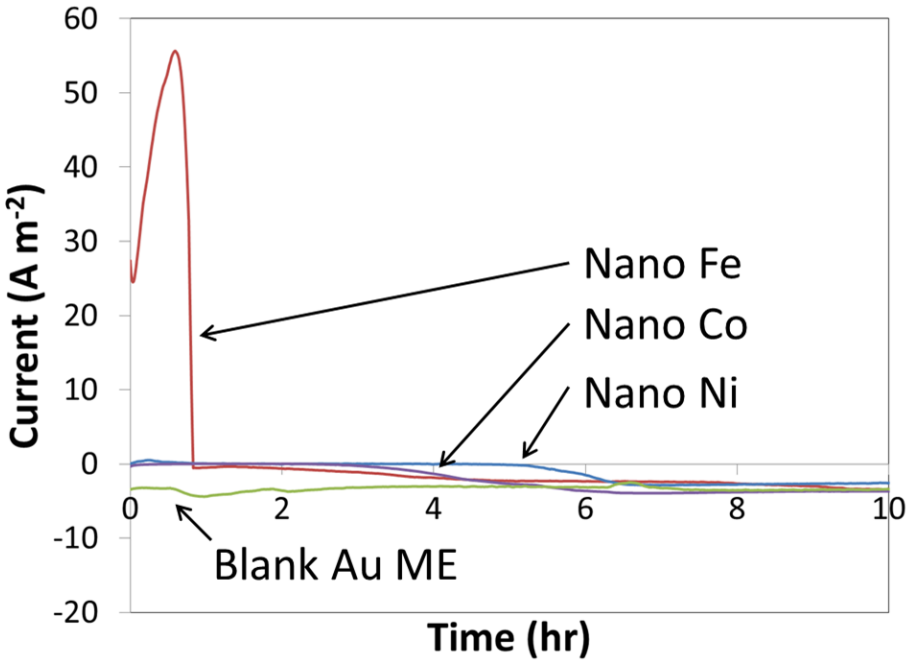

Figure 3.5: Chronoamperometry stability measurements of Fe, Co, and Ni catalysts in a SPE-cell at -0.25 V vs SHE.

subsequently changed to cathodic (negative) currents that were similar to the current exhibited by the underlying Au microelectrode. This behavior could be explained by the materials corroding and leaving the gold microelectrode underneath exposed. The current for these carbide catalysts decreased over time, which could be associated with a corrosion reaction or by a surface-reaction that results in a less active catalyst for the HER. The W_2C and W_2C-supported Pd catalysts, however, maintained relatively stable currents over the 10 hr measurements, which suggests that these materials are stable in the SPE cell.

One way to predict the stabilities of a material in an electrochemical cell is based on information in the Pourbaix diagram [5]. These diagrams depict the regions of electrochemical immunity, passivation, and corrosion for a given element over a range of applied potentials and pH. Platinum, for example, is predicted to be stable over the pH (~ 0) and potential region (-1.0 to -0.25 V vs SHE) of the cathode during operation

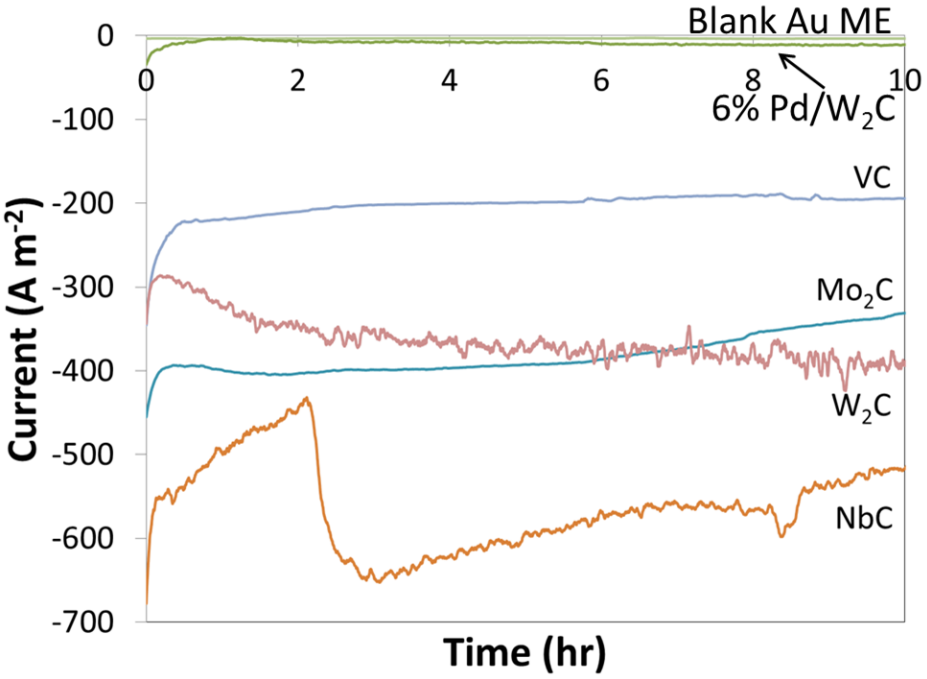

Figure 3.6: Chronoamperometry stability measurements of carbide and W_2C-supported Pd catalysts in a SPE-cell at -0.25 V vs SHE.

of the SPE reactor(Figure 3.7a). Iron, however, is predicted to be thermodynamically unstable and undergoes corrosion at low pH and potentials higher than -0.6 V vs SHE. Predicted stabilities for the catalysts used in this thesis are listed in Table 3.1.

Noble metal catalysts and selected base metal catalysts were demonstrated to be electrochemically stable, based on both TGA and SPE-cell measurements. The other base metals (i.e. Fe, Co, and Ni) were found to be unstable, ostensibly due to corrosion. These results are consistent with the predicted stabilities of these materials at -0.25 V vs SHE in an acidic environment. This suggests that in the future the Pourbaix diagrams provide a good indication of what materials might be stable in an SPE-cell for base and noble metals.

Pourbaix diagrams for the transition metal carbide catalysts have not been developed. The electrochemical stabilities predicted by the Pourbaix diagrams of their corresponding metals/metal oxides were not in all cases consistent with the stabilities

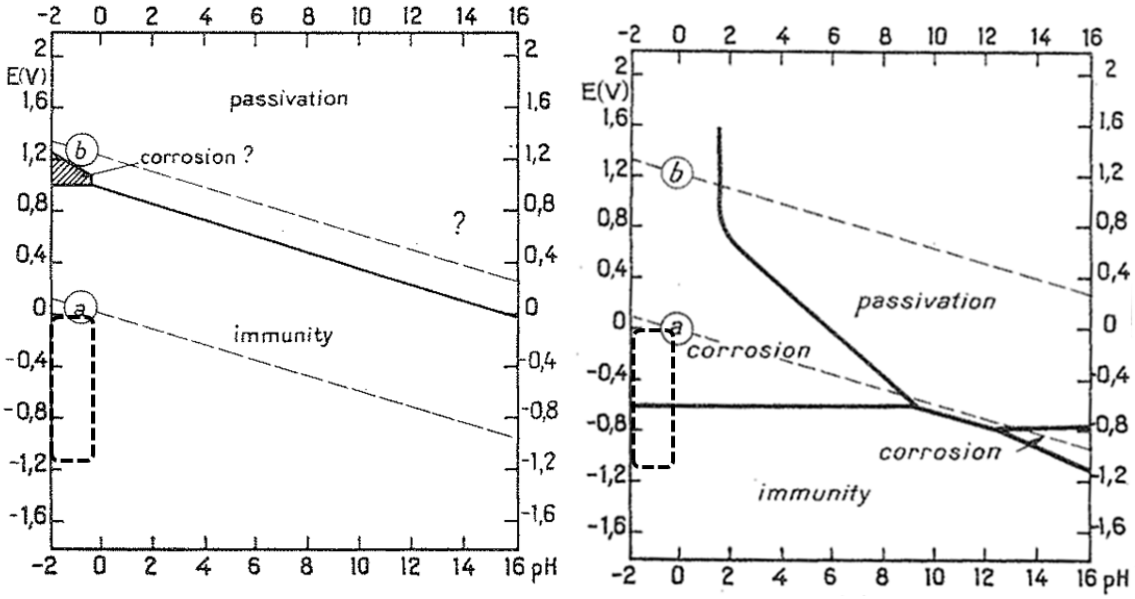

(a) Pourbaix diagram for Platinum

(b) Pourbaix diagram for Iron

Figure 3.7: Pourbaix diagrams for selected elements [5]. Area marked with dashed line indicates approximate pH and potential region during operation of SPE reactor.

measured for the transition metal carbides. For example, Nb/NbO is predicted by the Pourbaix diagram to be stable, but TGA and SPE-cell measurements demonstrated that NbC is not. V/VO and Mo/MoO are predicted to be unstable, and VC and Mo_2C were unstable based on the reduction in HER current that was observed over a 10 hr period (Figure 3.6). W/WO is predicted to be stable, and experiments demonstrated that W_2C was in fact stable. While the stabilities of noble and base metal materials were consistent with those predicted by their Pourbaix diagrams, this is apparently not always the case for carbide materials. This suggests that new Pourbaix diagrams should be developed specifically for transition metal carbides [8].

3.4 Conclusions

We demonstrated through the use of TGA and SPE-cell measurements that noble metals, W_2C, W_2C-supported Pd, and some base metals (i.e., Cu and Ag) were stable in the pH and potential environment experienced in the triglyceride hydrogenation

reactor. Other base metals and carbide catalysts were shown to be unstable. These observations suggest that the low rates of these materials for triglyceride hydrogenation may be related to their electrochemical instabilities in the SPE reactor.

References

[1] B. Liu and S. Creager. Carbon xerogels as pt catalyst supports for polymer electrolyte membrane fuel-cell applications. *Journal of Power Sources*, 195(7):1812–1820, 2010.

[2] M.S. Mamat, S.A. Grigoriev, K.A. Dzhus, D.M. Grant, and G.S. Walker. The performance and degradation of pt electrocatalysts on novel carbon carriers for pemfc applications. *International Journal of Hydrogen Energy*, 35(14):7580–7587, 2010.

[3] J. Jiang and A. Kucernak. Investigations of fuel cell reactions at the composite microelectrode— solid polymer electrolyte interface. I. Hydrogen oxidation at the nanostructured Pt Nafion membrane interface. *Journal of Electroanalytical Chemistry*, 567(1):123–137, 2004.

[4] D.T. Cromer and J.B. Mann. X-ray scattering factors computed from numerical Hartree-Fock wave functions. *Acta Crystallographica Section A: Crystal Physics, Diffraction, Theoretical and General Crystallography*, 24(2):321–324, 1968.

[5] M. Pourbaix. Atlas of electrochemical equilibria in aqueous solutions. *M. Pourbaix, published 1974 by NACE, 644*, 1974.

[6] A. Bonakdarpour, R. Löbel, S. Sheng, T.L. Monchesky, and J.R. Dahn. Acid stability and oxygen reduction activity of magnetron-sputtered ptta ($0 \leq x \leq 1$) films. *Journal of the Electrochemical Society*, 153:A2304, 2006.

[7] G.C.K. Liu, D.A. Stevens, J.C. Burns, R.J. Sanderson, G. Vernstrom, R.T. Atanasoski, M.K. Debe, and J.R. Dahn. Oxygen reduction activity of dealloyed pt(1-x)ni(x) catalysts. *Journal of the Electrochemical Society*, 158:B919–B926, 2011.

[8] M.C. Weidman, D.V. Esposito, I.J. Hsu, and J.G. Chen. Electrochemical stability of tungsten and tungsten monocarbide (wc) over wide ph and potential ranges. *Journal of The Electrochemical Society*, 157:F179, 2010.

CHAPTER IV

Electrocatalyst Performance in a SPE Reactor

4.1 Introduction

Solid polymer electrolyte reactors are attractive for use in carrying out a number of reactions that are typically performed using thermochemical reactors [1–10]. Pintauro and coworkers [6] demonstrated high activities and selectivities for the hydrogenation of triglycerides using a Pd catalyst in a SPE reactor. Central to this performance is the facile transport of hydrogen to the catalyst surface, which is diffusion-controlled under most conditions in thermochemical reactors [11]. The hydrogenation rate is influenced by the solubility of hydrogen gas in the triglyceride, which is a function of thermochemical operating variables (e.g., reactor temperature, pressure, agitation rate). In contrast, in the SPE reactor, protons are delivered to the cathode catalyst by means of the Nafion® membrane, which is primarily controlled by the applied potential and current (and to a lesser extent reactor temperature, anode gas pressure, and membrane hydration).

Similarly, Lux *et al.* [10] reported the use of an electrochemical reactor to selectively produce lactic acid from glycerol at moderate temperatures and pressures. In an electrochemical reactor, however, the driving force for the reaction is the applied potential rather than high temperatures and pressures. The electrocatalysts have typically been noble metals, either in bulk or on supports, which contribute significantly

to the overall capital cost of the reactor system. As such, there exists a motivation to develop highly active and selective electrocatalysts from relatively low cost materials.

Transition metal carbides have recently received a good deal of interest in this respect, because they are relatively inexpensive and have been demonstrated to have properties similar to those of noble metals [12]. These materials are electrically conductive [13–15], can be synthesized with high surface areas [16–18], and are catalytically active for a varietry of reactions, including benzene hydrogenation [19]. Among these materials, tungsten carbide has received the most attention and has been used as a support for various metals [20–23].

In this chapter, characterization of the activities and selectivities of a number of noble metal, base metal, carbide and carbide-supported metal catalysts for triglyceride hydrogenation in an electrochemical reactor is described. We demonstrate that the performance varies significantly with the type of material. Furthermore, we show that the hydrogenation rates and product selectivities are dependent on the applied potential, which may indicate that the rate determining step for the reaction is electrochemical in nature. We also used results from various characterization techniques, including XRD, BET surface area analysis, and ICP elemental analysis to support our conclusions.

4.2 Experimental

4.2.1 Electrocatalyst Synthesis and Characterization

4.2.1.1 Catalyst Synthesis

Noble metal (Pd, Pt, Rh, Ru, Ir, Au, and Ag) and base metal (Fe, Co, Ni, and Cu) catalysts were used as received from vendors (see Table 4.1). Transition metal carbide (VC, NbC, Mo_2C, and W_2C) catalysts were prepared via TPR of their respective oxides with 15% CH_4/H_2 (Table 2.1), according to methods described

in the literature [17, 18]. Carbide-supported Pd catalysts were synthesized using a wet impregnation method involving the dissolved metal salt ($Pd(NH_3)_4(NO_3)_2$) and unpassivated tungsten carbide [24].

4.2.1.2 BET Surface Area Analysis

Catalyst surface areas were measured via BET surface area analysis using a Micromeritics ASAP 2010 instrument for N_2 physisorption. Prior to these measurements, the catalysts were degassed at 300 °C for 4 hr.

4.2.1.3 X-ray Diffraction Analysis

XRD was performed using a Rigaku Miniflex Diffractometer with Cu Kα radiation and a Ni filter (λ = 1.540 Å). The diffraction angle range ($10° < 2\theta < 90°$) was scanned at a rate of 5 degrees min^{-1} with a 0.02 degree step size. The catalyst crystal structures and average crystallite sizes were determined from their XRD patterns using the Jade Software v. 9.0 (Materials Data, Inc.) package linked to the ICDD (International Center for Diffraction Data) PDF4 database (rev. 2009).

4.2.1.4 ICP Elemental Analysis

The elemental compositions of the carbide-supported metal catalysts were determined using a ICP-OES with a Varian 710-ES analyzer. Catalysts were dissolved in 5% aqua regia (3 parts HCl-1 part HNO_3 (Fisher Scientific, certified ACS Plus)) in 30% H_2O_2 (Fisher Scientific, certified ACS), and the emission spectra of dissolved species were compared to those for a series of standard solutions of known concentrations (Inorganic Ventures).

4.2.2 Electrocatalyst Performance Measurements

4.2.2.1 Membrane Electrode Assembly Fabrication

The MEAs used in the SPE reactor were prepared from two catalyst layers supported on carbon GDLs (E-tek cloth LT2500W ELAT© for constant current measurements or Toray paper TGP-H-090 for constant potential measurements) separated by a Nafion® 117 membrane (Ion Power, Inc.). Anode and cathode GDLs were prepared using a hand painting technique with a liquid catalyst suspension containing the catalyst and a 5 wt% Nafion® perfluorinated resin solution (Sigma-Aldrich). The target anode loading was 5 mg cm^{-2} of 20% Pt/C, and the target cathode loading was 1 mg cm^{-2} of the particular catalyst being characterized. MEAs were assembled and hot pressed at 800 psi for 5 min at 135 °C. During assembly of the reactor stack, the bolts were tightened to 50 foot-pounds of torque. Subsequently, the MEA was rehydrated overnight at 40 °C with 50 mL min^{-1} humidified H_2 gas (Cryogenic Gases, pre-purified) to restore moisture lost during the hot-press treatment.

4.2.2.2 SPE-Reactor Operation

Electrocatalytic activity measurements were performed using a SPE reactor, similar to that described by Pintauro *et al.* [6]. This reactor is similar in construction to a PEM fuel cell reactor, in that it includes anode and cathode graphite blocks separated by a Nafion®-based MEA (see Figure 2.3). Humidified hydrogen gas is circulated on the anode, while triglycerides (in this case, soybean oil) is circulated on the cathode side in a batch recycle manner. An external power supply exerts a potential across the cell stack via two copper current collectors. Hydrogen gas dissociates on the anode under the applied potential (Equation 4.1a).

$$H_2 \leftrightharpoons 2(H^+ + e^-) \tag{4.1a}$$

$$R - C = C - R^{'} + 2\left(H^+ + e^-\right) \leftrightharpoons R - C - C - R^{'} \tag{4.1b}$$

$$2(H^+ + e^-) \leftrightharpoons H_2 \tag{4.1c}$$

The resulting protons and electrons travel through the MEA and external circuit, respectively. On the cathode catalyst, hydrogen either reacts with absorbed triglycerides (Equation 4.1b) or bubbles off as H_2 gas (Equation 4.1c). Reactions were run under constant current (0.5 A) and constant potential (0.25 V, 0.50 V, 0.75 V, and 1.00 V) conditions. The reactor temperature was maintained at 70 °C via a PID temperature controller, as were the H_2 and triglyceride reactants. The H_2 and triglyceride flow rates were 100 mL min^{-1}, and the H_2 backpressure was 10 psig.

4.2.3 SPE-Reactor Product Characterization

Triglyceride samples were taken at the beginning of and periodically throughout each hydrogenation run at approximately 5 hr intervals. These samples were characterized according to standard methods from the American Oil Chemists' Society. First, the samples were transesterified to form FAMEs (AOCS Method Ce 2-66), and then these FAMEs were analyzed using GC a Varian GC-FID with a Varian CP 7487 column operating at 192 °C (AOCS Method Ce 1-62). The relative amounts of each FAME was calculated from the GC trace using PeakSimple Chromatography Software v. 3.93 (SRI Instruments). The FAME composition of the fresh soybean oil was measured to be approximately 4% methyl stearate (C18:0), 23% C18:1, 55% C18:2, and 8% C18:3.

The electrochemical current efficiency (CE%) represents the fraction of protons that are incorporated into reducing double bonds, as opposed to bubbling off as H_2

gas. By taking the difference between the compositions of the fresh and hydrogenated soybean oil samples, the number of reduced double bonds can be calculated. Equation 4.2 illustrates the current efficiency which is derived by dividing the number of reduced double bonds by the integrated flux of protons through the membrane (that is, the product of the applied current, I, and the total time of the experiment, t). The other terms in this equation are $\Delta_{\text{C18:1}}$, $\Delta_{\text{C18:2}}$, and $\Delta_{\text{C18:3}}$, which are the changes in the weight fractions of the glycerides C18:1, C18:2, and C18:3, respectively; M is the mass (in grams) of soybean oil, F is Faraday's constant, and MW is the molecular weight of each FAME component. The specific hydrogenation rates can also be calculated by dividing the moles of reduced double bonds by the reaction time and the catalyst BET surface area.

$$\text{CE } \% = \frac{FM\left[\frac{2\Delta_{\text{C18:1}}}{MW_{\text{C18:1}}} + \frac{4\Delta_{\text{C18:2}}}{MW_{\text{C18:2}}} + \frac{6\Delta_{\text{C18:3}}}{MW_{\text{C18:3}}}\right]}{It} \tag{4.2}$$

4.3 Results and Discussion

4.3.1 Electrocatalyst Synthesis and Characterization

XRD analysis of the catalyst materials (as-received or as-prepared) indicated that most of the materials were phase pure. XRD patterns of the carbides and carbide-supported Pd catalysts did not contain peaks associated with the oxide precursors, indicating that the carburization was complete. Previous researchers have reported that Mo_2C catalysts synthesized according to the method described in Table 2.1 [17, 25] produce a high surface area polyphasic material. The results of XRD analysis of the Mo_2C catalyst synthesized in this work are consistent with those findings. Average crystallite sizes were estimated using the Scherrer equation (Equation 4.3). The crystal structures, average crystallite sizes, BET surface areas and, for the carbide-

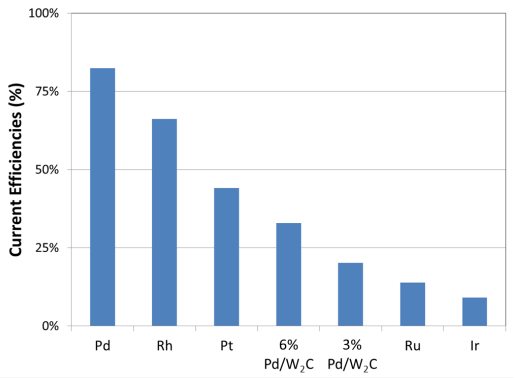

(a) Noble metal and W_2C-supported Pd catalysts

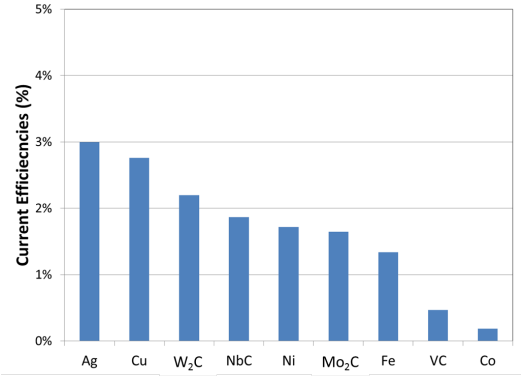

(b) Base metal and carbide catalysts

Figure 4.1: Electrochemical efficiencies of noble metal, base metal, and carbide electrocatalysts at 70 °C and 0.5 A constant current.

supported metal catalysts, elemental compositions are listed in Table 4.1.

$$d_c = \frac{K\lambda}{B\cos\theta} \tag{4.3}$$

Pd/W_2C catalysts were synthesized at two nominal weight loadings: 10% and 30% Pd/W_2C. ICP analysis of the synthesized catalysts indicated that their actual loadings were $2.8\% \pm 0.2\%$ and $6.4\% \pm 0.5\%$, respectively. Throughout this dissertation, these catalysts will be referred to be their approximate actual loadings of 3% Pd/W_2C and 6% Pd/W_2C.

4.3.2 Catalyst Performance Measurements

4.3.2.1 Constant Current Triglyceride Hydrogenation

The noble metal, base metal, carbide and carbide-supported Pd catalysts were tested in the electrochemical hydrogenation reactor. The electrochemical current efficiencies for these materials at 70 °C and 0.5 A constant current are illustrated in Figure 4.1a. The noble metal and W_2C-supported Pd catalysts exhibited relatively high efficiencies, while the base metal and carbide catalysts (Figure 4.1b) had efficiencies less than 5%.

Table 4.1: Results of XRD, BET, and ICP analysis of as-received and as-prepared catalysts.

Catalyst	Crystal Phase	Crystallite Size (nm)	BET (m^2 g^{-1})
Pt black[a]	fcc	7 ± 1	16
Rh black[a]	fcc	5 ± 1	43
Ru black[a]	hcp	15 ± 2	25
Ir black[a]	fcc	10 ± 2	17
Nano Pd[b]	fcc	4 ± 2	63
Nano Fe[b]	bcc	39 ± 15	21
Nano Cu[b]	fcc	36 ± 3	21
Nano Co[b]	unknown[c]	unknown[c]	38
Nano Ni[b]	fcc	3 ± 1	36
Nano Ag[b]	fcc	14 ± 2	11
VC	fcc	77 ± 9	4
Mo_2C	hcp & fcc	4 ± 2	82
NbC	fcc	43 ± 3	7
W_2C	fcc	7 ± 2	31
3% Pd/W_2C	hcp	6 ± 2	9
6% Pd/W_2C	hcp & fcc	7 ± 2	31

[a]Purchased from Alfa Aesar
[b]Purchased from Quantum Sphere
[c]Cobalt compounds cannot be characterized using Cu Kα radiation [26]

We show the trans fat and saturated fat selectivities in Figures 4.1b and 4.1b. One measure of selectivity is the ratio of trans fat or saturated fat produced to the extent of conversion (Equations 4.4 and 4.5). Since trans and saturated fats are undesired products, a lower number is preferred with this metric.

$$\text{Trans Selectivity} = \frac{\Delta\big(\%\text{ trans fat}\big)}{\Delta\big(\%\text{ conversion}\big)} \tag{4.4}$$

$$\text{Saturated Selectivity} = \frac{\Delta\big(\%\text{ saturated fat}\big)}{\Delta\big(\%\text{ conversion}\big)} \tag{4.5}$$

As a group, the noble metal and W_2C-supported Pd catalysts produced more saturated fat per unit conversion than the base metal and carbide catalysts. Noble metal, base metal, and W_2C-supported Pd catalysts all exhibited comparable selectivities toward trans fat production. Previous researchers reported the same trend for triglyceride hydrogenation in the thermochemical hydrogenation environment [27, 28], where the materials with the highest hydrogenation rates also contributed the highest production of trans fats. The base metal and carbide, which had comparatively lower rates for hydrogenation, also produced comparable amounts of trans fats.

With regard to saturated fat selectivity, the noble and base metals tended to make more saturated fat than the carbide catalysts (Figures 4.2a and 4.2b). Pt and Ru, specifically, produced high amounts of C18:0, while Pd, Rh, and Ir produced slightly less C18:0. Previous researchers also noted that Ru and Pt had high selectivities toward saturated fats than Pd and Rh [27]. The carbide-supported Pd catalysts had saturated fat selectivities that were lower than those of Pd, but higher than that of the tungsten carbide support alone.

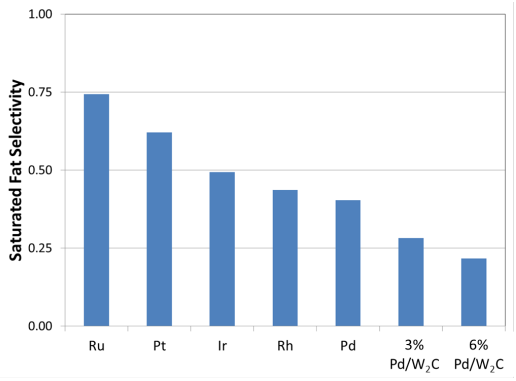

(a) Noble metal and W_2C-supported Pd catalysts

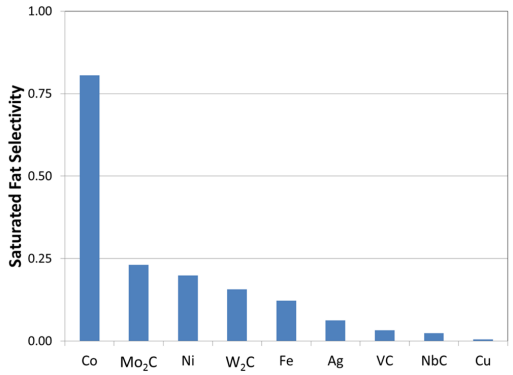

(b) Base metal and carbide catalysts

Figure 4.2: Saturated fat selectivities of noble metal, base metal, and carbide electrocatalysts at 70 °C and 0.5 A constant current. Since saturated fat is an undesired product, a lower number is preferred.

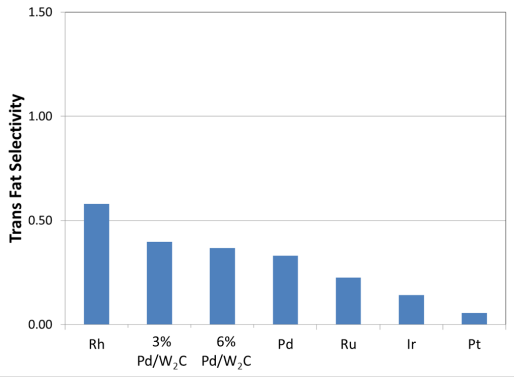

(a) Noble metal and W_2C-supported Pd catalysts

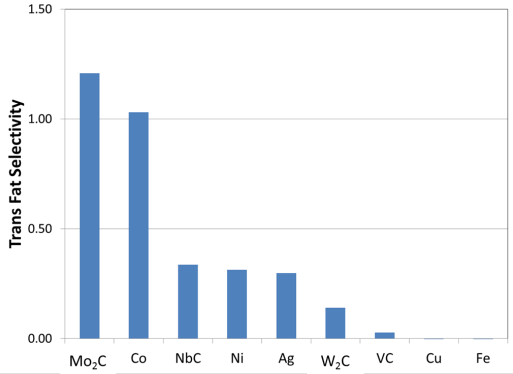

(b) Base metal and carbide catalysts

Figure 4.3: Trans fat selectivities of noble metal, base metal, and carbide electrocatalysts at 70 °C and 0.5 A constant current. Since trans fat is an undesired product, a lower number is preferred.

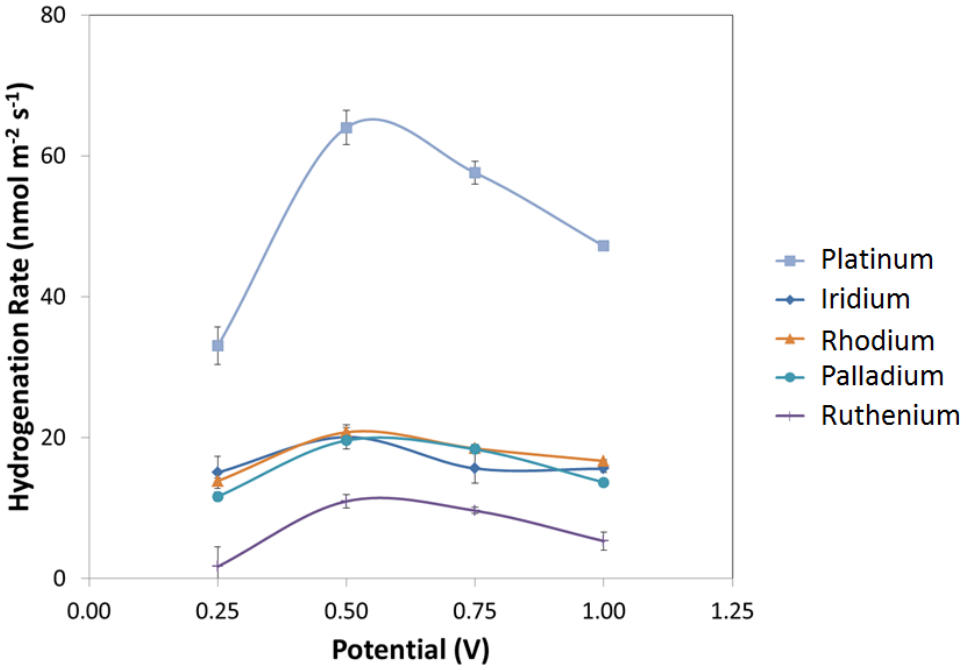

Figure 4.4: Electrochemical hydrogenation rates for noble metal catalysts at 70 °C and constant potentials from 0.25 V to 1.0 V.

4.3.2.2 Constant Potential Hydrogenation

We also performed triglyceride hydrogenation using the electrochemical reactor over the potential range 0.25 V to 1.0 V, in order to investigate the effect of applied potential on hydrogenation rates and selectivities. The areal hydrogenation rates for noble metal catalysts (Figure 4.4) was observed to vary with voltage between 0.25 V to 1.0 V. Initially the rate increased from 0.25 V to 0.5 V, but it subsequently decreased for 0.75 V and 1.0 V. This trend persisted for all the noble metal catalysts tested. The hydrogenation rates of the base metal, Mo_2C, NbC, and VC catalysts were too low for any trend to be observed. The hydrogenation rates of W_2C varied with applied voltage. This is consistent with the literature, which reports that carbides have similar overpotentials for the HER as noble metals [29]. Carbide-supported Pd catalysts behaved similarly, with areal rates that were comparable to the bulk noble metal catalysts (Figure 4.5).

The activity trends for the noble metal electrocatalysts follow approximately the

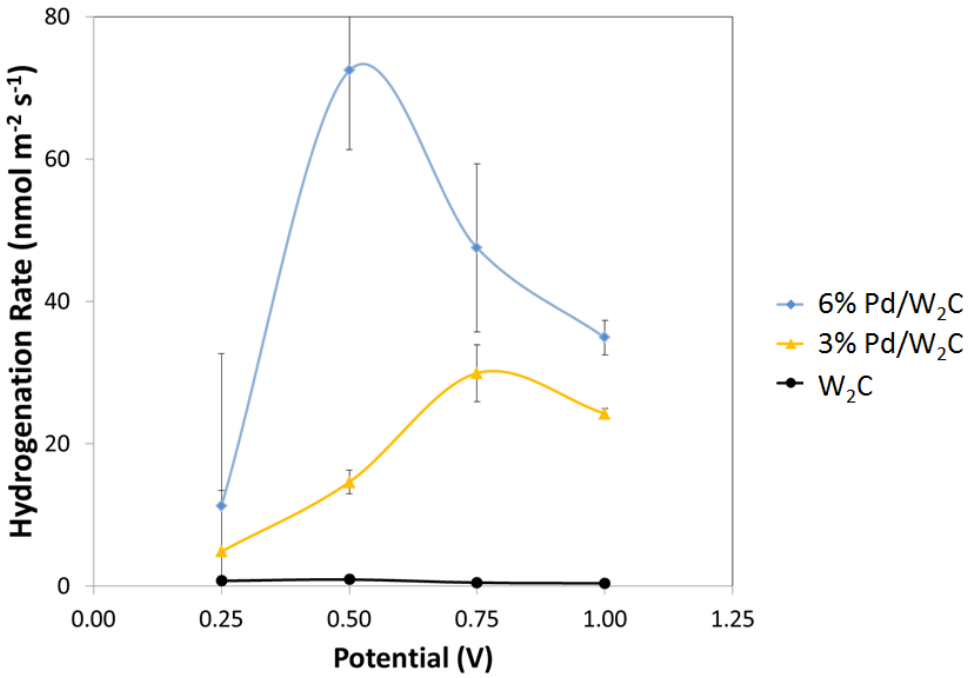

Figure 4.5: Electrochemical hydrogenation rates for W_2C and W_2C-supported Pd catalysts at 70 °C and constant potentials from 0.25 V to 1.0 V.

trends in activity of those metals in the thermochemical reactor. Rylander reported that, while activity sequences depended on the reaction conditions and the type of catalyst support used, generally speaking the thermochemical hydrogenation activity could be written:

$$\text{Pd} > \text{Rh} > \text{Pt} >> \text{Ir} > \text{Ru}$$

The areal hydrogenation rates for the electrocatalytic reactor followed a similar sequence, although in this case the Pt catalyst had an activity 3-4 times higher than the other noble metal catalysts.

$$\text{Pt} >> \text{Rh} > \text{Pd} >> \text{Ir} > \text{Ru}$$

One clear distinction, however, between the thermochemical and electrochemical hydrogenation rates, is the difference in rates for base metal catalysts such as Fe,

Co, Ni, and Cu, which have been shown to be active for hydrogenation [30–34]. The relative inactivity of these catalysts is perhaps related to reduced stability in the electrochemical system, or a different hydrogenation mechanism in the electrochemical environment.

4.4 Conclusions

We have used an electrochemical hydrogenation reactor to test the activities and selectivities of noble metal, base metal, carbide and carbide-supported Pd catalysts. We measured these in both constant current and constant potential operation modes. We demonstrated that noble metals and carbide-supported Pd catalysts had the highest efficiencies for hydrogenation. We also showed that hydrogenation rates are dependent on the applied potential. We conclude by noting that electrochemical stabilities and the electrochemical mechanism are likely causes of the differences in material performances.

References

[1] J.C. Smeltzer and P.S. Fedkiw. Reduction of Nitrobenzene in a Parallel-Plate Reactor. *Journal of The Electrochemical Society*, 139:1358, 1992.

[2] V. Anantharaman and P.N. Pintauro. The Electrocatalytic Hydrogenation of Glucose. *Journal of the Electrochemical Society*, 141:2729, 1994.

[3] L. Roquet, E.M. Belgsir, J.M. Léger, and C. Lamy. Kinetics and mechanisms of the electrocatalytic oxidation of glycerol as investigated by chromatographic analysis of the reaction products: potential and ph effects. *Electrochimica Acta*, 39(16):2387–2394, 1994.

[4] R. Lowrey, M. Doyle, and T. Andersona. A Novel Fluorine Production Process in a Proton Exchange Membrane Reactor. *Electrochemical and Solid-state Letters*, 2(10):519–521, 1999.

[5] X.Z. Yuan, Z.F. Ma, Q.Z. Jiang, and W.S. Wu. Cogeneration of cyclohexylamine and electrical power using PEM fuel cell reactor. *Electrochemistry communications*, 3(11):599–602, 2001.

[6] P.N. Pintauro, M.P. Gil, K. Warner, G. List, and W. Neff. Electrochemical hydrogenation of soybean oil with hydrogen gas. *Industrial & Engineering Chemistry Research*, 44(16):6188–6195, 2005.

[7] H. Li and C. Oloman. The electro-reduction of carbon dioxide in a continuous reactor. *Journal of Applied Electrochemistry*, 35(10):955–965, 2005.

[8] T. Fuchigami and T. Tajima. Development of new methodologies toward green sustainable organic electrode processes. *ChemInform*, 38(16):no–no, 2007.

[9] S. Sedighi and C.L. Gardner. A kinetic study of the electrochemical hydrogenation of ethylene. *Electrochimica Acta*, 55(5):1701–1708, 2010.

[10] S. Lux, P. Stehring, and M. Siebenhofer. Lactic Acid Production as a New Approach for Exploitation of Glycerol. *Separation Science and Technology*, 45(12):1921–1927, 2010.

[11] P.N. Rylander. Hydrogenation of natural oils with platinum metal group catalysts. *Journal of the American Oil Chemists' Society*, 47(12):482–486, 1970.

[12] R.B. Levy and M. Boudart. Platinum-like behavior of tungsten carbide in surface catalysis. *Science*, 181(4099):547, 1973.

[13] H.O. Pierson. *Handbook of chemical vapor depostion [ie deposition](CVD): principles, technology, and applications*. William Andrew, 1999.

[14] W.P. Leroy, C. Detavernier, R.L. Van Meirhaeghe, A.J. Kellock, and C. Lavoie. Solid-state formation of titanium carbide and molybdenum carbide as contacts for carbon-containing semiconductors. *Journal of Applied Physics*, 99:063704, 2006.

[15] L.W. Shacklette and W.S. Williams. Influence of order-disorder transformations on the electrical resistivity of vanadium carbide. *Physical Review B*, 7(12):5041, 1973.

[16] S.T. Oyama. *The chemistry of transition metal carbides and nitrides*. Kluwer Academic Publishers, 1996.

[17] J. Patt, D.J. Moon, C. Phillips, and L. Thompson. Molybdenum carbide catalysts for water–gas shift. *Catalysis Letters*, 65(4):193–195, 2000.

[18] S.T. Oyama and D.F. Cox. New catalysts for coal processing: Metal carbides and nitrides. Technical report, Federal Energy Technology Center, Morgantown, WV (US); Federal Energy Technology Center, Pittsburgh, PA (US), 1999.

[19] J.S. Lee, M.H. Yeom, K.Y. Park, I.S. Nam, J.S. Chung, Y.G. Kim, and S.H. Moon. Preparation and benzene hydrogenation activity of supported molybdenum carbide catalysts. *Journal of Catalysis*, 128(1):126–136, 1991.

[20] V. Marinovic, J. Stevanovic, B. Jugovic, and M. Maksimovic. Hydrogen evolution on Ni/WC composite coatings. *Journal of Applied Electrochemistry*, 36(9):1005–1009, 2006.

[21] C. Ma, J. Sheng, N. Brandon, C. Zhang, and G. Li. Preparation of tungsten carbide-supported nano Platinum catalyst and its electrocatalytic activity for hydrogen evolution. *International Journal of Hydrogen Energy*, 32(14):2824–2829, 2007.

[22] M. Wu, P.K. Shen, Z. Wei, S. Song, and M. Nie. High activity PtPd-WC/C electrocatalyst for hydrogen evolution reaction. *Journal of Power Sources*, 166(2):310–316, 2007.

[23] E.C. Weigert, D.V. Esposito, and J.G. Chen. Cyclic voltammetry and X-ray photoelectron spectroscopy studies of electrochemical stability of clean and Pt-modified tungsten and molybdenum carbide (WC and Mo2C) electrocatalysts. *Journal of Power Sources*, 193(2):501–506, 2009.

[24] W. Setthapun, S.K. Bej, and L.T. Thompson. Carbide and Nitride Supported Methanol Steam Reforming Catalysts: Parallel Synthesis and High Throughput Screening. *Topics in Catalysis*, 49(1):73–80, 2008.

[25] J.A. Schaidle, A.C. Lausche, and L.T. Thompson. Effects of sulfur on Mo2C and Pt/Mo2C catalysts: Water gas shift reaction. *Journal of Catalysis*, 272(2):235–245, 2010.

[26] B.B. He, J.H. Reibenspies, and N. Bhuvanesh. Two-Dimensional X-Ray Diffraction. *Powder Diffraction*, 25:200, 2010.

[27] M. Zajcew. Hydrogenation of fatty oils with palladium catalysts. v. products of the tall oil industry. *Journal of the American Oil Chemists' Society*, 37(10):473–475, 1960.

[28] C.H. Riesz and H.S. Weber. Catalysts for selective hydrogenation of soybean oil. 1 ii. commercial catalysts. *Journal of the American Oil Chemists' Society*, 41(6):400–403, 1964.

[29] D.V. Esposito, S.T. Hunt, A.L. Stottlemyer, K.D. Dobson, B.E. McCandless, R.W. Birkmire, and J.G. Chen. Low-Cost Hydrogen-Evolution Catalysts Based on Monolayer Platinum on Tungsten Monocarbide Substrates. *Angewandte Chemie International Edition*, 49(51):9859–9862, 2010.

[30] L. Kahlenberg and T.P. Pi. On the Catalytic Hydrogenation of Certain Oils. *The Journal of Physical Chemistry*, 28(1):59–70, 1924.

[31] K.J. Moulton, R.E. Beal, and E.L. Griffin. Hydrogenation of soybean oil with commercial copper-chromite and nickel catalysts: Winterization of low-linolenate oils. *Journal of the American Oil Chemists' Society*, 48(9):499–502, 1971.

[32] B.I. Rosen. Selective reduction of edible oils, May 24 1983. US Patent 4,385,001.

[33] S. Koritala. Homogeneous catalytic hydrogenation of soybean oil: Palladium acetylacetonate. *Journal of the American Oil Chemists' Society*, 62(3):517–520, 1985.

[34] J.A. Heldal, K.J. Moulton, and E.N. Fronkel. Fixed-bed continuous hydrogenation of soybean oil with palladium-polymer supported catalysts. *Journal of the American Oil Chemists' Society*, 66(7):979–982, 1989.

CHAPTER V

SPE Reaction Mechanisms

5.1 Introduction

In Chapter IV we demonstrated the hydrogenation of triglycerides in a SPE reactor. We reported the activities and selectivities for noble metal, base metal, carbide, and carbide-supported catalysts, and we noted that the rates for hydrogenation vary widely over the various materials. We also demonstrated that some of this variation can be explained through the varying electrochemical stabilities of the different materials. Some base metals, such as Fe, Co, and Ni, and carbides, such as VC, NbC, and Mo_2C, are not stable at the pH and potential environments of the SPE reactor. These instabilities are reflected in their low rates for hydrogenation.

The materials that have been demonstrated to be stable in the SPE-reactor exhibited a wide range of rates for triglyceride hydrogenation. In this chapter we elucidate the mechanisms for the cathodic reactions that occur during operation of the SPE-reactor: the HER and the triglyceride hydrogenation reaction. We compare the rates for the individual reaction steps to the hydrogenation rates of the different materials.

5.1.1 Hydrogen Evolution Reaction Mechanism

The HER is generally accepted to occur via two elementary steps [1, 2]. The first step involves the reduction of a proton from the electrolyte to a hydrogen atom ad-

sorbed on the electrode surface. This proton discharge step is called the Volmer reaction (Equation 5.1a). The second HER step involves the generation of H_2 gas via two pathways. In the Tafel pathway, two adsorbed hydrogens combine to form H_2 (Equation 5.1b). In the Heyrovský pathway, one adsorbed hydrogen is electrochemically desorbed along with an electron and a proton from the electrolyte (Equation 5.1c).

$$H^+ + e^- \leftrightharpoons H_{ads} \qquad \text{Volmer} \qquad (5.1a)$$

$$2H_{ads} \leftrightharpoons H_2 \qquad \text{Tafel} \qquad (5.1b)$$

$$H_{ads} + H^+ + e^- \leftrightharpoons H_2 \qquad \text{Heyrovský} \qquad (5.1c)$$

The rates for each of these elementary steps have been found to depend on a number of factors, including temperature, pH, metal type, as well as the cleanliness and nanostructure of the material surface [3].

A great deal of effort has been expended to determine which of the two pathways (Volmer-Tafel or Volmer-Heyrovský) may dominate under different conditions [1, 4–12]. Much of this effort has involved measuring the current-voltage response of a given system, and comparing its behavior to that of a given theoretical model for the pathways [12]. It was demonstrated by Butler [4] and Volmer [5] that for a reversible, one-electron transfer reaction at equilibrium, the current-voltage relationship can be modeled using the following equation:

$$i = i_0\left(\exp\left[\frac{\alpha F\eta}{RT}\right] - \exp\left[\frac{(1-\alpha)F\eta}{RT}\right]\right) \qquad \text{Butler-Volmer Eqn} \qquad (5.2)$$

where i is the current density (A cm^{-2}), i_0 is the exchange current density (A cm^{-2}), F is Faraday's constant (C mol^{-1}), R is the ideal gas constant (J mol^{-1} K^{-1}), T is the temperature (K), α is the transfer coefficient, and η is the voltage (V). Previous

Table 5.1: Tafel slope method for determining the rate limiting step of the HER.

Rate Determining Step (RDS)	$\alpha^a = \mathrm{n}_p + \frac{1}{2}\mathrm{n}_q + \mathrm{n}_r$	Slope (mV decade^{-1})^b
Volmer	$\alpha = 0 + \frac{1}{2}(1) + 0 = \frac{1}{2}$	120
Tafel	$\alpha = 2 + \frac{1}{2}(0) + 0 = 2$	30
Heyrovský	$\alpha = 1 + \frac{1}{2}(1) + 0 = \frac{3}{2}$	40

[a]Transfer coefficient is the sum of electrons transferred before (n_p) and after (n_r) the RDS, and one-half of electrons transferred during (n_q) the RDS.

[b]Tafel slope at 25 °C.

research [12] has demonstrated that at large overpotentials ($\eta \to \infty$), the Butler-Volmer equation simplifies to:

$$\log[i] = \log[i_0] - \frac{\alpha F \eta}{2.303RT} \qquad \text{Butler-Volmer Eqn as } \eta \to \infty \qquad (5.3)$$

where the transfer coefficient α is equal to the sum of the electrons transferred before (n_p) and after (n_q) the rate determining step, plus one-half the electrons transferred during the rate-determining step (n_r) [12]. A plot of the potential versus the logarithm of the current (i.e. a Tafel plot), in the absence of mass-transfer limitations, yields a straight line. The slope of this line is indicative of which elementary step (Volmer, Tafel, or Heyrovský) is the rate-determining step for the HER.

Despite decades of research, however, it is still unclear which mechanism prevails under different conditions, even on a well-studied material like Pt [2]. For example, some research has concluded, using the Tafel slope method, that the Volmer-Tafel mechanism prevails for Pt in acidic electrolytes [6, 7, 11], with the Tafel step being rate determining. Other research using theoretical and kinetic models have begun to question whether these conclusions are accurate, and have proposed that the mechanism may actually be Volmer-Heyrovský [13, 14]. The challenge with determining the HER mechanism using the Tafel slope method lies in the necessity to measure

changes in the HER rate over several orders of magnitude in current without influence from ohmic distortion, mass-transfer limitations, or background currents from other surface reactions [12]. Early research recognized the difficulty of meeting these requirements and described the need for more sophisticated methods of determining the prevailing reaction mechanisms [6, 15].

More recent research has developed methods that rely on fitting the current-voltage data to kinetic and theoretical models using nonlinear regression software. For example, Quaino *et al.* developed a kinetic method that describes the relationship between each of the three equations over the whole range of potentials [1, 8–10]. This model also has the added benefit of incorporating the diffusion limitation of H_2 through the electrolyte.

5.1.2 Hydrogenation Reaction Mechanism

Electrochemical hydrogenation of unsaturated compounds ($A + 2H \leftrightharpoons AH_2$) in general can occur via three types of mechanisms [16]:

1. Direct electron transfer

$$A + e^- \leftrightharpoons A^- + 2H^+ + e^- \leftrightharpoons AH_2 \tag{5.4}$$

2. Catalytic hydrogenation

$$A + 2H_{ads} \leftrightharpoons AH_2 \tag{5.5}$$

3. Electrocatalytic hydrogenation

$$A + 2H^+ + 2e^- \leftrightharpoons AH_2 \tag{5.6}$$

The direct electron transfer mechanism (Equation 5.4) is generally believed to

occur over materials with high HER overpotentials, such as Hg, Bi, Sn and Cd [17]. These materials have very low surface coverages of hydrogen, so reduction of unsaturated compounds occurs via the production of a radical cation intermediate, which is subsequently reacted to form the saturated organic [18].

The catalytic and electrocatalytic hydrogenation mechanisms involve the reaction of adsorbed unsaturated compounds with either adsorbed hydrogen atoms (Equation 5.5) or protons (Equation 5.6), respectively. One difference between these two reaction pathways is the effect that the electron transfer in Equation 5.6 has on the characteristic rate equation [18]. While the catalytic hydrogenation rate expression involves the surface coverages of the organic (θ_{Org}) and hydrogen (θ_{H}) reactants:

$$\mathrm{Rate} = k\theta_{\mathrm{Org}}^{a}\theta_{\mathrm{H}}^{b} \tag{5.7}$$

the rate expression for the electrocatalytic pathway incorporates an exponential term to account for the potential dependence of the electron transfer [19]:

$$\mathrm{Rate} = k\theta_{\mathrm{Org}}^{a}\theta_{\mathrm{H}}^{b}\exp\left(\frac{\alpha FV}{RT}\right) \tag{5.8}$$

where V is the applied potential, k is the reaction rate constant, and a and b are the orders of reaction. The implication from the electrochemical pathway is that an applied potential will have the effect of increasing the reaction rate. Nevertheless, the chemisorption of the organic and hydrogen reactants may also depend on the applied potential, which will likewise affect the rate [20].

Previous research has investigated the hydrogenation of unsaturated compounds, and has postulated both the catalytic hydrogenation [21–24] and electrocatalytic hydrogenation [18, 25–27] mechanisms. The fact that a proton is electrochemically generated under the applied potential in the SPE reactor employed in this work means that the hydrogenation reaction may proceed by either mechanism. This work gener-

ally asserted the given mechanism rather than employing any systematic experimental effort to determine whether the mechanism was catalytic or electrocatalytic.

In 1970, Wagner proposed a method by which the particular mechanism, thermocatalytic or electrocatalytic, may be elucidated [28]. He proposed that these mechanisms should govern the current-voltage response for a catalytic system in the presence and absence of the organic in different ways. By polarizing the cell across a range of voltages and measuring the current, both with and without the organic, the mechanism can be determined. For example, Takehara reported the hydrogenation of quinone, allyl alcohol, and vinyl alcohol in an electrochemical cell over Pt and Pt-Ag catalysts [29]. Using the method proposed by Wagner, they concluded that quinone hydrogenation followed an electrochemical mechanism, while allyl alcohol and vinyl alcohol hydrogenation followed a combination of catalytic and electrocatalytic mechanisms. They were unable to explain, however, the increase in hydrogenation rates at increasingly negative potentials. Subsequent research has demonstrated that the surface coverage of hydrogen species increases with more negative potentials [10].

By building on the methods reported by these researchers, this thesis develops a kinetic method to determine the hydrogenation mechanism using a nonlinear regression technique similar to that used to determine the HER mechanism.

5.2 Experimental

The mechanisms for HER and triglyceride hydrogenation, the cathodic reactions that occur in the SPE reactor, were investigated for various catalysts in an aqueous three-electrode cell at room temperature (25 °C).

For the HER, the catalyst materials were supported on a polished glassy carbon RDE [30]. The glassy carbon disk (d = 0.5 cm) was polished using 15 micron polishing paper (Fiber Instrument Sales, Inc.) and thoroughly rinsed with ultrapure H_2O (Millipore-Q system, 18 MΩ cm). A catalyst ink was prepared by mixing 10

mg catalyst with 0.5 mL ultrapure H_2O and 0.5 mL isopropanol (Aldrich, 99.5+%). An small aliquot (10 μL) of the catalyst suspension was deposited on the electrode and dried at room temperature in air, while rotating at 100 rpm to ensure a smooth catalyst film covered the entire electrode. Subsequently, $\sim$5 μL of a 5 wt% Nafion ionomer solution was deposited on the film and dried. A platinum wire was used as a counter electrode. Cell potentials were measured with respect to a SMSE (Bioanalytical Systems, Inc.). Analytical grade sulfuric acid (Aldrich, 99.999% purity) was used to prepare the supporting electrolyte solution. The glassy carbon RDE was attached to a MSR Analytical Rotator (Pine Instrument Company), and the three-electrode circuit was controlled by an Autolab PGSTAT302N potentiostat (Metrohm USA).

In order to characterize the triglyceride hydrogenation rates, methyl linoleate was used as a surrogate for triglycerides, since it is soluble in CH_3OH and is the methyl ester of the most abundant glycerides found in soybean oil. Measurements for the methyl linoleate hydrogenation reaction were performed with the catalyst materials abraded on a gold microelectrode. The electrolyte was composed of 0.5 M H_2SO_4 in 96% CH_3OH in ultrapure H_2O.

5.3 Results and Discussion

5.3.1 Hydrogen Evolution Reaction

To elucidate the mechanisms for the cathodic reactions that occur in the SPE-reactor, we characterized the various electrochemically stable catalysts using a number of electrochemical techniques. H_2 gas was bubbled through the electrolyte until it was saturated with H_2 at a rotation of 5000 rpm. We determined that the solution was saturated when the open circuit voltage (OCV) stopped changing, which was typically after about 30 min. Once saturation was achieved, we performed LSV in the region surrounding the OCV (Figure 5.1). The overall shape of the HER curve is

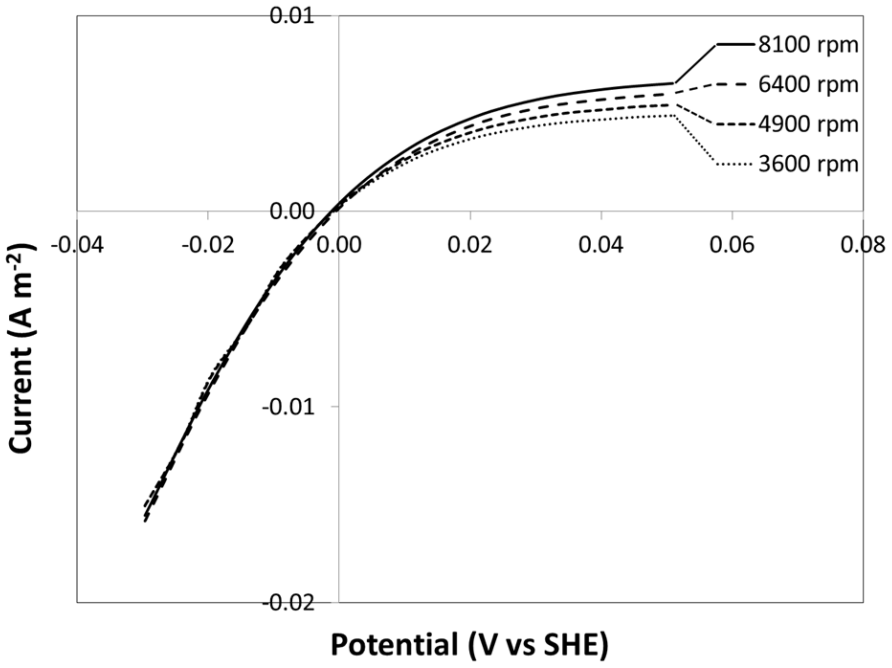

Figure 5.1: HER data for Pt black on a glassy carbon RDE rotating at 3600, 4900, 6400, and 8100 rpm in H_2 saturated 0.5 M H_2SO_4. Scan rate was 1 mV s^{-1}.

determined by the relative magnitudes of the Volmer, Heyrovský, and Tafel exchange current densities ($i_{V,0}$, $i_{H,0}$, and $i_{T,0}$, respectively). The current reaches a plateau at increasingly positive potentials due to mass-transfer limitations of H_2 to the surface.

We used nonlinear regression to fit HER LSV curves for noble metal, base metal, W_2C, and W_2C-supported Pd catalysts to the HER model (Section 2.5.2.1), as reported in the literature [10] and described in Section 2.5.2.1. This analysis was used to determine the exchange current densities for the three elementary reaction steps (Volmer, Tafel, and Heyrovský), the hydrogen coverage at OCV, and the limiting current (Table 5.2). The mass-transfer limitation associated with H_2 was characterized by the Koutecky-Levich equation, which relates the electrode area and rotation rate to the limiting current. The effect of rotation rate between 3600 to 8100 rpm on the limiting current was measured (Figure 5.2) for Pt black on a glassy carbon RDE. Since the limiting current is independent of the catalyst being tested, during nonlinear regression we fixed the value of the limiting currents for the different

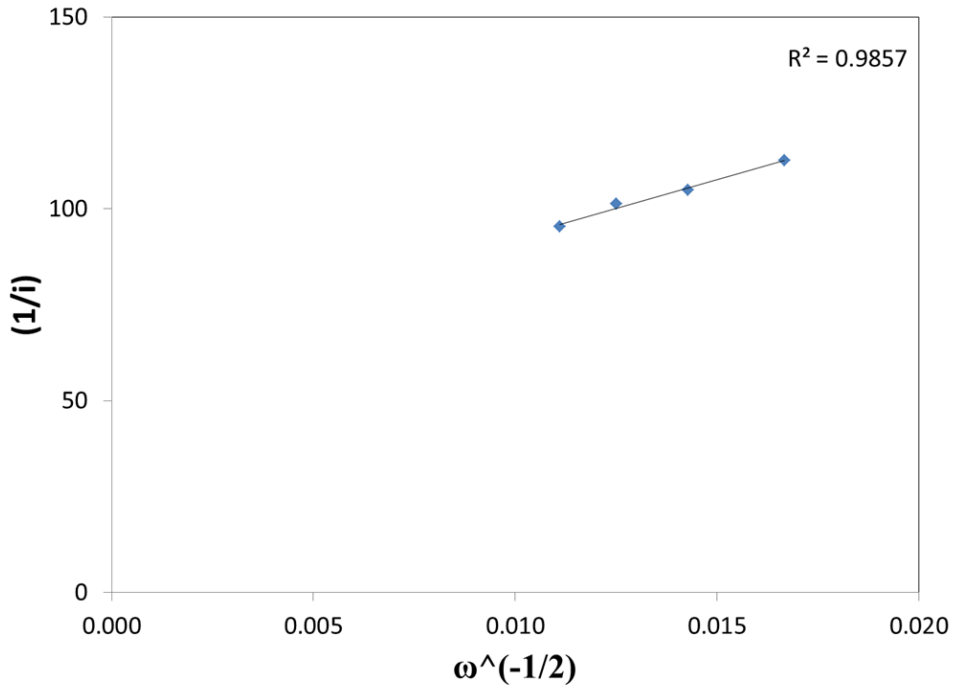

Figure 5.2: Koutecky-Levich plot for limiting currents from Table 5.2. Data is from HER of Pt black on a glassy carbon RDE rotating at 3600, 4900, 6400 and 8100 rpm in H_2 saturated 0.5 M H_2SO_4.

Table 5.2: HER data and best fit line from HER model for Pt black on a glassy carbon RDE rotating at 3600, 4900, 6400, and 8100 rpm in H_2 saturated 0.5 M H_2SO_4. Scan rate was 1 mV s^{-1}.

Parameter	Rotation Rate (rpm)				Average	Error
	3600	4900	6400	8100		
i_L x 10^2 (A m^{-2})	8.9	9.5	9.9	10.5	N/A	N/A
θ^e_H	0.1726	0.1729	0.1724	0.1729	0.1727	0.0002
$i_{H,0}$ x 10^{10} (A m^{-2})	5.8	6.8	6.8	7.0	6.6	0.6
$i_{T,0}$ x 10^8 (A m^{-2})	5.4	5.5	5.7	5.9	5.6	0.2
$i_{V,0}$ x 10^8 (A m^{-2})	38.4	36.0	37.1	37.4	37	1

Table 5.3: HER kinetic parameters from nonlinear regression of LSV data for Pt black, Rh black, Pd black, and Ru black on a glassy carbon RDE rotating between 2000 to 8000 rpm in H_2 saturated 0.5 M H_2SO_4 with a 1 mV s^{-1} scan rate.

Parameters	Pt	Rh	Pd	Ru
θ_H^e	0.1727 ± 0.002	0.1631 ± 0.0005	0.22 ± 0.04	0.16 ± 0.01
$i_{H,0}$ x 10^{11} (A m^{-2})	6.6 ± 0.6	6.73 ± 0.02	2.7 ± 0.3	6.0 ± 0.7
$i_{T,0}$ x 10^{7} (A m^{-2})	5.6 ± 0.2	6.4 ± 0.2	8 ± 2	6.2 ± 0.2
$i_{V,0}$ x 10^{7} (A m^{-2})	37 ± 1	81 ± 3	120 ± 40	79 ± 1

Table 5.4: HER kinetic parameters from nonlinear regression of LSV data for Ir, Ag, W_2C, and 6% Pd/W_2C on a glassy carbon RDE rotating between 2000 to 8000 rpm in H_2 saturated 0.5 M H_2SO_4 with a 1 mV s^{-1} scan rate.

Parameters	Ir	Ag	W_2C	6% Pd/W_2C
θ_H^e	0.163 ± 0.003	0.169 ± 0.008	0.17 ± 0.02	0.22 ± 0.01
$i_{H,0}$ x 10^{10} (A m^{-2})	9.7 ± 1.4	5.2 ± 0.9	5.9 ± 0.6	23 ± 23
$i_{T,0}$ x 10^{7} (A m^{-2})	4.3 ± 0.9	0.7 ± 0.1	0.2 ± 0.1	7.6 ± 0.7
$i_{V,0}$ x 10^{6} (A m^{-2})	24 ± 2	3 ± 2	1 ± 2	100 ± 1

rotation rates for subsequent analyses for all catalysts. The results of this analysis are listed in Table2 5.3 and 5.4. These results indicated that the HER follows the Volmer-Tafel pathway for all these materials, since the exchange current densities for the Heyrovský step were essentially zero. This result is consistent with the conclusions of other researchers (e.g., Pt [13, 14, 31], Pd [32], Ru [33–35], Ir [36, 37], and W_2C [38–40]), although some research has concluded that the HER pathway for certain materials follows the Volmer-Heyrovský pathway [13, 14]. We also observed that the exchange current density for the Tafel step for HER correlated approximately with the triglyceride hydrogenation rates from the SPE reactor (Figure 5.3).

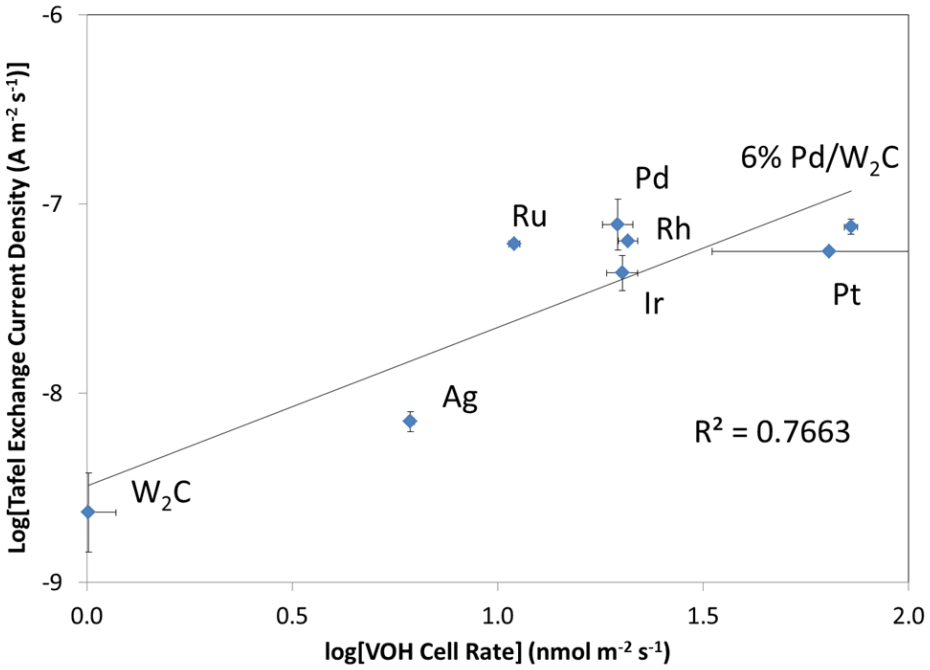

Figure 5.3: Trend of Tafel exchange current densities versus rate from SPE reactor.

5.3.2 Triglyceride Hydrogenation Reaction

In order to interrogate the mechanism for triglyceride hydrogenation, we again employed a LSV technique. Each catalyst was tested in 15 mL of an electrolyte composed of H_2 saturated 0.5 M H_2SO_4 in 96% CH_3OH and 4% H_2O. The CH_3OH was added to the electrolyte in order to make it miscible with methyl linoleate, the methyl ester of the glyceride with two unsaturated carbon-carbon bonds. This methyl ester is used as a surrogate molecule to study the hydrogenation activities of the catalyst materials for triglyceride hydrogenation. The catalysts were supported on a gold microelectrode, while a Pt wire was used as the counter electrode and potentials were measured with respect to a SMSE.

Thermochemical Hydrogenation Mechanism

$$\text{R-CH=CH-R'}_{aq} \leftrightharpoons \text{R-CH=CH-R'}_{ad} \tag{5.9a}$$

$$\text{H}_{2,ad} \leftrightharpoons 2\text{H}_{ad} \tag{5.9b}$$

$$\text{R-CH=CH-R'}_{ad} + \text{H}_{ad} \leftrightharpoons \text{R-CH-C-R'}_{ad} \tag{5.9c}$$

$$\text{R-CH-C-R'}_{aq} + \text{H}_{ad} \leftrightharpoons \text{R-CH-CH-R'}_{ad} \tag{5.9d}$$

$$\text{R-CH-CH-R'}_{ad} \leftrightharpoons \text{R-CH-CH-R'}_{aq} \tag{5.9e}$$

Electrochemical Hydrogenation Mechanism

$$\text{R-C=C-R'}_{aq} \leftrightharpoons \text{R-C=C-R'}_{ad} \tag{5.10a}$$

$$\text{R-C=C-R'}_{ad} + \text{H}^{+}_{aq} \leftrightharpoons \text{R-CH}^{+}\text{-C-R'}_{ad} \tag{5.10b}$$

$$\text{R-CH}^{+}\text{-C-R'}_{ad} + \text{e}^{-} \leftrightharpoons \text{R-CH-C-R'}_{ad} \tag{5.10c}$$

$$\text{R-CH-C-R'}_{ad} + \text{H}^{+}_{aq} \leftrightharpoons \text{R-CH-CH}^{+}\text{-R'}_{ad} \tag{5.10d}$$

$$\text{R-CH-CH}^{+}\text{-R'}_{ad} + \text{e}^{-} \leftrightharpoons \text{R-CH-CH-R'}_{ad} \tag{5.10e}$$

$$\text{R-CH-CH-R'}_{ad} \leftrightharpoons \text{R-CH-CH-R'}_{aq} \tag{5.10f}$$

As described previously, the rate determining step for hydrogenation of methyl linoleate is assumed to occur by either thermochemical or electrochemical hydrogenation on the catalyst surface (i.e., not direct electron transfer to unadsorbed organic in the electrolyte) [28, 29, 41]. The thermochemical mechanism (also known as the Horiuti-Polanyi mechanism [42–44]), involves two hydrogenation steps where the adsorbed organic reacts with adsorbed hydrogen atoms (Equation 5.9). The electrochemical mechanism also involves two hydrogenation steps where the adsorbed organic reacts with protons in the electrolyte and is subsequently reduced by an

electron (Equation 5.10).

Since both mechanisms involves an adsorbed organic, the rate expression should be proportional to the coverage of methyl linoleate (θ_{ML}). Previous research has related the surface coverage of an organic to its bulk electrolyte concentration using a Langmuir isotherm [45] (Equation 5.11), where θ_{ML} is the ML coverage, C_{ML} is the bulk concentration of ML in the electrolyte, and Γ_{ML} is the Langmuir adsorption constant for ML. If hydrogenation proceeds via the electrochemical route, the rate expression should include an exponential term involving the applied potential ($\exp[\alpha f \eta]$, where η is the applied potential); if the mechanism is thermochemical, the rate expression would not contain this term. Finally, if the mechanism is thermochemical, it should contain a term involving the hydrogen coverage.

$$\theta_{\mathrm{ML}} = \frac{\Gamma_{\mathrm{ML}} C_{\mathrm{ML}}}{1 + \Gamma_{\mathrm{ML}} C_{\mathrm{ML}}} \tag{5.11}$$

The effect of adding the unsaturated organic to the electrolyte is illustrated in Figure 5.4. As the concentration of methyl linoleate in the electrolyte is increased, the limiting current decreased and the OCV shifted to the right. Using nonlinear regression (Section 2.5.2.2), we fit rate expressions for both catalytic (Equation 5.7) or electrolytic (Equation 5.8) hydrogenation rate limiting step mechanisms to the data (Table 5.5). By comparing the goodness of fit for each rate expression, we determined that the hydrogenation reaction followed the electrolytic mechanism (Figure 5.5). The best fit values for the parameters Γ_{ML} and k_{Hyd} for each catalyst material are listed in Tables 5.6 and 5.7.

Finally, we consider the effect of applied potential on the measured hydrogenation rates. As observed earlier, hydrogenation rates varied with applied potential (Figure 5.6a). The initial increase may have been caused by the effect of potential on the hydrogenation reaction, which has been shown to proceed via an electrochemical mechanism. We propose that the subsequent plateau and decrease may be related

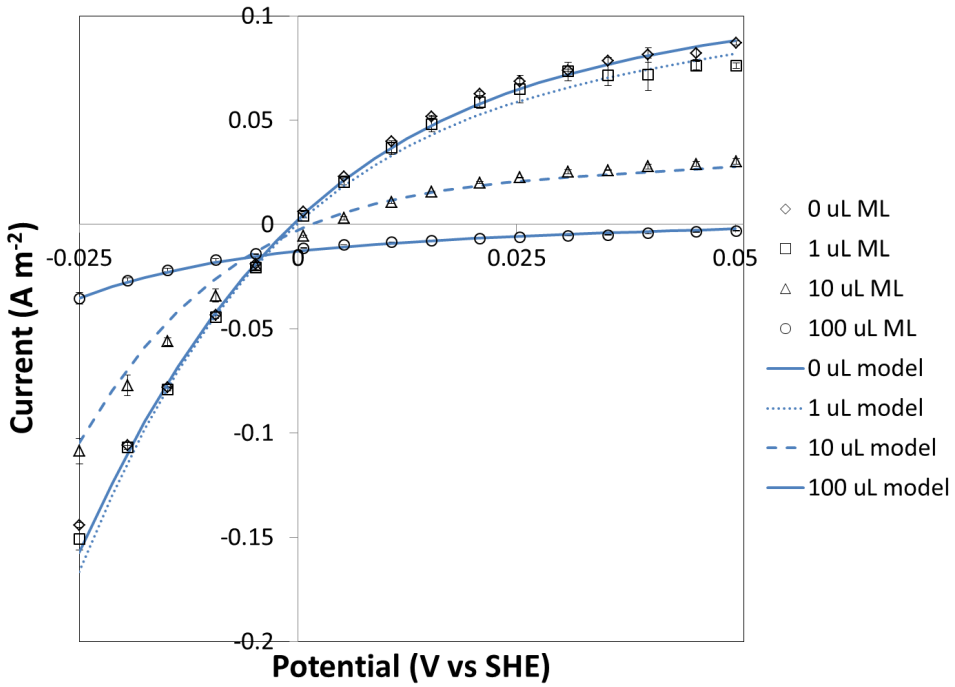

Figure 5.4: HER and ML hydrogenation data and best fit lines from HER/hydrogenation model for Pt black on a Au microelectrode in 15 mL of H_2 saturated 0.5 M H_2SO_4 in 96% CH_3OH in H_2O with 0, 1 μL, 10 μL, and 100 μL methyl linoleate.

Table 5.5: Rate expressions for thermochemical and electrochemical hydrogenation mechanisms.

	Thermochemical	Electrochemical
θ_{H}^0	$r_{Hyd} = k_{Hyd}\theta_{\mathrm{ML}}$	$r_{Hyd} = k_{Hyd}\theta_{\mathrm{ML}} \exp(\alpha f \eta)$
θ_{H}^1	$r_{Hyd} = k_{Hyd}\theta_{\mathrm{ML}}\theta_{\mathrm{H}}$	$r_{Hyd} = k_{Hyd}\theta_{\mathrm{ML}}\theta_{\mathrm{H}} \exp(\alpha f \eta)$
θ_{H}^2	$r_{Hyd} = k_{Hyd}\theta_{\mathrm{ML}}\theta_{\mathrm{H}}^2$	$r_{Hyd} = k_{Hyd}\theta_{\mathrm{ML}}\theta_{\mathrm{H}}^2 \exp(\alpha f \eta)$

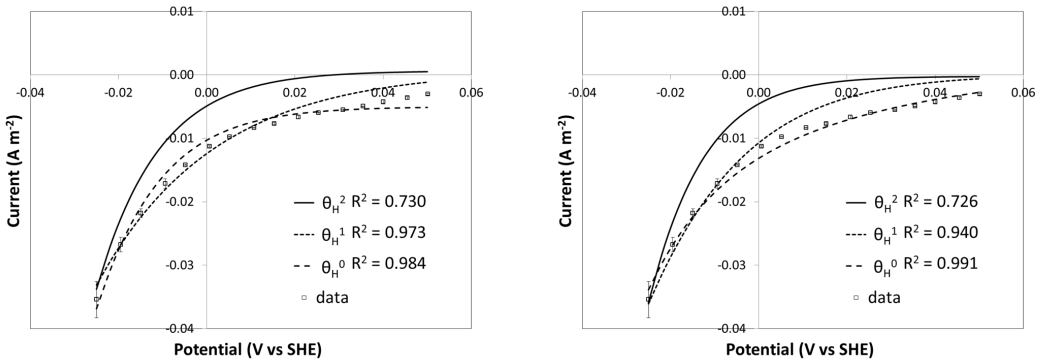

(a) Thermochemical rate determining steps (b) Electrochemical rate determining steps

Figure 5.5: HER and ML hydrogenation data and best fit lines from thermochemical and electrochemical rate laws for Pt black on a Au microelectrode in H_2 saturated 0.5 M H_2SO_4 in 96% CH_3OH in H_2O.

Table 5.6: Hydrogenation kinetic parameters from nonlinear regression of LSV data for Pt black, Rh black, Pd black, and Ru black in 15 mL of H_2 saturated 0.5 M H_2SO_4 in 96% CH_3OH in H_2O with 0, 3.86 x 10^{-5} M, 3.86 x 10^{-4} M, and 3.86 x 10^{-3} M methyl linoleate with a 1 mV s^{-1} scan rate.

Parameters	Pt	Rh	Pd	Ru
v_H^e x 10^{10} (A m^{-2})	0.07	0.09	0.07	0.06
v_V^e x 10^7 (A m^{-2})	15.8	4.69	106	0.42
v_T^e x 10^7 (A m^{-2})	31.7	30.0	3,100	5.4
Γ_{ML} x 10^2	4.3 ± 0.7	5 ± 2	6 ± 2	1.2 ± 0.2
k_{Hyd} x 10^7	5 ± 4	5 ± 1	8 ± 10	0.11 ± 0.05

Table 5.7: Hydrogenation kinetic parameters from nonlinear regression of LSV data for Ir, Ag, W_2C, and 6% Pd/W_2C in 15 mL of H_2 saturated 0.5 M H_2SO_4 in 96% CH_3OH in H_2O with 0, 3.86 x 10^{-5} M, 3.86 x 10^{-4} M, and 3.86 x 10^{-3} M methyl linoleate with a 1 mV s^{-1} scan rate.

Parameters	Ir	Ag	W_2C	6% Pd/W_2C
v_H^e x 10^{10} (A m^{-2})	0.01	0.01	100	1.6
v_V^e x 10^7 (A m^{-2})	2.77	0.67	4.8	77
v_T^e x 10^7 (A m^{-2})	64.4	22.1	6.8	47
Γ_{ML} x 10^2	3 ± 1	6 ± 3	8 ± 2	10 ± 15
k_{Hyd} x 10^7	4.7 ± 0.9	3 ± 1	80 ± 100	7 ± 3

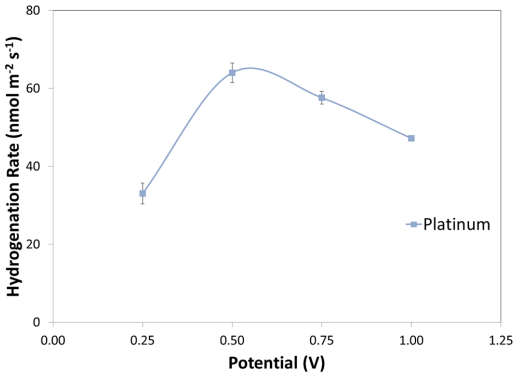

(a) Triglyceride hydrogenation rates for Pt black in a SPE reactor at 70 °C for constant potentials from 0.25 V to 1.0 V.

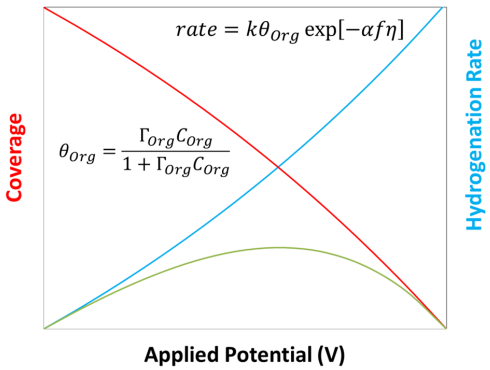

(b) Schematic of the effect of applied potential on triglyceride coverage and hydrogenation rates

Figure 5.6: Effect of applied potential on triglyceride coverage and hydrogenation rates.

to mass-transfer limitations of the triglyceride to the catalyst surface. Pintauro and coworkers observed that an increase in oil flow rate and a decrease in the thickness of the GDL resulted in an increase of the hydrogenation rate [46]. This mass-transfer limitation is likely caused by the present hydrogen gas, which is produced in greater amounts at higher applied potentials.

5.4 Conclusions

We measured rates for the HER and hydrogenation reactions over the potential range 0.25 V to 1.0 V. We observed that the mechanism for the HER was Volmer-Tafel, which agrees with the literature for those materials. We also observed that the rate determining step for methyl linoleate hydrogenation was electrocatalytic. The rates for hydrogenation in the SPE reactor correlated with those from the aqueous hydrogenation of methyl linoleate. The rates also correlated with those for the Tafel step of the HER.

References

[1] P.M. Quaino, M.R.G. de Chialvo, and A.C. Chialvo. Hydrogen diffusion effects on the kinetics of the hydrogen electrode reaction. *Physical Chemistry Chemical Physics*, 6(18):4450–4455, 2004.

[2] E. Skulason, V. Tripkovic, M.E. Bjorketun, S. Gudmundsdottir, G. Karlberg, J. Rossmeisl, T. Bligaard, H. Jonsson, and J.K. Nørskov. Modeling the electrochemical hydrogen oxidation and evolution reactions on the basis of density functional theory calculations. *The Journal of Physical Chemistry C*, 114:18182–18197, 2010.

[3] J.O.M. Bockris and E.C. Potter. The mechanism of the cathodic hydrogen evolution reaction. *Journal of the Electrochemical Society*, 99:169, 1952.

[4] J.A.V. Butler. Studies in heterogeneous equilibria. part ii.-the kinetic interpretation of the nernst theory of electromotive force. *Transactions of the Faraday Society*, 19(March):729–733, 1924.

[5] T. Erdey-Gruz and M. Volmer. The theory of hydrogen overvoltage. *Zeitschrift für Physikalische Chemie*, 150:203–13, 1930.

[6] J.O.M. Bockris, I.A. Ammar, and A. Huq. The mechanism of the hydrogen evolution reaction on platinum, silver and tungsten surfaces in acid solutions. *The Journal of Physical Chemistry*, 61(7):879–886, 1957.

[7] M. Nicolas, L. Dumoulin, and J.P. Burger. Hydrogen evolution reaction on platinum films in aqueous and methanolic solutions between 343 and 163 k. *Journal of Electroanalytical Chemistry and Interfacial Electrochemistry*, 172(1):389–395, 1984.

[8] M.R.G. de Chialvo and A.C. Chialvo. Hydrogen diffusion effects on the kinetics of the hydrogen electrode reaction. part i. theoretical aspects. *Physical Chemistry Chemical Physics*, 6(15):4009–4017, 2004.

[9] P.M. Quaino, J.L. Fernandez, M.R. Gennero de Chialvo, and A.C. Chialvo. Hydrogen oxidation reaction on microelectrodes: Analysis of the contribution of the kinetic routes. *Journal of Molecular Catalysis A: Chemical*, 252(1-2):156–162, 2006.

[10] P.M. Quaino, M.R. Gennero de Chialvo, and A.C. Chialvo. Hydrogen Electrode Reaction: A Complete Kinetic Description. *Electrochimica Acta*, 52(25):7396–7403, 2007.

[11] K. Kunimatsu, T. Senzaki, G. Samjeské, M. Tsushima, and M. Osawa. Hydrogen adsorption and hydrogen evolution reaction on a polycrystalline pt electrode studied by surface-enhanced infrared absorption spectroscopy. *Electrochimica Acta*, 52(18):5715–5724, 2007.

[12] S. Fletcher. Tafel slopes from first principles. *Journal of Solid State Electrochemistry*, 13(4):537–549, 2009.

[13] M.C. Tavares, S.A.S. Machado, and L.H. Mazo. Study of hydrogen evolution reaction in acid medium on pt microelectrodes. *Electrochimica Acta*, 46(28):4359–4369, 2001.

[14] Y. Cai and A.B. Anderson. The reversible hydrogen electrode: Potential-dependent activation energies over platinum from quantum theory. *The Journal of Physical Chemistry B*, 108(28):9829–9833, 2004.

[15] B.E. Conway and M. Salomon. Electrochemical reaction orders: Applications to the hydrogen-and oxygen-evolution reactions* 1. *Electrochimica Acta*, 9(12):1599–1615, 1964.

[16] D. Pletcher. Electrocatalysis: present and future. *Journal of Applied Electrochemistry*, 14(4):403–415, 1984.

[17] C.L. Wilson. Analogies Between Electrolytic and Chemical Methods of Reduction. Experiments with Sorbic Acid. Remarks on Mechanism. *Transactions of The Electrochemical Society*, 75:353, 1939.

[18] G.C. Bond, G. Webb, M.D. Birkett, and A.T. Kuhn. *The catalytic hydrogenation of organic compounds–a comparison between the gas–phase, liquid–phase, and electrochemical routes*, pages 61–89. RSC Publishing, 1983.

[19] F. Beck. Electrochemical and catalytic hydrogenation: common features and differences. *International Chemical Engineering*, 19(1):1–11, 1979.

[20] M. Byrne and A.T. Kuhn. Electro-catalytic reduction of ethylene on platinum and ruthenium. *Journal of the Chemical Society, Faraday Transactions 1: Physical Chemistry in Condensed Phases*, 68:355–368, 1972.

[21] E. Lamy-Pitara, L. Bencharif, and J. Barbier. Effect of sulphur on the properties of platinum catalysts as characterized by cyclic voltammetry. *Applied Catalysis*, 18(1):117–131, 1985.

[22] I. Willner, M. Rosen, and Y. Eichen. Characterization of the hydrogenation process of allyl alcohol at a pt electrode using a double galvanostatic pulse technique. *Journal of the Electrochemical Society*, 138:434–439, 1991.

[23] D.S. Santana, G.O. Melo, M.V.F. Lima, J.R.R. Daniel, M.C.C. Areias, and M. Navarro. Electrocatalytic hydrogenation of organic compounds using a nickel sacrificial anode. *Journal of Electroanalytical Chemistry*, 569(1):71–78, 2004.

[24] M.V.F. Lima, F.D. Menezes, B. de Barros Neto, and M. Navarro. A factorial design analysis of (+)-pulegone electrocatalytic hydrogenation. *Journal of Electroanalytical Chemistry*, 613(1):58–66, 2008.

[25] G. Horányi, G. Inzelt, and K. Torkos. Reductive cleavage of c-oh bonds in allyl position-formation of gaseous products in the course of the cathodic reduction of some simple unsaturated alcohols. *Journal of Electroanalytical Chemistry*, 101(1):101–108, 1979.

[26] G. Horanyi and K. Torkos. Effect of chemisorbed methanol on the rate and selectivity of electroreduction processes at a platinized platinum electrode. *Journal of Electroanalytical Chemistry and Interfacial Electrochemistry*, 111(2-3):279–286, 1980.

[27] L. Ploense, M. Salazar, B. Gurau, and E.S. Smotkin. Proton spillover promoted isomerization of n-butylenes on pd-black cathodes/nafion 117. *Journal of the American Chemical Society*, 119(47):11550–11551, 1997.

[28] C. Wagner. Considerations on the mechanism of the hydrogenation of organic compounds in aqueous solutions on noble metal catalysts. *Electrochimica Acta*, 15(6):987–997, 1970.

[29] Z. Takehara. Hydrogenation of some organic compounds in acidic aqueous solutions on noble metal catalysts. *Electrochimica Acta*, 15(6):999–1012, 1970.

[30] M.I. Awad, M.M. Saleh, and T. Ohsaka. Impact of SO2 poisoning of platinum nanoparticles modified glassy carbon electrode on oxygen reduction. *Journal of Power Sources*, 2011.

[31] B. Babic, J. Gulicovski, L. Gajic-Krstajic, N. Elezovic, V.R. Radmilovic, N.V. Krstajic, and L.M. Vracar. Kinetic study of the hydrogen oxidation reaction on sub-stoichiometric titanium oxide-supported platinum electrocatalyst in acid solution. *Journal of Power Sources*, 193(1):99–106, 2009.

[32] F. Hernandez and H. Baltruschat. Hydrogen evolution and cu upd at stepped gold single crystals modified with pd. *Journal of Solid State Electrochemistry*, 11(7):877–885, 2007.

[33] A.T. Kuhn and P.M. Wright. The cathodic evolution of hydrogen on ruthenium and osmium electrodes. *Journal of Electroanalytical Chemistry*, 27(2):319–323, 1970.

[34] M. Fleischmann and M. Grenness. Electrocrystallization of ruthenium and electrocatalysis of hydrogen evolution. *Journal of the Chemical Society, Faraday Transactions 1: Physical Chemistry in Condensed Phases*, 68:2305–2315, 1972.

[35] M.S. Rau, M.R. Gennero de Chialvo, and A.C. Chialvo. A feasible kinetic model for the hydrogen oxidation on ruthenium electrodes. *Electrochimica Acta*, 55(17):5014–5018, 2010.

[36] L. Chen, D. Guay, and A. Lasia. Kinetics of the hydrogen evolution reaction on ruo2 and iro2 oxide electrodes in h2so4 solution: An ac impedance study. *Journal of The Electrochemical Society*, 143:3576, 1996.

[37] T. Pauporté, F. Andolfatto, and R. Durand. Some electrocatalytic properties of anodic iridium oxide nanoparticles in acidic solution. *Electrochimica Acta*, 45(3):431–439, 1999.

[38] H. Bohm. Adsorption und anodische oxydation von wasserstoff an wolframcarbid. *Electrochimica Acta*, 15(7):1273–1280, 1970.

[39] P. Zóltowski. Hydrogen evolution reaction on smooth tungsten carbide electrodes. *Electrochimica Acta*, 25(12):1547–1554, 1980.

[40] P. Zoltowski. An immitance study of the mechanism of hydrogen reactions on a tungsten carbide electrode:: Part ii. analysis in terms of a non-linear model. *Journal of Electroanalytical Chemistry*, 260(2):287–301, 1989.

[41] W. An, J.K. Hong, P.N. Pintauro, K. Warner, and W. Neff. The electrochemical hydrogenation of edible oils in a solid polymer electrolyte reactor. I. Reactor design and operation. *Journal of the American Oil Chemists' Society*, 75(8):917–925, 1998.

[42] Y.B. Vassiliev, V.S. Bagotzky, O.A. Khazova, V.V. Cherny, and A.M. Meretsky. Mechanism of adsorption, electroreduction and hydrogenation of compounds with ethylenic bonds on platinum and rhodium:: Part II. Comparison of the electroreduction and catalytic hydrogenation processes. *Journal of Electroanalytical Chemistry*, 98(2):273–282, 1979.

[43] P. Simon, A. Celkova, and S. Schmidt. A simplified Horiuti-Polanyi scheme for the hydrogenation of triacylglycerols. *Journal of the American Oil Chemists' Society*, 68(2):74–78, 1991.

[44] A. Bernas, P. Maki-Arvela, N. Kumar, B. Holmbom, T. Salmi, and D.Y. Murzin. Heterogeneously catalytic isomerization of linoleic acid over supported ruthenium catalysts for production of anticarcinogenic food constituents. *Industrial Engineerring Chemistry Research*, 42(4):718–727, 2003.

[45] V. Anantharaman and P.N. Pintauro. The Electrocatalytic Hydrogenation of Glucose. *Journal of the Electrochemical Society*, 141:2729, 1994.

[46] W. An, J.K. Hong, P.N. Pintauro, K. Warner, and W. Neff. The electrochemical hydrogenation of edible oils in a solid polymer electrolyte reactor. II. Hydrogenation selectivity studies. *Journal of the American Oil Chemists' Society*, 76(2):215–222, 1999.

CHAPTER VI

Conclusions and Future Work

6.1 General Conclusions

Electrochemical reactors have recently received an increase in attention due to the possibility of influencing the activities and selectivities of chemical reactions via the applied potential. The work described in this thesis has explored the utility of this approach in the context of triglyceride hydrogenation. A range of catalyst materials have been evaluated in therms of their activities and selectivities for the triglyceride hydrogenation reaction, including noble metals, base metals, early transition metal carbides, and carbide-supported metals. The conclusions derived from these investigations have broad application in the context of other reactions and electrochemical reactor configurations. A brief summary of these conclusions include:

- We found that certain catalysts had high activities for triglyceride hydrogenation, such as the noble metals (Pt, Rh, Pd, Ru and Ir). Other catalysts, such as the base metals (Fe, Co, and Ni) as well as Mo_2C, VC, and NbC had low or negligible activities. The best catalysts, in terms of high activities and high selectivities in terms of trans and saturated fat production, were the W_2C-supported Pd catalysts. The high surface areas and high electrical conductivities of the carbide materials make them attractive for use as catalyst supports. The devel-

opment of these carbide-supported metal catalysts will likely be an important area of research for the development of electrocatalytic reactor systems.

- We demonstrated that the catalyst stabilities of the materials we tested were an important factor in determining their utility for triglyceride hydrogenation. We characterized the spent membrane electrode assemblies for the catalysts tested, and found that the low rates observed for the base metals and certain of the carbides were likely due to their instability in the potential and pH ranges used. We further characterized their stabilities in a SPE three-electrode cell, and found that corrosion rates for the different materials were on the order of hours to days. These observations are particularly relevant when considering the different properties necessary for thermochemical and electrochemical catalysts. For example, a Ni/SiO_2 catalyst is used in the thermochemical triglyceride hydrogenation reactor in industry. But a similar catalyst would be unsuitable for use in electrochemical hydrogenation, since the support is nonconductive and the Ni is unstable.

- We observed that the hydrogenation rates for the catalysts tested varied with applied potential. Detailed electrochemical experiments in aqueous three-electrode cells demonstrated that this dependence is due to the electrochemical mechanisms for the cathode reactions (i.e., HER and hydrogenation). These reactions involve the transfer of an electron, and as such their rate expressions are dependent on the applied potential. This has important ramifications on the operating parameters chosen for the reactor operation. Since higher potentials result in higher hydrogenation rates as well as higher HER rates, it is important to balance these to make best use of the electricity.

- We further observed that the hydrogenation rates decreased at very high potentials (up to 1 V), and we propose that this is due to mass transfer limitations

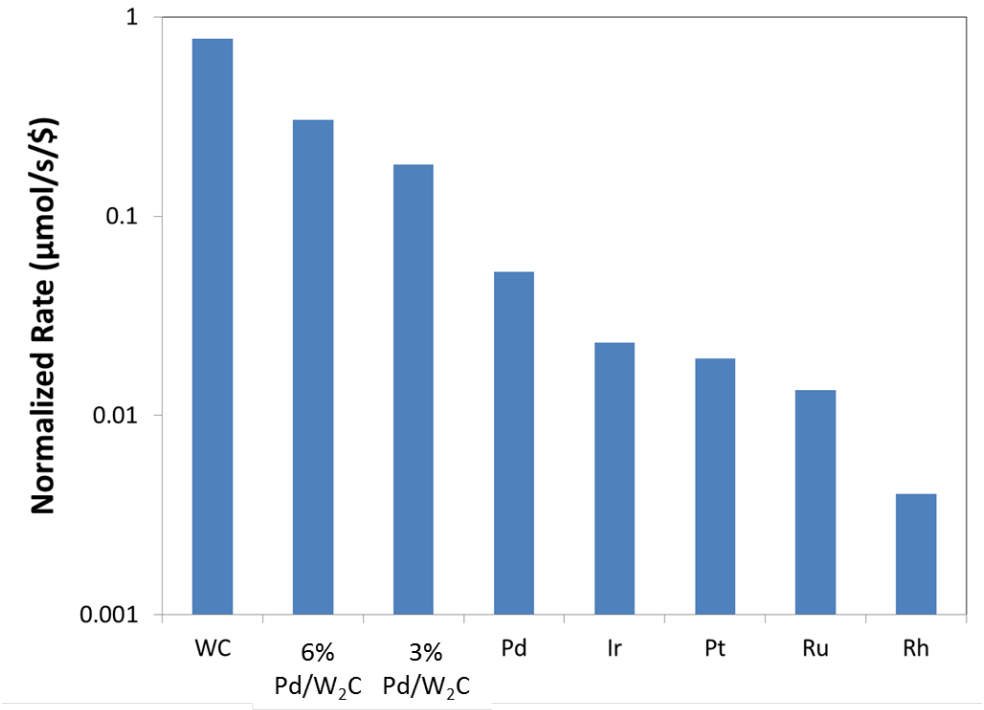

Figure 6.1: Triglyceride hydrogenation rates at 70 °C and 0.5 V normalized by material costs for noble metal, base metal, W_2C, and W_2C-supported Pd catalysts.

with respect to the triglyceride. This is a marked departure from the operation of the thermochemical reactor, which is mass transfer limited with respect to hydrogen gas. The high conductivity of the ion conducting membrane provides facile transport of hydrogen to the catalyst surface, and at high potential this creates an excess of hydrogen on the surface of the cathode catalyst. This excess limits the effective concentration of oil near the surface and effectively decreases the rate. Future reactor designs should incorporate strategies for mitigating the evolution of hydrogen gas and facilitating the transfer of triglyceride to the catalyst surface.

6.2 Economics of Triglyceride Hydrogenation

Finally, in Figure 6.1, we compare the activities of the different electrocatalysts against their cost (as of 3/18/2011) [1]. The cost for W_2C was assumed to be the

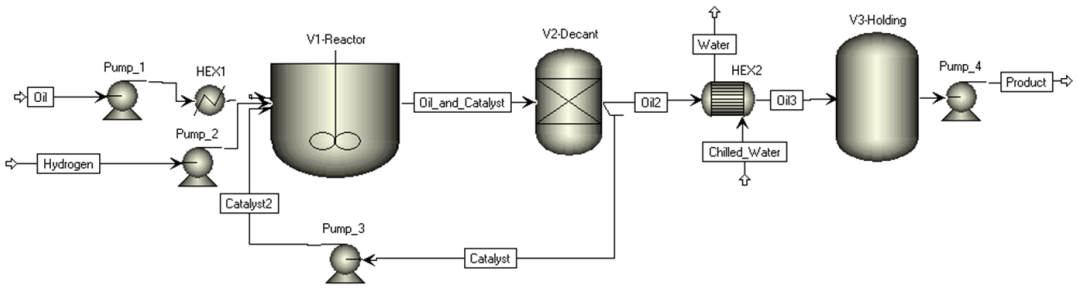

Figure 6.2: Schematic of a thermochemical triglyceride hydrogenation plant.

same as that of W metal, and the costs for the W_2C-supported Pd catalysts were estimated to be the weighted average of the costs for W and Pd. We note that although Pd, Rh, and Pt exhibited the highest rates for triglyceride hydrogenation, these materials have the highest material cost. W_2C-supported Pd catalysts had the highest hydrogenation rates when normalized by material cost. This suggests that these materials may be interesting for use in an industrial setting.

Using Capcost, a software package for capital cost estimation and financial analysis, we have investigated the viability of an electrochemical hydrogenation plant and compared it to that of a thermochemical plant [2]. We based the designs for these plants on that of a typical oil hydrogenation plant described in the literature [3]. Both plants process 25 metric tons of soybean oil a day using hydrogen gas, and produce margarine. All equipment are made of stainless steel. While an real plant would make use of heat integration to reduce utility costs, this was not taken into account for simplicity. Reactants are heated with natural gas and products are cooled with chilled water.

The thermochemical plant uses a Ni/SiO_2 catalyst (0.02% catalyst/oil) in a stirred tank reactor at 140 °C and 3 atm (Figure 6.2 and Table 6.1). The catalyst is separated from the product in a separate decanting tank and recycled back to the reactor. The product is subsequently cooled and stored in an intermediate holding tank. It is assumed that the catalyst loading is replaced once per year. The net present value of

Table 6.1: Capital cost and utilities usage of an thermochemical triglyceride hydrogenation plant[a].

Equipment	Bare Module Cost ($)	Utilities	Annual Cost ($)
V1 - Reactor[b]	$160,000	N/A	-
V2 - Decanter[b]	$160,000	N/A	-
V3 - Storage[b]	$160,000	N/A	-
Pump 1[c]	$36,500	Electricity	$592
Pump 2[c]	$36,500	Electricity	$592
Pump 3[c]	$36,500	Electricity	$592
Pump 4[c]	$36,500	Electricity	$592
Heat Exchanger 1[d]	$13,200	Natural Gas	$13,900
Heat Exchanger 2[d]	$13,200	Chilled Water	$740

[a]Assumes 2 yr construction period and a 10 yr project life after construction; taxation rate is 42% and annual interest rate is 10%. Labor cost is $600,000 per year. Cost of raw materials and products (soybean oil - $0.69 kg^{-1} [4]; hydrogen - $2.00 kg^{-1} [5]; margarine - $2.53 kg^{-1} [6]) are estimated from literature.

[b]Reactor and storage vessels are sized to accommodate up to 10 metric tons of oil, are made of stainless steel, and are rated to a maximum pressure of 4 barg.

[c]Pumps are centrifugal type, stainless steel pumps operating at 1 kW with 85% efficiency; Pumps 1, 2, and 3 have an outlet pressure of 3 barg, while Pump 4 has an outlet pressure of 1 barg. Bare module costs also includes cost of 2 spare pumps on hand. Cost of electricity is estimated to be $16.67 GJ^{-1}.

[d]Heat exchangers are 1 m^2 double pipe type exchangers constructed of stainless steel, which are rated for a tube pressure of 4 barg. Heating cost is estimated to be $6 GJ^{-1} (from natural gas), while cooling cost is estimated to be $0.35 GJ^{-1} (from chilled water).

Table 6.2: Capital cost and utilities usage of an electrochemical triglyceride hydrogenation plant[a].

Equipment	Bare Module Cost ($)	Utilities	Annual Cost ($)
V1 - Reactor[b]	$113,000	Electricity	$119,190
V3 - Storage[b]	$113,000	N/A	-
Pump 1[c]	$36,500	Electricity	$592
Pump 2[c]	$36,500	Electricity	$592
Pump 4[c]	$36,500	Electricity	$592
Heat Exchanger 1[d]	$13,200	Natural Gas	$5,600
Heat Exchanger 2[d]	$13,200	Chilled Water	$290

[a]Assumes 2 yr construction period and a 10 yr project life after construction; taxation rate is 42% and annual interest rate is 10%. Labor cost is $600,000 per year. Cost of raw materials and products (soybean oil - $0.69 kg^{-1} [4]; hydrogen - $2.00 kg^{-1} [5]; margarine - $2.53 kg^{-1} [6]) are estimated from literature.

[b]Cost and structure of the electrochemical reactor vessel is assumed to be of similar cost to a thermochemical reactor of a similar size. Reactor and storage vessels are sized to accommodate up to 10 metric tons of oil, are made of stainless steel, and are rated to a maximum pressure of 1 barg. The electrochemical reactor is assumed to operate at 0.5 V and 0.3 A cm^{-2}. Catalyst loading is assumed to be 1 mg cm^{-2} of 6% Pd/W_2C, and will require approximately 1,600 m^2 of active surface area.

[c]Pumps are centrifugal type, stainless steel pumps operating at 1 kW with 85% efficiency; Pumps 1, 2, and 4 have an outlet pressure of 1 barg, while Pump 3 (from Figure 6.2) is unnecessary since the catalyst does not need to be separated recycled in this plant). Bare module costs also includes cost of 2 spare pumps on hand. Cost of electricity is estimated to be $16.67 GJ^{-1}.

[d]Heat exchangers are 1 m^2 double pipe type exchangers constructed of stainless steel, which are rated for a tube pressure of 1 barg. Heating cost is estimated to be $6 GJ^{-1} (from natural gas), while cooling cost is estimated to be $0.35 GJ^{-1} (from chilled H_2O).

the thermochemical plant for 10 yr of operation is $16.43 million.

The electrochemical plant takes advantage of the improved catalyst-product separation available due to the SPE-reactor design; since the catalyst remains fixed in the membrane, a separate decanting vessel is not required (Figure 6.3). Furthermore, since the hydrogen for reducing the triglycerides is supplied to the catalyst surface by the applied potential, the reactor operates at a lower temperature (70 °C) and pressure (1 atm). This reduces the capital cost associated with having a high system pressure (Table 6.2). The electrochemical reactor uses a 6 wt% Pd/W_2C catalyst with

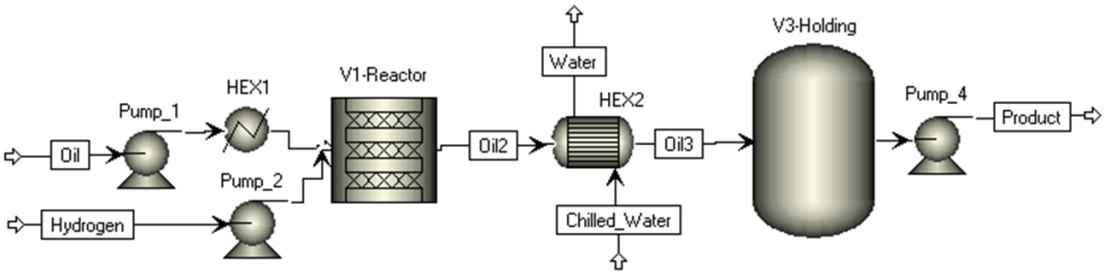

Figure 6.3: Schematic of an electrochemical triglyceride hydrogenation plant.

the same activity measured in this work. It is similarly assumed that the catalyst loading is replaced once per year. The net present value of the electrochemical plant for 10 yr of operation is $16.38 million. The cumulative cash flow (discounted) for the two plants is illustrated in Figure 6.4, which demonstrates how the electrochemical system approximately equal to the thermochemical system in profitability. Another scenario is also illustrated, which shows the projected profitability of a plant with a product that sells for 5% more, due to its more desirable product selectivity (lower concentrations of saturated and *trans* fat contents), with a net present value of $18.9 million after 10 yr. In this case, the electrochemical plant is slightly more profitable than the thermochemical plant. While the accuracy of this analysis is likely limited to an order of magnitude, these results suggest that an SPE industrial triglyceride hydrogenation reactor is at least possible.

6.3 Future Research Directions

Throughout this thesis we have looked at the intersection between catalysis and electrochemistry in the context of an electrochemical reactor. The hydrogenation of triglycerides has provided a unique platform for this reaction, since the chemistry involved is rather complex. While the majority of the detailed mechanistic work in this thesis has focused on elucidating the activity trends for different electrocatalysts,

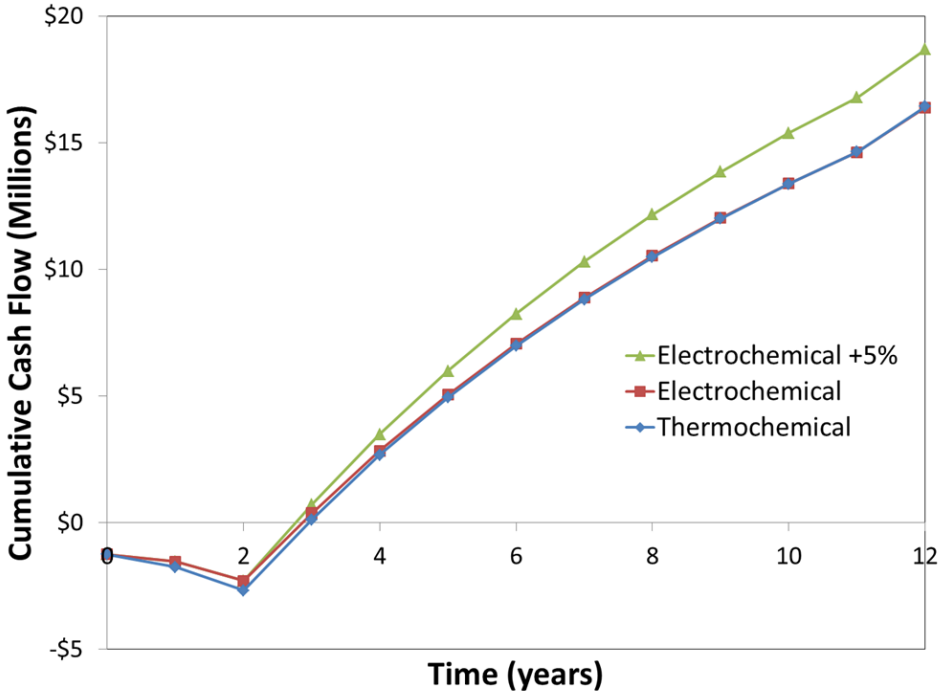

Figure 6.4: Comparison of discounted cumulative cash flows for thermochemical and electrochemical triglyceride hydrogenation plants.

the selectivities of these catalysts need to be further studied.

For example, the *trans* fat and saturated fat selectivities of a Pt catalyst in the triglyceride hydrogenation reactor were found to be a function of the applied potential. This behavior could be related to different coverages of the *cis* and *trans* isomers being present under a given potential. Or it could be dependent on different reactivities of these species under reaction conditions. It is important for the operation of electrochemical reactors to understand how these processes work, so this area should be investigated further.

Another logical extension of this thesis would be to investigate the activities of other W_2C-supported metal catalysts. Pd/W_2C catalysts were found to have high activities and selectivities. Other catalysts comprised of other noble metals (e.g., Pt, Rh, Ru, Ir, and Au) supported on W_2C may likewise exhibit interesting performance.

References

[1] Metal prices, March 2011.

[2] R. Turton, R.C. Bailie, and W.B. Whiting. *Analysis, Synthesis and Design of Chemical Processes*. Prentice Hall, Old Tappan, NJ (United States), 1998.

[3] R.C. Hastert. Practical aspects of hydrogenation and soybean salad oil manufacture. *Journal of the American Oil Chemists' Society*, 58(3):169–174, 1981.

[4] A. Radich. Biodiesel performance, costs, and use. *Combustion*, 24(2):131–132, 1998.

[5] F.D. Doty. A realistic look at hydrogen price projections. *Doty Scientific, Inc. Columbia*, 2004.

[6] Margarine and Cooking Oil Processing in the US. Technical report, IBISWorld, 2008.